DISSERTATION

THE PH-DEPENDENT ACTIVITY AND THE PROTONOPHORIC MECHANISM OF PYRAZINOIC ACID AND ITS STRUCTURAL ANALOGUES

Submitted by

Fabio Levi Piedade Neto Guerra Fontes

Graduate Degree Program in Cell and Molecular Biology

In partial fulfillment for the requirements

For the Degree of Doctor of Philosophy

Colorado State University

Fort Collins, Colorado

Fall 2019

Doctoral Committee:

Advisor: Dean C. Crick

Co-Advisor: Debbie C. Crans

Deborah Roess

Eric Ross

ABSTRACT

THE PH-DEPENDENT ACTIVITY AND THE PROTONOPHORIC MECHANISM OF PYRAZINOIC ACID AND ITS STRUCTURAL ANALOGUES

Pyrazinamide is an anti-tubercle drug used in the standard treatment regimen against *Mycobacterium tuberculosis*, the cause of tuberculosis infections. The mechanism of action of pyrazinamide requires its enzymatic conversion to pyrazinoate, but the final molecular target of pyrazinoate is controversial. Pyrazinamide also exhibits pH-dependent activity *in vitro*, but the phenomenon was seldom explained by the mechanisms of action proposed in literature. Moreover, pyrazinamide is known to synergize with other anti-mycobacterial drugs *in vivo* but reports of this synergistic activity *in vitro* are scarce. The work presented here aimed to gain insight on the mechanism of action of pyrazinamide that explains both its activity and the pH-dependent behavior *in vitro*, while seeking to understand the synergism of pyrazinamide *in vitro*.

The results presented here show the pH-dependent activity is not caused by pH sensitivity of *M. tuberculosis*, as the data demonstrates the bacilli are able to maintain pH homeostasis in a pH range between 5.5 and 7.3. Additionally, *M. tuberculosis* actively replicates in physiologically extreme pH environments (pH 5.5 and pH 8.5), albeit at a slower rate than at neutral pH values. Mycobacterial cultures treated with pyrazinoic acid showed growth inhibition that correlates with the relative concentration of the acid (but not of its conjugated base, pyrazinoate). Treatment with pyrazinoic acid also leads to concentration-dependent acidification of the cytoplasm of mycobacterial bacilli and concentration-dependent dissipation of the electric potential across the cytosolic membrane. These results led to the conclusion that pyrazinoic acid, but not pyrazinoate,

is the active form of pyrazinamide. The mechanism involves the enzymatic conversion of pyrazinamide into pyrazinoate. Pyrazinoate then crosses the cytosolic membrane and is exposed to the acidic environment, where an acid-base equilibrium is established with pyrazinoic acid. Pyrazinoic acid crosses the membrane and reaches the cytosol, where the more neutral pH leads to the loss of the proton it carried from the extracellular environment. The acid-base equilibrium outside the cell generates a higher relative concentration of pyrazinoic acid as the pH of the environment becomes more acidic, leading to the pH-dependent activity of pyrazinamide. The work presented here demonstrates the pH-dependence is not replicated by other anti-tubercle drugs, such as rifampin, isoniazid or bedaquiline. However, structural analogues of pyrazinoic acid, such as salicylic acid, and a known protonophore, carbonyl cyanide *m*-chlorophenyl hydrazone, mimic the pH-dependent growth inhibition of pyrazinoic acid. A model for the pH-dependent activity of these compounds was derived, based on chemical assumptions. The model demonstrates that pyrazinoic acid acts as a protonophore, causing the disruption of proton motive force, and that this mechanism is only possible if no other cellular target exists.

The synergism of pyrazinoic acid with rifampin and isoniazid *in vitro* was determined, using the median effect principle, at different pH environments. Additionally, salicylic acid was tested in combination with rifampin or isoniazid to determined if the drug-drug interactions of pyrazinoic acid with these drugs was mimicked by its structural analogues, like its mechanism was shown to be. The results indicate pyrazinoic acid behaves additively with both rifampin and isoniazid *in vitro*, which was seen in salicylic acid as well. The data indicates that the drug-drug interactions of pyrazinoic acid are replicated by salicylic acid. Additionally, the results suggest the synergism of pyrazinamide *in vivo* may originate from some type of host effect that was not present in the *in vitro* studies conducted.

ACKNOWLEDGEMENTS

The work presented here would have been impossible to finish without the guidance and support of my two advisors, Debbie Crans and Dean Crick. Debbie gave me the opportunity to join her group and work with her, first as a research assistant and then as a graduate student under her supervision and, even in the worst of times, she never gave up on me; for that and all the rest, I am grateful for her help and support. Dean became my supervisor almost by accident, but, apparently, some accidents have positive outcomes. The results shown here are the consequence as much his guidance as his patience to let me explore and make my own path, even if he lost some hair because of it. I guess irreverence never disappears, even in more formal documents. I am also greatly appreciated to the other members of my graduate advisory committee, Deborah Roess and Eric Ross, whom always showed support and incentivized me during our brief interactions.

It is unmeasurable the amount of gratitude I have for my family. So distant in space and somewhat in time with the seven hours of difference between our clocks, my parents and little sister were my biggest supporters during this time, never giving up when I wanted to give up and always present. I do not have words to thank them.

I have left a few friends behind when I moved to pursuit my studies, but they never left me. I would like to name a few close friends that, either with a stupid joke or a simple text supported me over the years in manners they probably do not realize: Ricardo Praça and Carlos Afonso, thank you for all the moments of silliness that allowed me to stay sane.

Speaking of insanity, I have to name the members that shared the laboratory space with me and that I drove absolutely crazy, very likely. Venugopal Pujari, Vicki Cox-Jones, Santosh Kumar and Kaitlin Doucette, I am sorry and thankful for everything. I am also deeply grateful to Janine

Crick, who made her mission to become almost my surrogate mother and went to the extreme of making sure I was fed. I clearly was not starving, but she made sure I had enough soup.

I also have to thank Steven Rooker and Jamie Lynn-Barbe for allowing me to advise them during their time as undergraduate students in our laboratory. They probably do not realize I learned as much with them as they think they did with me.

Finally, I would like to thank the NIH/NSAID for funding this work.

TABLE OF CONTENTS

LIST OF FIGURES

Chapter 1

Pyrazinamide

Tuberculosis (TB) is an infectious disease responsible for the death of 1.3 million people in 2017 alone.[1] The standard regimen against infections with *Mycobacterium tuberculosis*, the etiological cause of TB, includes rifampin, isoniazid, ethambutol and pyrazinamide (PZA). While the other drugs in the regimen have known mechanisms of action,[2–4] PZA's molecular target remains unknown. Additionally, *M. tuberculosis* is mildly resistant to PZA *in vitro*, when optimal growth conditions are used.[5] When used in combination *in vivo*, however, PZA exhibits synergism with other anti-tubercle drugs, leading to a reduction of the time required for treatment with the standard regimen from 12 to 6 months.[6,7] The use of PZA with other drug combinations have also been recommended,[8] despite the lack of understanding on the mechanism of PZA's synergism. Thus, the poorly understood activity of PZA has hindered the development of antibiotics with similar properties against *M. tuberculosis*.

Historical background

The discovery of PZA's anti-mycobacterial properties occurred simultaneously at the Merck Laboratories and at the Lederle Laboratories, in 1952, using a mouse model.[9,10] The studies, which also discovered the anti-tubercle activities of isoniazid and ethaniomide,[11,12] were conducted following the reports of the inhibitory activity of nicotinamide in *M. tuberculosis*, in a murine model.[13] The use of PZA to successfully treat human TB patients was reported shortly afterwards.[14] The activity of PZA *in vitro* was also examined and it was concluded that PZA was only active against *M. tuberculosis in vitro* at acidic pH.[15] In 1967, PZA was also shown to be a

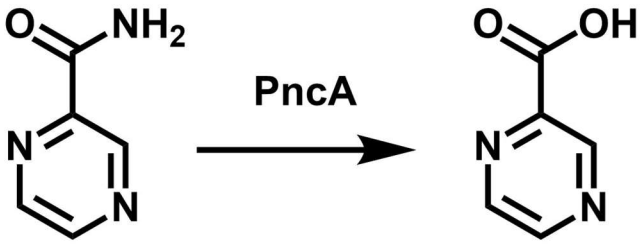

Figure 1.1 – Pyrazinamide conversion by PncA. Pyrazinamide requires enzymatic conversion inside the bacterium by a nicotinamidase, PncA, to pyrazinoic acid. Mutations in PncA are the cause of over 95% of the cases of resistance to PZA in patients.

pro-drug, requiring activation by a mycobacterial nicotinamidase, PncA (Figure 1.1).[16] While the activity of PZA was comparable to that of isoniazid in patients with TB, the high doses required for the treatment of TB with PZA and the subsequent liver damage led to PZA being used mainly as a second-line drug until the early 1980s.[17] A study conducted in East Africa, however, indicated a combination between PZA and rifampin shortened the time required for disease clearance by half and, with the HIV/AIDS epidemics amplifying the number of TB patients, PZA was added to the standard regimen.[6,7] Currently, the World Health Organization recommends the use of PZA in, at least, the first couple months of the regimen in first-line combinations, while use of PZA in second-line is still advisable for most combinations.[8]

In vivo activity of pyrazinamide

The discovery of PZA as an anti-TB drug occurred in a murine model, but human studies were reported almost simultaneously.[9,10,14] In mice, PZA was shown to exhibit prolonged activity, with an initial delayed effect (~2 days).[18,19] However, PZA is not active in guinea pigs with no proven explanation for the differential activity in the two animal models. In humans, PZA used alone was shown to reduce initial TB symptoms, such as fever and cough.[14] Additionally, was shown to be as effective as rifampin when any of the drugs were added to regimens containing isoniazid and streptomycin.[6] The observation led to the discovery of PZA's synergy with rifampin

when subsequent studies were implemented,[7] which led to PZA's addition to the standard regimen.

The activity of PZA against *M. tuberculosis* inside macrophages is controversial, with reports asserting either bacteriostatic or bactericidal effect in intracellular bacilli,[20–22] while other literature describes no inhibitory effect of PZA in mycobacterial cells inside macrophages.[23,24] Additionally, pyrazinoic acid (POA), the product of PZA's conversion by PncA (Figure 1.1) was shown to be inactive against cultured macrophages infected with *M. tuberculosis*.[25,26] Hypotheses to explain the different observations were presented elsewhere,[27] based on the small but significant experimental protocols used in all the reports. Recently, it was shown that PZA also exhibits differential activity dependent on the pathology of the TB lesions.[28] The different pH of the lesions was suggested as the explanation for this observation,[29] correlating with previous observations on the requirement of acidic pH for PZA activity.[15]

In vitro activity of pyrazinamide

As described above, PZA's activity was initially shown to require acidic environments,[15] acting in a pH-dependent manner *in vitro*.[30] The pH-dependence is reported to correlate with the Henderson-Hasselbalch equation.[27] The activity of PZA is higher in acidic environments and gets progressively worse as the pH increases.[30] The pH-dependent activity was also demonstrated with POA, albeit PZA showing lower efficacy at the same pH values and POA exhibiting mild, but observable activity in neutral environments while PZA does not.[27] The activity of PZA in neutral environments is stimulated by overexpression of PncA,[31] suggesting POA undergoes efflux after conversion from PZA.

Multiple mechanisms of action have been proposed for PZA.[27,32–35] Independent studies have recently suggested POA inhibits PanD, an enzyme involved in the pantothenate biosynthetic

pathway.[32,33] Pantothenate is a precursor of coenzyme A (CoA) and it was shown to antagonize the activity of PZA.[32] The enzyme PanD acts as an aspartate decarboxylase, resulting in the synthesis of β-alanine, and both β-alanine and pantetheine were shown to also antagonize PZA's and POA's activity.[32,33] As pantothenate, pantetheine and β-alanine are all downstream of PanD in the pantothenate pathway, the results suggest POA may target this pathway. Additionally, POA was also shown to inhibit the activity of GpsI, a bifunction enzyme involved in the metabolism of RNA, single-stranded DNA and guanosine tetraphosphate.[34] Recently, PZA was also shown to inhibit NadC, a quinolinic acid phosphoribosyltransferase; POA was also shown to inhibit NadC, but the inhibition was weaker than when PZA was used.[35] However, none of the mechanisms described above provide any insight into the pH-dependent activity of PZA and POA.

Conversely, POA was proposed to cause the acidification of the cytoplasm of *M. tuberculosis*.[27] The mechanism suggested involves the conversion of PZA by PncA into POA inside the cytosol and posterior efflux of POA to the exterior of the mycobacterial bacilli. In an acidic extracellular environment, the acid-base equilibrium of POA would shift towards the protonated form of the acid (as seen in Figure 1.2), when compared with the acid-base equilibrium inside the cell. This form can permeate the mycobacterial membrane and transport protons across,

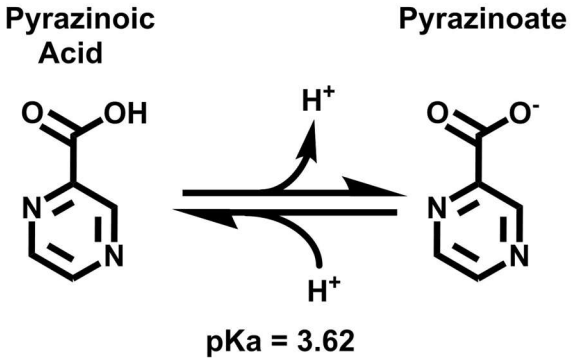

Figure 1.2 – The acid base equilibrium of pyrazinoic acid. In solution, pyrazinoic acid is in equilibrium with its conjugated base, pyrazinoate, and the relative amounts of each form depend on the pH of the solution and the pK_a of pyrazinoic acid, following the Henderson Hasselbalch equation.

leading to the eventual acidification of the cytoplasm.[27] This mechanism is pH-dependent and is similar to the mechanism describing the activity of chemical uncouplers.[36]

References

(1) World Health Organization. *Global Tuberculosis Report 2018*; Geneva, 2018.

(2) Lancini, G.; Pallanza, R.; Silvestri, L. G. Relationships between bactericidal effect and inhibition of ribonucleic acid nucleotidyl-transferase by rifampicin in *Escherichia coli* K-12. *J. Bacteriol.* **1969**, *97* (2), 761–768.

(3) Winder, F. G. A.; Collins, P.; Rooney, S. A. Effects of isoniazid on mycolic acid synthesis in *Mycobacterium tuberculosis* and on its cell envelope. *Biochem. J.* **1970**, *117* (2), 27P-27P. https://doi.org/10.1042/bj1170027Pa.

(4) Goude, R.; Amin, A. G.; Chatterjee, D.; Parish, T. The arabinosyltransferase EmbC is inhibited by ethambutol in *Mycobacterium tuberculosis*. *Antimicrob. Agents Ch.* **2009**, *53* (10), 4138–4146. https://doi.org/10.1128/AAC.00162-09.

(5) Tarshis, M. S.; Weed, W. A. Lack of significant *in vitro* sensitivity of *Mycobacterium tuberculosis* to pyrazinamide on three different solid media. *Am. Rev. Tuberc.* **1953**, *67* (3), 391–395. https://doi.org/10.1164/art.1953.67.3.391.

(6) British Thoracic and Tuberculosis Association. Short-course chemotherapy in pulmonary tuberculosis: a controlled trial by the British Thoracic and Tuberculosis Association. *The Lancet* **1976**, *308* (7995), 1102–1104. https://doi.org/10.1016/S0140-6736(76)91085-0.

(7) British Thoracic Society. A controlled trial of six months' chemotherapy in pulmonary tuberculosis, final report: results during the 36 months after the end of chemotherapy and beyond. *Brit. J. Dis. Chest* **1984**, *78*, 330–336. https://doi.org/10.1016/0007-0971(84)90165-7.

(8) World Health Organization. *WHO Consolidated Guidelines on Drug-Resistant Tuberculosis Treatment*; Geneva, 2019.

(9) Solotorovsky, M.; Gregory, F. J.; Ironson, E. J.; Bugie, E. J.; O'Neill, R. C.; Pfister, K. Pyrazinoic acid amide: an agent active against experimental murine tuberculosis. *P. Soc. Exp. Biol. Med.* **1952**, *79* (4), 563–565. https://doi.org/10.3181/00379727-79-19447.

(10) Malone, L.; Schurr, A.; Lindh, H.; McKenzie, D.; Kiser, J. S.; Williams, J. H. The effect of pyrazinamide (aldinamide) on experimental tuberculosis in mice. *Am. Rev. Tuberc.* **1952**, *65* (5), 511–518. https://doi.org/10.1164/art.1952.65.5.511.

(11) Fox, H. H. The chemical approach to the control of tuberculosis. *Science* **1952**, *116* (3006), 129–134. https://doi.org/10.1126/science.116.3006.129.

(12) Rist, N.; Grumbach, F.; Libermann, D. Experiments on the antituberculous activity of alpha-ethyl-thioisonicotinamide,. *Am. Rev. Tuberc. Pulm. Dis.* **1959**, *79* (1), 1–5. https://doi.org/10.1164/artpd.1959.79.1.1.

(13) McKenzie, D.; Malone, L.; Kushner, S.; Oleson, J. J.; SubbaRow, Y. The effect of nicotinic acid amide on experimental tuberculosis of white mice. *J. Lab. Clin. Med.* **1948**, *33* (10), 1249–1253. https://doi.org/10.5555/uri:pii:0022214348903217.

(14) Yeager, R. L.; Munroe, W. G. C.; Dessau, F. I. Pyrazinamide (aldinamide) in the treatment of pulmonary tuberculosis. *Am. Rev. Tuberc.* **1952**, *65* (5), 523–546. https://doi.org/10.1164/art.1952.65.5.523.

(15) McDermott, W.; Tompsett, R. Activation of pyrazinamide and nicotinamide in acidic environments *in vitro*. *Am. Rev. Tuberc.* **1954**, *70* (4), 748–754. https://doi.org/10.1164/art.1954.70.4.748.

(16) Konno, K.; Feldmann, F. M.; McDermott, W. Pyrazinamide susceptibility and amidase activity of tubercle bacilli. *Am. Rev. Respir. Dis.* **1967**, *95* (3), 461–469. https://doi.org/10.1164/arrd.1967.95.3.461.

(17) Matthews, J. H. Pyrazinamide and isoniazid used in the treatment of pulmonary tuberculosis. *Am. Rev. Respir. Dis.* **1960**, *81* (3), 348–351. https://doi.org/10.1164/arrd.1960.81.3.348.

(18) McCune, R. M.; Tompsett, R. Fate of *Mycobacterium tuberculosis* in mouse tissues as determined by the microbial enumeration technique: I. The persistence of drug-susceptible tubercle bacilli in the tissues despite prolonged antimicrobial therapy. *J. Exp. Med.* **1956**, *104* (5), 737–762. https://doi.org/10.1084/jem.104.5.737.

(19) McCune, R. M.; Tompsett, R.; McDermott, W. Fate of *Mycobacterium tuberculosis* in mouse tissues as determined by the microbial enumeration technique: II. the conversion of tuberculous infection to the latent state by the administration of pyrazinamide and a companion drug. *J. Exp. Med.* **1956**, *104* (5), 763–802. https://doi.org/10.1084/jem.104.5.763.

(20) Mackaness, G. B. The intracellular activation of pyrazinamide and nicotinamide. *Am. Rev. Tuberc. Pulm. Dis.* **1956**, *74* (5), 718–728. https://doi.org/10.1164/artpd.1956.74.5.718.

(21) Scorpio, A.; Zhang, Y. Mutations in *pncA*, a gene encoding pyrazinamidase/nicotinamidase, cause resistance to the antituberculous drug pyrazinamide in tubercle bacillus. *Nat. Med.* **1996**, *2* (6), 662. https://doi.org/10.1038/nm0696-662.

(22) Boshoff, H. I.; Mizrahi, V.; Barry, C. E. Effects of pyrazinamide on fatty acid synthesis by whole mycobacterial cells and purified fatty acid synthase I. *J. Bacteriol.* **2002**, *184* (8), 2167–2172. https://doi.org/10.1128/JB.184.8.2167-2172.2002.

(23) Heifets, L.; Higgins, M.; Simon, B. Pyrazinamide is not active against *Mycobacterium tuberculosis* residing in cultured human monocyte-derived macrophages. *Int. J. Tuberc. Lung Dis.* **2000**, *4* (6), 491–495.

(24) Rastogi, N.; Potar, M. C.; David, H. L. Pyrazinamide is not effective against intracellularly growing *Mycobacterium tuberculosis*. *Antimicrob. Agents Ch.* **1988**, *32* (2), 287. https://doi.org/10.1128/AAC.32.2.287.

(25) Salfinger, M.; Crowle, A. J.; Reller, L. B. Pyrazinamide and Pyrazinoic Acid Activity against Tubercle Bacilli in Cultured Human Macrophages and in the BACTEC System. *J. Infect. Dis.* **1990**, *162* (1), 201–207. https://doi.org/10.1093/infdis/162.1.201.

(26) Crowle, A. J.; Sbarbaro, J. A.; May, M. H. Inhibition by pyrazinamide of tubercle bacilli within cultured human macrophages. *Am. Rev. Respir. Dis.* **1986**, *134* (5), 1052–1055. https://doi.org/10.1164/arrd.1986.134.5.1052.

(27) Zhang, Y.; Mitchison, D. The curious characteristics of pyrazinamide: a review. *Int. J. Tuberc. Lung Dis.* **2003**, *7* (1), 6–21.

(28) Lanoix, J.-P.; Lenaerts, A. J.; Nuermberger, E. L. Heterogeneous disease progression and treatment response in a C3HeB/FeJ mouse model of tuberculosis. *Dis. Model. Mech.* **2015**, *8* (6), 603–610. https://doi.org/10.1242/dmm.019513.

(29) Lanoix, J.-P.; Ioerger, T.; Ormond, A.; Kaya, F.; Sacchettini, J.; Dartois, V.; Nuermberger, E. Selective inactivity of pyrazinamide against tuberculosis in C3HeB/FeJ mice is best explained by neutral pH of caseum. *Antimicrob. Agents Ch.* **2016**, *60* (2), 735–743. https://doi.org/10.1128/AAC.01370-15.

(30) Salfinger, M.; Heifets, L. B. Determination of pyrazinamide MICs for *Mycobacterium tuberculosis* at different pHs by the radiometric method. *Antimicrob. Agents Ch.* **1988**, *32* (7), 1002–1004. https://doi.org/10.1128/AAC.32.7.1002.

(31) Peterson, N. D.; Rosen, B. C.; Dillon, N. A.; Baughn, A. D. Uncoupling environmental pH and intrabacterial acidification from pyrazinamide susceptibility in *Mycobacterium tuberculosis*. *Antimicrob. Agents Ch.* **2015**, *59* (12), 7320–7326. https://doi.org/10.1128/AAC.00967-15.

(32) Dillon, N. A.; Peterson, N. D.; Rosen, B. C.; Baughn, A. D. Pantothenate and pantetheine antagonize the antitubercular activity of pyrazinamide. *Antimicrob. Agents Ch.* **2014**, *58* (12), 7258–7263. https://doi.org/10.1128/AAC.04028-14.

(33) Shi, W.; Chen, J.; Feng, J.; Cui, P.; Zhang, S.; Weng, X.; Zhang, W.; Zhang, Y. Aspartate decarboxylase (PanD) as a new target of pyrazinamide in *Mycobacterium tuberculosis*. *Emerg. Microbes Infec.* **2014**, *3* (1), 1–8. https://doi.org/10.1038/emi.2014.61.

(34) Njire, M.; Wang, N.; Wang, B.; Tan, Y.; Cai, X.; Liu, Y.; Mugweru, J.; Guo, J.; Hameed, H. M. A.; Tan, S.; et al. Pyrazinoic acid inhibits a bifunctional enzyme in *Mycobacterium tuberculosis*. *Antimicrob. Agents Ch.* **2017**, *61* (7), e00070-17. https://doi.org/10.1128/AAC.00070-17.

(35) Kim, H.; Shibayama, K.; Rimbara, E.; Mori, S. Biochemical characterization of quinolinic acid phosphoribosyltransferase from *Mycobacterium tuberculosis* H37Rv and inhibition of its activity by pyrazinamide. *PLOS ONE* **2014**, *9* (6), e100062. https://doi.org/10.1371/journal.pone.0100062.

(36) McLaughlin, S. G.; Dilger, J. P. Transport of protons across membranes by weak acids. *Physiol. Rev.* **1980**, *60* (3), 825–863. https://doi.org/10.1152/physrev.1980.60.3.825.

Chapter 2

Mechanisms of action of chemical uncouplers

The reducing products of glucose respiration, such as NADH and $FADH_2$, provide a source of electrons and energy that the enzyme complexes in the electron transport chain (ETC) can use to drive protons through a semi-permeable membrane and against the concentration gradient. Additionally, electrons flow from these initial donors to oxygen, which accepts the electrons to form water (as seen in Figure 2.1). The electron flux occurs through a series of oxidation-reduction reactions catalyzed by the enzymes in the ETC. The energy produced through these reactions is used to shuttle the protons across the membrane and the electrochemical potential generated by this process is then converted to the high-energy ATP bonds by the ATP synthase. The flux of protons and electrons was described by Mitchell in 1961 and provides the basis of his chemiosmotic theory.[1] The chemiosmotic theory was developed to explain ATP synthesis by mitochondria, but also describes the prokaryotic energy production mechanism,[2,3] given the following assumptions:

a) the membrane separating the reducing environment that provides electrons to the ETC and the environment to which protons are being transferred to is essentially impermeable to ions, including protons.[1] The topology of this membrane is distinct in eukaryotic cells, where the ETC and ATP synthase machinery exist in the inner membrane of mitochondria,[4] and prokaryotic cells, which have the complexes responsible for most of the energy production embedded in the cytosolic membrane.[3]

b) the respiratory chain consists of proton translocators and electron carriers, which use the energy obtained from the oxidation of substrate to transport protons from the proton-poor side of

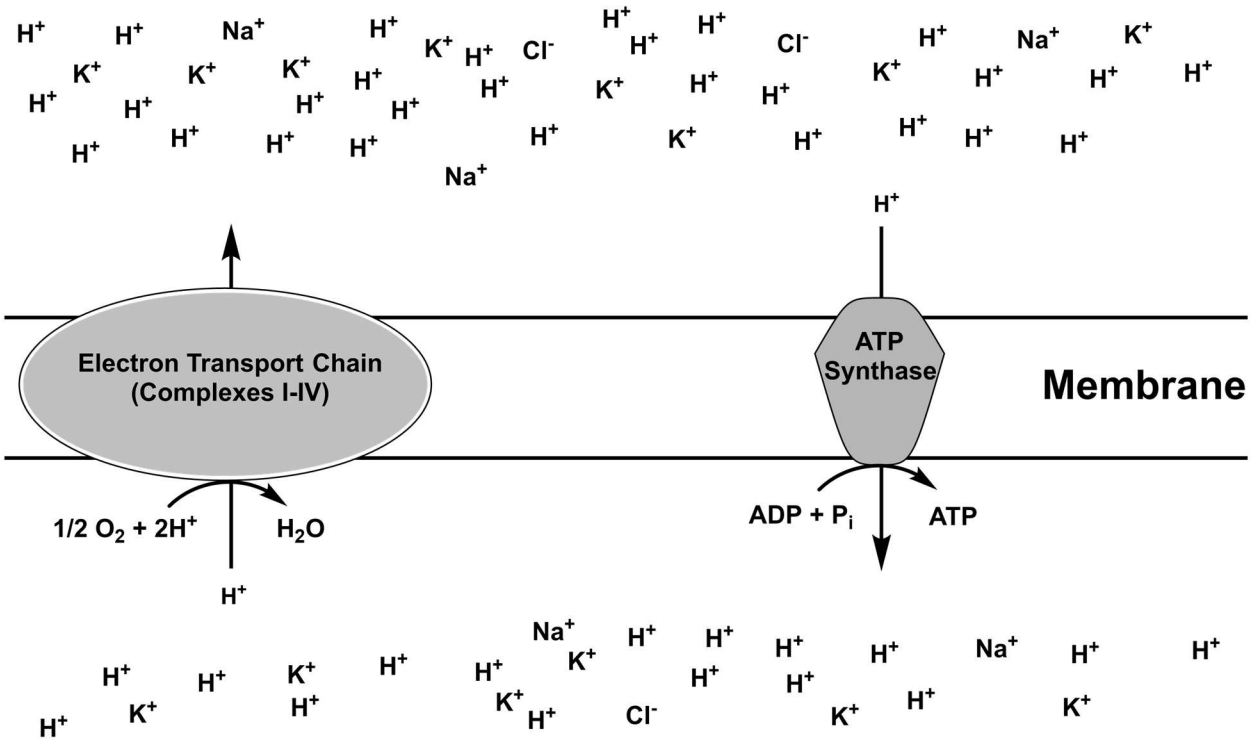

Figure 2.1 – Mitchell's chemiosmotic theory. Peter Mitchell postulated the electron flux through the electron transport chain (ETC) generated energy which was used to establish an electrochemical potential across the membrane. The electrons going through the ETC are accepted by oxygen to form water while the electrochemical gradient is converted to ATP through translocation of a proton along the gradient by ATP synthase, which converts the potential energy into a phosphate-phosphate bond in ATP. The electrochemical gradient is mainly generated through efflux of protons, which led Mitchell to designate the potential as proton motive force.

the membrane to a proton-rich side of the membrane. This proton flux is accompanied by electron transfer to cofactors (such as FAD or iron-sulfur clusters) or electron carriers (such as ubiquinone or menaquinone) to a final electron acceptor (commonly oxygen or others, in the case of anaerobic cells).[1,3–5]

Based on these assumptions above, a proton electrochemical potential is generated by the movement of ions across the semi-permeable membrane.[1] Mitchell designated this potential as proton motive force, or PMF. Apart from the role in ATP synthesis,[2] PMF is utilized for a variety of cellular processes, from suppling the energy for bacterial flagellar movement to xenobiotics efflux.[3,6] The conservation of PMF, in particular in bacteria given the absence of specialized compartments, is an active process that cells maintain by regulating ion gradients across

membranes.[7] During his derivation of PMF, Mitchell demonstrated how PMF depends on two components: the electric potential across the membrane ($\Delta\Psi$), which reflects the overall charge separation across the membrane, and the gradient of protons (ΔpH), resulting in a differential pH environment on each side of the membrane.[2] In eukaryotes, the control of PMF is achieved by maintaining the concentrations of charged entities in the matrix and in the intermembrane space and through the acidification of the intermembrane space and regulation other ions' concentration on both sides of the mitochondrial inner membrane.[4] In prokaryotes, the control is exerted at the cytoplasm level, as PMF is established with the extracellular environment;[7,8] therefore, it is impossible for the cell to regulate the concentrations of the environment. In both cases, however, dissipation of either $\Delta\Psi$ or ΔpH has been shown to lead to PMF disruption,[9] despite the existence of compensatory mechanisms.[7] The disruption of PMF was shown to be a regulatory mechanism in mitochondria, involving the efflux of protons or other ions by uncoupling proteins,[10] but in most cases, this disruption is a catastrophic event that leads to cell growth arrest.[11] Thus, chemical uncouplers, known to be able to disrupt one (or both) components of PMF, can lead to catastrophic events and, in the case of bacteria, have the potential to be used as chemotherapeutic agents.[12,13]

Mechanisms of uncoupling activity

While mitochondria and bacteria have highly regulated mechanisms to control PMF, other compounds have been discovered to cause disruption of PMF. These xenobiotics are structurally and mechanistically diverse and are traditionally grouped under the same designation: uncouplers. The nomenclature originated from the ability to uncouple the oxidative processes in the ETC from the ADP phosphorylation by the ATP synthase.[2] The structural nature of uncouplers ranges from small molecular weight molecules (such as 2,4-dinitrophenol, also termed DNP) to peptides (such

as gramicidin or valinomycin).[2] Given the structural diversity, the mechanisms of action of the various uncouplers is also diverse, albeit with a common target: uncouplers affect PMF, either disrupting one of its components or both.

Valinomycin is an ionophore able to transport cations across a semi-permeable membrane down the membrane electrochemical potential.[14] While valinomycin can transport Na^+, Cs^+, Rb^+ and NH_4^+, the binding constant to K^+ was shown to be the highest at ~10^6 M^{-1}.[15] Mechanistically, valinomycin acts as a uniporter of cations, transporting these ions in a single way through the membrane and, as such, collapsing $\Delta\Psi$ and causing the disruption of PMF through this collapse.[14] Gramicidin is also known to lead to increased permeabilization of the membrane to the ions transported by valinomycin, but gramicidin acts in a distinct way: a gramicidin dimer spontaneously forms in the presence of a membrane, creating a ion-permeable pore that causes the disruption of membrane $\Delta\Psi$ like valinomycin.[16] Hence, both valinomycin and gramicidin are commonly used in the bioenergetics field due to their uncoupling activity.

Nigericin is also used in bioenergetics studies, given its ability to collapse PMF.[14] While valinomycin acts as a uniporter cation transporter, nigericin (and the structurally similar monensin) behaves like an antiporter shuttle. The catalytic mechanism of nigericin involves the protonation of its carboxylic acid in the proton-rich side of the membrane (corresponding to the mitochondrial intermembrane space or the extracellular environment, in bacteria). The protonated nigericin diffuses through the membrane, reaching the proton-poor side of the membrane (the matrix in mitochondria and the cytoplasm in bacteria). Here, the carboxylic group loses its proton as a consequence of the acid-base equilibrium at the proton-poor side of the membrane favoring the formation of the charged form of nigericin. Then, the charged nigericin forms a complex with a K^+ ion, folding around the cation.[17] Monensin forms a similar complex with Na^+, but the

mechanism is otherwise identical to that of nigericin.[14] The nigericin-K^+ complex will then diffuse through the membrane to the proton-rich side of the membrane, where the cation will be exchanged for a proton (given the more favorable acid-base equilibrium of the carboxylic acid group in the proton-rich environment) and the cycle will start anew.[17] This electroneutral cycle means nigericin causes a collapse of the ΔpH, but not of $\Delta\Psi$, as the exchange of a proton for a K^+ implies the overall charge is maintained. However, the proton flux leads to a change in the proton gradient across the membrane and, therefore, a dissipation of the ΔpH.

Carbonyl cyanide *m*-chlorophenyl hydrazone (CCCP) and DNP are examples of another class of uncoupler that behaves differently from valinomycin or nigericin. The mechanism of action of these uncouplers involves the transport of protons across the membrane,[18] similarly to the mechanism described for the first step of the catalytic cycle of nigericin. Yet, while nigericin then conjugates with a cation counterion, CCCP or DNP do not, and the mechanism can vary from that point, as described below. These ionophoric uncouplers that specifically transport protons are called protonophores, although the names classical or chemical uncouplers can also be found. Since the flux of positively charged protons is not compensated by an inverse flux of a cation, protonophores trigger the disruption of PMF through the dissipation of both $\Delta\Psi$ and ΔpH.[19] Protonophores also share a set of structural similarities, namely the requirement for one (or more) protonatable group within its structure and a hydrophobic moiety, such as a benzene-like ring, likely to augment the protonophore membrane solubility.[9,20]

However, depending on the specific mechanism cycle, protonophores are often divided into two classes: class 1, which follows a monomolecular mechanism (or A^- mechanism), and class

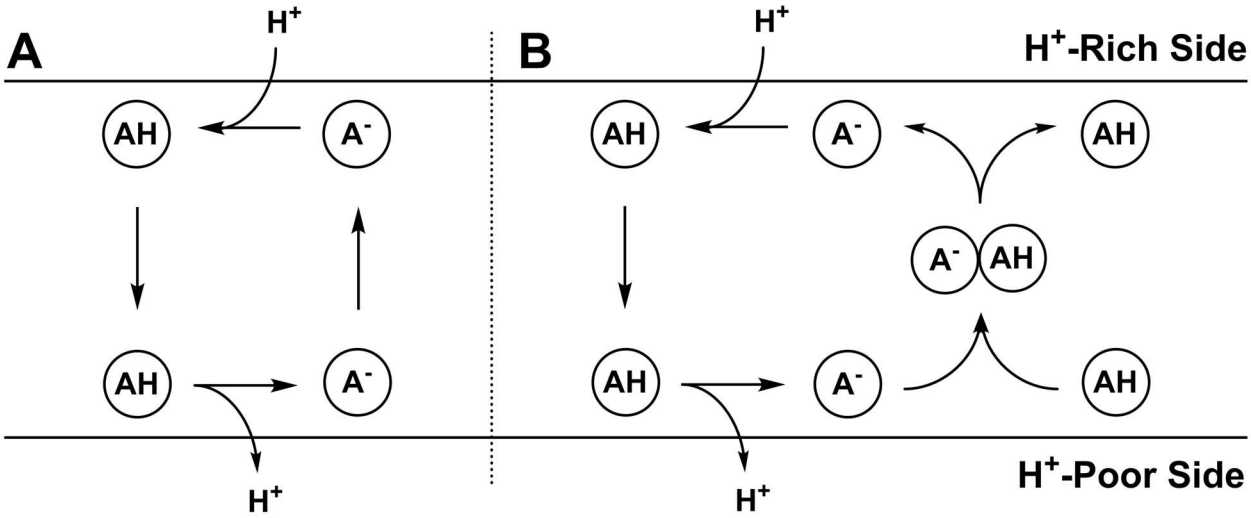

Figure 2.2 – The mechanisms of action of protonophores. Protonophores have two distinct mechanism of action, with the A^- mechanism shown in Panel A and the AHA^- mechanism shown in Panel B. The A^- mechanism involves the monomolecular diffusion of the protonophore to both sides of the membrane, albeit in different states of protonation. The AHA^- mechanism, however, requires the formation of the heterodimer AHA^- for A^- to diffuse through the membrane and complete the cycle. The proton-rich side of the membrane corresponds to the intermembrane space of mitochondria or the extracellular milieu of bacteria, while the proton-poor side corresponds to the mitochondrial matrix or the bacterial cytosol. Adapted from McLaughlin and Dilger.[23]

2, acting through a bimolecular mechanism (or AHA^- mechanism).[21] An example of a class 1 protonophore is CCCP,[22,23] while DNP operates through a class 2 mechanism.[23] In class 1 protonophores, when the uncoupler is exposed to the proton-rich side of the membrane, the compound enters in an acid-base equilibrium between its protonated form (AH) and its conjugated base (A^-). The form AH is generally accepted to permeate the membrane at a much faster rate than A^- and, thus, the AH is more likely to be exposed to the proton-poor side of the membrane. The acid-base equilibrium between AH and A^- in the proton-poor side of the membrane is shifted to the generation of A^- and AH is deprotonated. The cycle is completed by A^- crossing the membrane with no counterion like nigericin and is commonly termed as A^- mechanism given A^- diffusion through the membrane.[22] The electrogenic transport of protons causes the disruption of PMF though both $\Delta\Psi$ and ΔpH and is illustrated in Figure 2.2 (Panel A). Class 2 compounds function through a bimolecular mechanism, in which the first step is similar to the beginning of the mechanism of class 1 compounds: the protonophore is exposed to the proton-rich side of the

membrane and enters in an acid-base equilibrium between AH and A^-. The AH form diffuses through the membrane and reaches the proton-poor side of the membrane where it loses the proton. However, instead of freely crossing the membrane, in class 2 protonophores the A^- form forms a heterodimer with a molecule AH and it is under the AHA^- dimer form that A^- crosses the membrane. The AHA^- dimer falls apart on the proton-rich side of the membrane, releasing A^- and the cycle starts anew, with A^- in equilibrium with AH.[23] Therefore, the class 2 mechanism has been termed AHA^- mechanism. Examples of protonophores acting through this mechanism include DNP and salicylic acid, the active form of aspirin. The cycle is shown in Figure 2.2 (Panel B).

The ability for uncouplers to be utilized as antibiotics is far from a novel concept,[24] but has gained traction as new drugs are found to behave as uncouplers or to exhibit uncoupling activity under specific conditions.[12,13,25] Moreover, previously reports show uncouplers may also heighten the activity of other antibiotics.[25,26] Thus, the potential for use of classical or novel uncouplers of PMF as antibiotics exists and may open the way to new classes of compounds used against infectious diseases.

The work presented here proposes that pyrazinamide (PZA), a first-line anti-tubercle drug, acts as a protonophore. The growth inhibitory activity of PZA was shown to exhibit pH-dependent *in vitro*,[27] which would be explained by the general mechanism of chemical uncouplers. Moreover, the activity of PZA requires the conversion to pyrazinoate, the conjugated base of pyrazinoic acid.[28–31] The acid-base equilibrium of pyrazinoic acid and pyrazinoate exhibits the same properties of the equilibrium between A^- and AH. Additionally, pyrazinoic acid is a structural analogue of both benzoic acid and salicylic acid, which were shown to behave like protonophores previously.[32,33] Thus, the aim of the present work is to investigate the pH-dependent activity of

pyrazinoic acid in *Mycobacterium tuberculosis*, the cause of tuberculosis infections, and to determine if pyrazinoic acid behaves as a protonophore, leading to the disruption of PMF in mycobacterial cells.

References

(1) Mitchell, P. Coupling of phosphorylation to electron and hydrogen transfer by a chemi-osmotic type of mechanism. *Nature* **1961**, *191* (4784), 144–148. https://doi.org/10.1038/191144a0.

(2) Mitchell, P. Chemiosmotic coupling in oxidative and photosynthetic phosphorylation. *Biol. Rev.* **1966**, *41* (3), 445–502. https://doi.org/10.1111/j.1469-185X.1966.tb01501.x.

(3) Harold, F. M. Membranes and energy transduction in bacteria. In *Current Topics in Bioenergetics*; Sanadi, D. R., Ed.; Elsevier, 1977; Vol. 6, pp 83–149. https://doi.org/10.1016/B978-0-12-152506-4.50010-8.

(4) Brand, M. D.; Lehninger, A. L. H+/ATP ratio during ATP hydrolysis by mitochondria: modification of the chemiosmotic theory. *PNAS* **1977**, *74* (5), 1955–1959. https://doi.org/10.1073/pnas.74.5.1955.

(5) Skulachev, V. P. Solution of the problem of energy coupling in terms of chemiosmotic theory. *J. Bioenerg. Biomembr.* **1972**, *3* (1), 25–38. https://doi.org/10.1007/BF01515994.

(6) Manson, M. D.; Tedesco, P.; Berg, H. C.; Harold, F. M.; Drift, C. V. der. A protonmotive force drives bacterial flagella. *PNAS* **1977**, *74* (7), 3060–3064. https://doi.org/10.1073/pnas.74.7.3060.

(7) Bakker, E. P.; Mangerich, W. E. Interconversion of components of the bacterial proton motive force by electrogenic potassium transport. *J. Bacteriol.* **1981**, *147* (3), 820–826.

(8) Booth, I. R. Regulation of cytoplasmic pH in bacteria. *Microbiol. Mol. Biol. R.* **1985**, *49* (4), 359–378.

(9) Heytler, P. G. [58] Uncouplers of oxidative phosphorylation. In *Methods in Enzymology*; Biomembranes Part F: Bioenergetics: Oxidative Phosphorylation; Academic Press, 1979; Vol. 55, pp 462–472. https://doi.org/10.1016/0076-6879(79)55060-5.

(10) Krauss, S.; Zhang, C.-Y.; Lowell, B. B. The mitochondrial uncoupling-protein homologues. *Nat. Rev. Mol. Cell Biol.* **2005**, *6* (3), 248–261. https://doi.org/10.1038/nrm1592.

(11) Terada, H. The interaction of highly active uncouplers with mitochondria. *Biochim. Biophys. Acta* **1981**, *639* (3), 225–242. https://doi.org/10.1016/0304-4173(81)90011-2.

(12) Hards, K.; McMillan, D. G. G.; Schurig-Briccio, L. A.; Gennis, R. B.; Lill, H.; Bald, D.; Cook, G. M. Ionophoric effects of the antitubercular drug bedaquiline. *PNAS* **2018**, *115* (28), 7326–7331. https://doi.org/10.1073/pnas.1803723115.

(13) Darby, C. M.; Ingólfsson, H. I.; Jiang, X.; Shen, C.; Sun, M.; Zhao, N.; Burns, K.; Liu, G.; Ehrt, S.; Warren, J. D.; et al. Whole cell screen for inhibitors of pH homeostasis in *Mycobacterium tuberculosis*. *PLOS ONE* **2013**, *8* (7), e68942. https://doi.org/10.1371/journal.pone.0068942.

(14) Nicholls, D. G.; Ferguson, S. J. Ion transport across energy-conserving membranes. In *Bioenergetics (Fourth Edition)*; Nicholls, D. G., Ferguson, S. J., Eds.; Academic Press: Boston, 2013; pp 13–25. https://doi.org/10.1016/B978-0-12-388425-1.00002-6.

(15) Stillwell, W. Membrane transport. In *An Introduction to Biological Membranes (Second Edition)*; Stillwell, W., Ed.; Elsevier, 2016; pp 423–451. https://doi.org/10.1016/B978-0-444-63772-7.00019-1.

(16) Stein, W. D.; Litman, T. Ion channels across cell membranes. In *Channels, Carriers, and Pumps (Second Edition)*; Stein, W. D., Litman, T., Eds.; Elsevier: London, 2015; pp 81–130. https://doi.org/10.1016/B978-0-12-416579-3.00003-4.

(17) Bhagavan, N. V. Electron transport and oxidative phosphorylation. In *Medical Biochemistry (Fourth Edition)*; Bhagavan, N. V., Ed.; Academic Press: San Diego, 2002; pp 247–274. https://doi.org/10.1016/B978-012095440-7/50016-0.

(18) Terada, H. Uncouplers of oxidative phosphorylation. *Environ. Health Persp.* **1990**, *87*, 213–218. https://doi.org/10.1289/ehp.908721 3.

(19) Finkelstein, A. Weak-acid uncouplers of oxidative phosphorylation: mechanism of action on thin lipid membranes. *BBA-Bioenergetics* **1970**, *205* (1), 1–6. https://doi.org/10.1016/0005-2728(70)90055-1.

(20) Hanstein, W. G. Uncoupling of oxidative phosphorylation. *Biochim. Biophys. Acta* **1976**, *456* (2), 129–148. https://doi.org/10.1016/0304-4173(76)90010-0.

(21) Neumcke, B.; Bamberg, E. The action of uncouplers on lipid bilayer membranes. In *Lipid bilayers and biological membranes: dynamic properties*; Dekker: New York, 1975; Vol. 3, pp 215–253.

(22) Kasianowicz, J.; Benz, R.; McLaughlin, S. The kinetic mechanism by which CCCP (carbonyl cyanide m-chlorophenylhydrazone) transports protons across membranes. *J. Membrane Biol.* **1984**, *82* (2), 179–190. https://doi.org/10.1007/BF01868942.

(23) McLaughlin, S. G.; Dilger, J. P. Transport of protons across membranes by weak acids. *Physiol. Rev.* **1980**, *60* (3), 825–863. https://doi.org/10.1152/physrev.1980.60.3.825.

(24) Brody, T. M. The uncoupling of oxidative phosphorylation as a mechanism of drug action. *Pharmacol. Rev.* **1955**, *7* (3), 335–363.

(25) Voskuil, M. I.; Covey, C. R.; Walter, N. D. Antibiotic lethality and membrane bioenergetics. In *Advances in Microbial Physiology*; Poole, R. K., Ed.; Academic Press, 2018; Vol. 73, pp 77–122. https://doi.org/10.1016/bs.ampbs.2018.06.002.

(26) Meyer-Rosberg, K.; Scott, D. R.; Rex, D.; Melchers, K.; Sachs, G. The effect of environmental pH on the proton motive force of *Helicobacter pylori*. *Gastroenterology* **1996**, *111* (4), 886–900. https://doi.org/10.1016/S0016-5085(96)70056-2.

(27) Salfinger, M.; Heifets, L. B. Determination of pyrazinamide MICs for *Mycobacterium tuberculosis* at different pHs by the radiometric method. *Antimicrob. Agents Ch.* **1988**, *32* (7), 1002–1004. https://doi.org/10.1128/AAC.32.7.1002.

(28) Konno, K.; Feldmann, F. M.; McDermott, W. Pyrazinamide susceptibility and amidase activity of tubercle bacilli. *Am. Rev. Respir. Dis.* **1967**, *95* (3), 461–469. https://doi.org/10.1164/arrd.1967.95.3.461.

(29) Boshoff, H. I. M.; Mizrahi, V. Expression of *Mycobacterium smegmatis* pyrazinamidase in *Mycobacterium tuberculosis* confers hypersensitivity to pyrazinamide and related amides. *J. Bacteriol.* **2000**, *182* (19), 5479–5485. https://doi.org/10.1128/JB.182.19.5479-5485.2000.

(30) Scorpio, A.; Zhang, Y. Mutations in *pncA*, a gene encoding pyrazinamidase/nicotinamidase, cause resistance to the antituberculous drug pyrazinamide in tubercle bacillus. *Nat. Med.* **1996**, *2* (6), 662. https://doi.org/10.1038/nm0696-662.

(31) French, J. B.; Cen, Y.; Vrablik, T. L.; Xu, P.; Allen, E.; Hanna-Rose, W.; Sauve, A. A. Characterization of nicotinamidases: steady state kinetic parameters, classwide inhibition by nicotinaldehydes, and catalytic mechanism. *Biochemistry* **2010**, *49* (49), 10421–10439. https://doi.org/10.1021/bi101251 8.

(32) Peters, B. J.; Groninger, A. S.; Fontes, F. L.; Crick, D. C.; Crans, D. C. Differences in interactions of benzoic acid and benzoate with interfaces. *Langmuir* **2016**, *32* (37), 9451–9459. https://doi.org/10.1021/acs.langmuir.6b02073.

(33) Gutknecht, J. Salicylates and proton transport through lipid bilayer membranes: A model for salicylate-induced uncoupling and swelling in mitochondria. *J. Membrane Biol.* **1990**, *115* (3), 253–260. https://doi.org/10.1007/BF01868640.

Chapter 3

The acid-base equilibrium of pyrazinoic acid drives the pH dependence of pyrazinamide-induced *Mycobacterium tuberculosis* growth inhibition

Pyrazinamide (PZA) is an essential component of the antibiotic regimen used to treat *Mycobacterium tuberculosis*, the etiological cause of tuberculosis (TB), infections. The addition of PZA to the first-line treatment of TB led to a decrease in the average time of treatment from 9-12 months to 6.[1,2] PZA also synergizes with second-line antibiotics *in vivo* and has been part of most of the current regimens against multi- and extensively-drug resistant TB.[3,4] PZA is a pro-drug, requiring cytosolic activation by a nicotinamidase (PncA, encoded by *Rv2043c*).[5–7] Thus, the deamidation of PZA, specifically forming the deprotonated, negatively charged pyrazinoate (POA_C),[8] is required for activity.[6,7] However, once POA_C forms in the bacterial cytosol, it rapidly establishes an acid-base equilibrium with the protonated, neutral pyrazinoic acid (POA_N). Thus, the total pyrazinoic acid (POA_T) in the system equals the sum of POA_C and POA_N, with the relative concentrations of the acid and its conjugate base being pH-dependent. The relative concentration of each form in solution are calculated as indicated in Figure 3.1.

While several molecular targets have been proposed in *M. tuberculosis*,[9–13] the mode of action of PZA remains controversial more than 65 years after the discovery of PZA's anti-tubercle activity. Similarly, the mechanism behind PZA's synergism is unknown, thwarting the ability to replicate or improve on PZA's impact on the time of treatment. A third unexplained characteristic of PZA is its pH-dependent activity *in vitro*. When exposed to PZA in neutral pH environments, *M. tuberculosis* is modestly tolerant to PZA, with high doses of PZA required to produce an effect.[14] However, when the pH of the culture medium is lowered, the concentration of PZA

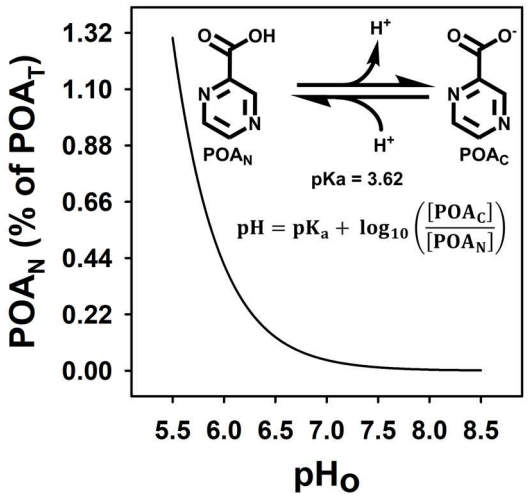

Figure 3.1 – Effect of pH on the relative amount of POA_N. The percentage of POA_N was calculated using the Henderson-Hasselbalch equation (HHE), assuming a pK_a of 3.62 (determined using Chemicalize, www.chemicalize.com).

required to produce the same effect is progressively lower.[15] A previous report suggested that the activity of PZA can be predicted by the Henderson-Hasselbalch equation (HHE, Figure 3.1), based on results showing PZA's pH-dependent activity in acidic environments.[16] Zhang and Mitchison argued that the ratio of POA_C to POA_N correlates with the minimum inhibitory concentrations (MIC) reported by Salfinger.[15,16] However, the distinction between POA_C and POA_N is seldom considered in studies of PZA.

Of the multiple potential targets for POA_T (or PZA without hydrolysis) proposed in recent literature, none provides a simple explanation for the pH-dependent activity of PZA.[9–13] The proposed targets are all cytosolic enzymes or enzymatic activities. For an enzymatic activity to be affected by environmental pH, the likely explanation is that PZA uptake is altered. However, two separate studies agree that PZA uptake in mycobacteria is independent of environmental pH, ruling out this possibility.[17,18] Furthermore, it has been suggested PZA (or its active form) may target the pH stress mechanism triggered at low extracellular pH;[19] however, this hypothesis does not explain the ability to predict the efficacy of PZA using the HHE. The observations that formation of a form of POA_T is required to activate PZA and that its effect is altered in a predictable manner by

the pH of the environment, suggest that either the bacteria do not maintain cytoplasmic pH homeostasis or that POA_T is exposed to the external environment prior to action. The loss of pH homeostatic control could explain the acidification of the cytoplasm proposed elsewhere.[16]

The exposure of one or both forms of POA_T to the extracellular environment is supported by previous observations of POA_T in the supernatant of cells treated with PZA.[18] Zhang and Mitchison suggest POA_C leaves the cell (either by efflux or diffusion) and, given the lower pH of the environment relative to the cytoplasm, the acid-base equilibrium of POA_T shifts towards POA_N. They propose POA_N then enters the cell through diffusion or an active mechanism, causing acidification of the cytoplasm.[16] Nevertheless, cytoplasmic acidification has not previously been shown to occur in live cells[14,18] and the only evidence for such a phenomenon comes from treatment of membrane vesicles with POA_T.[20] Furthermore, the dependence of PZA's activity on pH has been questioned, with reports that both overexpression of PncA and lower temperatures (28 °C versus 37 °C) lead to PZA susceptibility in neutral environments.[14,21]

Hypothetically, the existence of a pH-dependent activity could be linked to the mechanism of action of PZA and/or to the mechanism of synergism with other anti-tubercle drugs. Therefore, the present work was carried out to investigate the mycobacterial pH homeostasis changes with environmental pH and if the pH homeostasis of *M. tuberculosis* is affected during treatment with PZA.

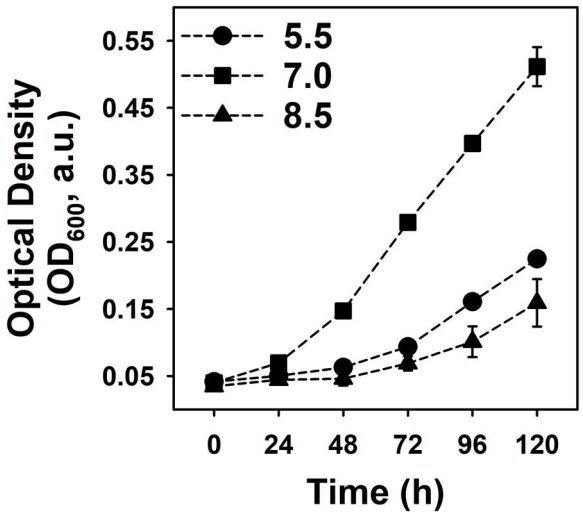

Figure 3.2 – Effect of environmental pH on *M. tuberculosis* growth. *M. tuberculosis* H37Ra cells were grown in supplemented 7H9 broth, harvested and re-suspended in supplemented 7H9 broth at the indicated pH. Cultures incubated at 37 °C for 5 days and optical density at 600 nm was determined every 24 hours. Values shown are the averages of three independent replicates, with standard deviation shown as error bars. Dashed lines between data points were added for ease of visualization.

Results

Mycobacterium tuberculosis H37Ra growth in different pH environments.

Supplemented 7H9 broth (pH 5.5, 7.0 or 8.5) was inoculated with bacilli and growth in culture was followed over a period of five days. The results are shown in Figure 3.2. The cells at the extreme pH values tested (5.5 and 8.5) were still able to replicate, although at a much slower rate than at neutral pH, suggesting that *M. tuberculosis* H37Ra maintains viability despite the stress induced by the two extremes of environmental pH.

Dependence of pyrazinoic acid-induced growth inhibition of *Mycobacterium tuberculosis* H37Ra on pH.

The results presented in Figure 3.3 show the pH-dependent growth inhibition of *M. tuberculosis* H37Ra caused by exposure to POA_T over a range of environmental pH values (6.4-7.3), which corresponds to the pH range likely to be encountered in the host organism.[22–27]

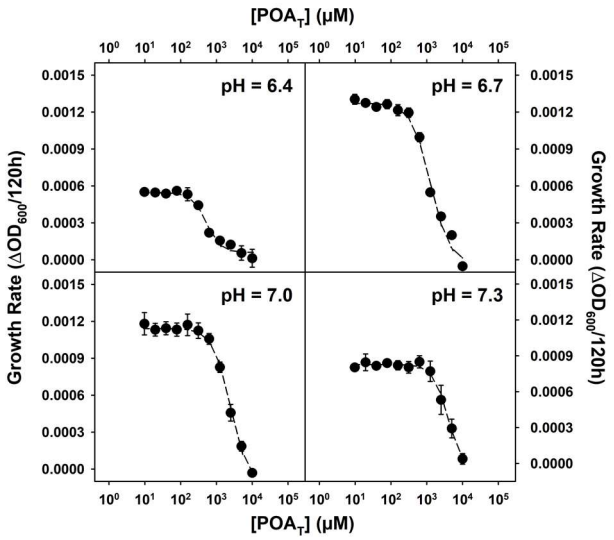

Figure 3.3 – Effect of POA_T on *M. tuberculosis* H37Ra growth. *M. tuberculosis* H37Ra was grown in supplemented 7H9 broth containing the indicated POA_T concentrations at 37 °C. The OD_{600} was measured every 24 hours for 5 days, with the growth rate at day 5 shown. Growth rate are expressed in terms of change of OD_{600} divided by the time of exposure. The results shown are the averages of four independent replicates, with standard deviation shown as the error bars. The regression line was calculated using a non-linear 4 parameter E_{max} model.

The concentrations required to inhibit 50% growth (GIC_{50}) were calculated from the growth rates observed at 120 hours of incubation with POA_T.

While the growth rates near neutrality (pH 6.7-7.0) are similar, the effect of pH on bacterial growth is evident in *M. tuberculosis* at the extremes of the environmental pH values tested (6.4 and 7.3, with a 2-fold decrease from the growth rates observed in neutral pH environments). The use of kinetic growth measurements allows for unconfounded determination of the GIC_{50} for each pH, represented graphically in Figure 3.4. The GIC_{50} values linearly correlate with the environmental pH ($R^2 = 0.97$).

Mycobacterium tuberculosis H37Ra pH homeostasis.

To determine if *M. tuberculosis* maintains a constant cytoplasmic pH over a range of environmental pH values, a constant ionic strength buffer (MMA) containing 2',7'-bis-(2-carboxyethyl)-5-(and-6)-carboxyfluorescein acetoxymethyl ester (BCECF-AM) was inoculated

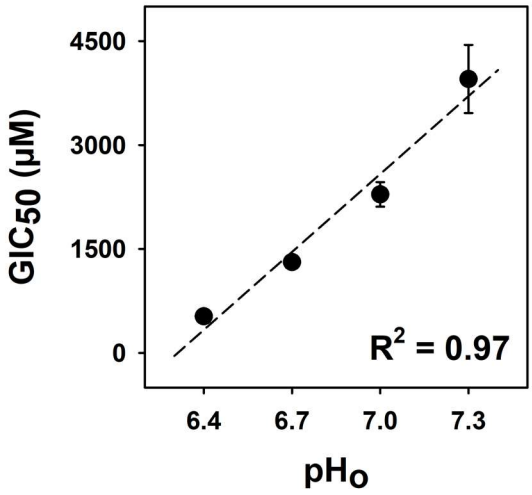

Figure 3.4 – POA_T concentration responsible for 50% growth inhibition. The GIC_{50} values extracted from the E_{max} model regression are presented at each external pH tested (pH_o). The error bars of each point correspond to the standard error calculated during the regression. The calculated linear regression and corresponding R^2 value are shown.

with bacilli. The results are presented in Figure 3.5. The fluorescence ratio 485/440 is dependent on the internal pH of cells when BCECF-AM is used; BCECF-AM is not fluorescent, but upon exposure to the cytoplasm, the acetoxymethyl ester modification is hydrolyzed by non-specific esterases. The resulting 2',7'-bis-(2-carboxyethyl)-5-(and-6)-carboxyfluorescein (BCECF) fluoresces in a pH-dependent manner.[28] In acidic medium (pH 5.5-7.0), the fluorescence ratio is stable, indicating the dye-loaded cells maintain a constant internal pH over that range. As the pH of the assay buffer becomes increasingly alkaline (pH 7.6-8.5), the fluorescence ratio increases linearly with the external pH, suggesting *M. tuberculosis* H37Ra no longer controls the cytoplasmic pH and, therefore, the pH homeostasis seen in acidic environments is lost as the external pH increases. The internal pH of *M. tuberculosis* H37Ra was estimated as the intercept of the two linear trends, at pH = 7.3, which is consistent with the measurements described by Rao and colleagues in *Mycobacterium smegmatis* and *Mycobacterium bovis* BCG using a different methodology than the one described above.[29]

Pyrazinoic acid effect on proton motive force of *Mycobacterium tuberculosis* H37Ra.

The pH-dependent effect of POA_T has been associated with its ability to cause acidification of the cytoplasm of *M. tuberculosis*, despite the unsuccessful attempts to demonstrate such an event.[14,18] A property of semi-permeable membranes, proton motive force (PMF) is a measure of the potential energy stored in the form of the electric potential ($\Delta\Psi$) and the proton gradient (ΔpH, internal pH minus environmental pH) across the membrane. To cause a disruption of PMF, one (or both) of these components must be affected. The effect of a range of concentrations of POA_T on both the internal pH and the $\Delta\Psi$ of *M. tuberculosis* H37Ra was evaluated using fluorescence ratiometric techniques to test if POA_T has an effect on PMF.

The results in Figure 3.6 show the effect of POA_T on the pH differential across mycobacterial membrane (ΔpH) when bacilli were exposed to different external pH values. The percentage of ΔpH remaining was estimated taking the BCECF's 485/440 ratio after 30 minutes incubation with POA_T for each replicate and dividing the ratio by the ΔpH (the estimated internal pH minus the pH of the MMA buffer). The average of the non-treated replicates (dimethyl sulfoxide, DMSO, control) was considered 0% dissipation or 100% remaining ΔpH. The results

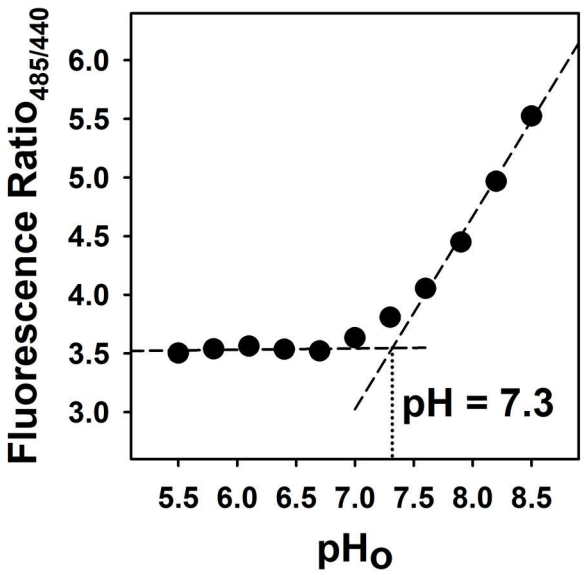

Figure 3.5 – Effect of environmental pH on cytoplasmic pH in *M. tuberculosis* H37Ra. *M. tuberculosis* H37Ra cells were suspended in MMA buffer at the indicated external pH (pH_o). BCECF-AM was added and fluorescence emission 540 nm was recorded at 37 °C, with excitation at both 440 and 485 nm. The results shown are averages of four replicates. Error bars indicate standard deviation. The dashed lines correspond to the linear regressions between pH 5.5-6.7 and 7.6 8.5, with the intercept of the lines corresponding to the estimated internal pH (pH = 7.3).

indicate POA_T causes the acidification of the cytoplasm in a concentration-dependent manner. The dissipation of the pH gradient is more obvious when the pH of the MMA buffer is lower.

The acidification of the cytoplasm by POA_T alone may lead to disruption of PMF, but it was unclear if POA_T also affected the $\Delta\Psi$ of *M. tuberculosis* H37Ra, as an increase in $\Delta\Psi$ can counteract the decrease of cytoplasmic pH to maintain PMF.[30] A $\Delta\Psi$-dependent fluorescent dye, $DiOC_2(3)$, was used to determine if POA_T also caused dissipation of mycobacterial $\Delta\Psi$ under the same conditions used to observe the cytoplasmic acidification. Figure 3.7 shows the change of $\Delta\Psi$ in *M. tuberculosis* H37Ra exposed to a range of POA_T concentrations, at different MMA buffer pH values, after incubation with POA_T for 30 minutes. The percentage of $\Delta\Psi$ remaining shown in Figure 3.7 was calculated based on the fluorescence ratio of $DiOC_2(3)$ at 590/540, with 100% corresponding to the ratio of the buffer alone subtracted from the ratio of the untreated control (DMSO only). As seen in both the growth inhibition and the internal pH dissipation experiments,

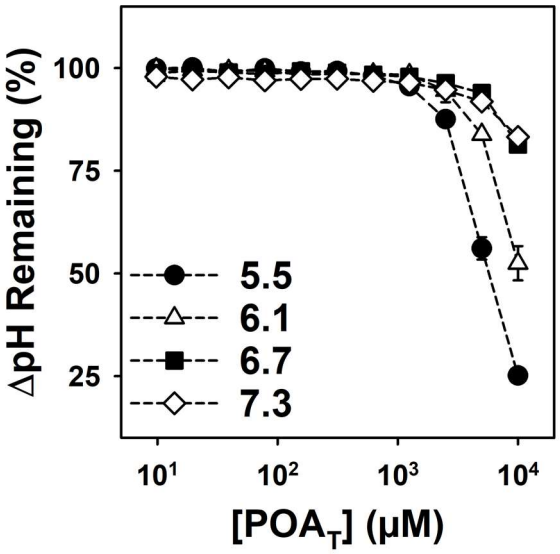

Figure 3.6 – Effect of POA_T concentration on ΔpH over a range of external pH values. *M. tuberculosis* H37Ra cells were incubated in MMA buffer containing 0.5 μM BCECF-AM at the indicated pH and concentration of POA_T for 30 minutes. Fluorescence was measured at 37 °C with excitation at 440 and 485 nm and emission recorded at 540 nm with four replicates for each concentration of POA_T. The percentage of ΔpH remaining was estimated with the BCECF's 485/440 ratio after 30 minutes of incubation with POA_T divided by the estimated ΔpH (using pH 7.4 as the cytoplasmic pH); the untreated (DMSO control) was considered 100%. Dashed lines between data points were added to facilitate visualization of trends.

the membrane potential disruption by POA_T is dependent on the pH of the MMA buffer and the concentration of POA_T. The disruption is more evident when the environmental pH is 5.5 and it seems to plateau at around 25% of the membrane potential. The disruption is progressively less obvious as the pH of the MMA buffer increases, which is consistent with the previous observations for growth inhibition and cytoplasmic acidification. Thus, there is a clear collapse of both components of PMF that correlates with the pH of the culture medium.

Discussion

Mycobacterium tuberculosis H37Ra growth in different pH environments.

The present work aims to clarify the pH-dependent activity of PZA, with two hypotheses considered. Either *M. tuberculosis* cannot maintain pH homeostasis in acidic environments, leading to acidification of the bacillary internal pH and to a change in the acid-base equilibrium of

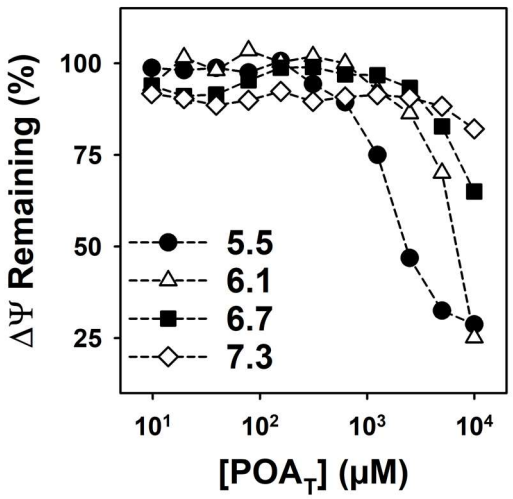

Figure 3.7 – Effect of POA_T concentration on ΔΨ over a range of external pH values. *M. tuberculosis* H37Ra cells were incubated in MMA buffer at the desired external pH, in the presence of 2 μM $DiOC_2(3)$ and a range of concentrations of POA_T. Fluorescence was measured with excitation at 440 nm and emission at 540 and 590 nm, at 37 °C. The fluorescence ratio 590/540 was converted to percentage of the difference between no treatment with POA_T (DMSO control) and no cells (buffer only control). The results shown are the average of four independent replicates. Error bars indicate standard deviation and dashed lines between data points were added to ease visualization of trends.

POA_T trapped inside the mycobacterial cells, or POA_T is exposed to the extracellular milieu and undergoes further conversion to its active form. The initial approach to understand the pH-dependent activity of PZA entailed the evaluation of the viability of *M. tuberculosis* H37Ra in acidic, neutral and alkaline environments (Figure 3.2). The results show a short lag phase in the neutral environment followed by consistent replication, while in both acidic and alkaline environments longer lag phases (~48h, compared to less than 24h at pH 7.0) and slower growth rates were observed. The data is supported by previous reports of mycobacterial growth in acidic environments.[31] The adaptation of *M. tuberculosis* to acidic environments and the mycobacterial metabolic changes responsible for the adaptation have been described elsewhere.[31–33] However, results indicate *M. tuberculosis* H37Ra is still viable in acidic and alkaline environments, even if pH stress causes a metabolic slowdown, suggesting mycobacteria possess mechanisms to endure both acid and alkaline environments. Additionally, the similar growth response of *M. tuberculosis* to the extreme environmental pH values tested (pH 5.5 and 8.5) suggests the pH-dependent activity

of PZA (and/or POA_T) is independent of stress caused by the environmental pH. The efficacy of PZA should increase at higher pH environments if the activity of the antibiotic was, simply, linked to mycobacterial stress. However, this increase has not been reported previously nor observed in the work presented here.

The results shown in Figure 3.2 also led to changes in subsequent experimental design. The longer lag phase at pH extremes indicated *M. tuberculosis* undergoes a metabolic adaptation to different pH environments and such changes, coupled with antibiotic treatment, could obfuscate or amplify the drug effect. Thus, cultures intended for drug susceptibility assays were incubated at the final pH of the assay until the bacterial culture was in exponential growth phase, assuring metabolic pre-adaptation to the pH of the assay. Furthermore, mycobacterial drug susceptibility assays are often conducted with endpoint measurements, comparing the drug activity after a prolonged incubation with the compound of interest. However, given the different growth rates in different pH environments, comparisons of absolute growth can confound growth rate and drug efficacy. Therefore, growth rates, as previously reported,[34] were determined in order to minimize discrepancy. Moreover, utilizing growth rate inhibition, drug susceptibility can be determined with significantly shorter incubation times (5 days, compared to the usual 10 or more days in resazurin-based microtiter plate assays). The methodology used also ensures the surveillance of inhibitor stability throughout the assay and the ability to observe time-dependent effects, as recently reported for fluorinated anthranilate-induced inhibition of *M. tuberculosis* growth.[35]

Dependence of pyrazinoic acid-induced growth inhibition of *Mycobacterium tuberculosis* H37Ra on pH.

The growth inhibition of *M. tuberculosis* H37Ra by POA_T is shown in Figure 3.3, with the calculated GIC_{50} values plotted in Figure 3.4, demonstrating the pH-dependent effect of POA_T is detectable even over small increments of environmental pH. These observations are supported by previous reports of POA_T activity dependence on pH.[14,36] The use of kinetic growth measurements, as opposed to the use of endpoint growth measurements as an evaluation of drug effect, has the benefit of minimizing the impact of the slower growth seen at pH 6.4 and 7.3 on the determination of drug toxicity. Thus, it is possible to determine the GIC_{50} at each pH (Figure 3.4).

The external pH values used were chosen so that the proton concentration at each point differs from the next pH tested by a factor of 2. The GIC_{50} observed doubles at each increase of pH increment, so the efficacy of POA_T in *M. tuberculosis* decreases linearly ($R^2 = 0.97$, Figure 3.4) as the proton concentration of the medium decreases. As such, POA_T exhibits around 8-fold greater potency at pH 6.4 than at pH 7.3 (530 μM versus 4000 μM). The results are consistent with the increase in the relative amount of POA_N in the extracellular milieu, which, using the HHE, is 8-fold more abundant at pH 6.4 than at pH 7.3. The calculated POA_N GIC_{50} is ~950 nM at all of the pH values tested. Thus, the active form of PZA appears to be POA_N rather than POA_C.

As indicated earlier, formation of POA_N is dependent on pK_a, providing an explanation for the multiple reports that lower temperatures enhance PZA's activity.[21,37] Hertog and colleagues reported that PZA has increased efficacy in neutral pH environments at 28 °C (compared to cultures treated with PZA at 37 °C), with exception of PncA-linked resistant strains where no effect was detected at either temperature;[21] Coleman and colleagues made similar observations, with a wider range of temperatures (16-37 °C).[37] Hertog's report on PncA mutants demonstrated

that PZA deamidation is required and the temperature-dependent effect linked to POA_T. Given that pK_a increases as temperature decreases,[38] the relative amount of POA_N in solution at 37 °C is lower than at temperatures below 37 °C. Similarly, reports of increased PZA susceptibility of *M. tuberculosis* at neutral pH when PncA is overexpressed[14] can be explained by an increase in the amount of POA_T (and, consequentially, POA_N) in solution, supporting the hypothesis that PZA's activity is dependent on POA_N.

***Mycobacterium tuberculosis* H37Ra pH homeostasis.**

The viability of *M. tuberculosis* H37Ra in acidic and alkaline environments is insufficient to assess the ability of mycobacteria to maintain internal pH homeostasis during exposure to acidic and alkaline environments. The internal pH of *M. tuberculosis* H37Ra at a range of external pH values was determined using the pH-sensitive fluorescence of BCECF, as shown in Figure 3.5. Consistent with earlier reports,[29,39] *M. tuberculosis* H37Ra maintains a stable internal pH when exposed to external pH values ranging between 5.5 and 7.0. The work of Rao and colleagues with *M. smegmatis* and *M. bovis* BCG shows the increase of the pH gradient across the membrane (ΔpH), as the external pH decreases, indicating a stable internal pH, also results in a decrease of the electric membrane potential (ΔΨ). Thus, the bacilli maintained a stable proton motive force (PMF) in addition to a stable internal pH.[29] The equilibration of ΔpH and ΔΨ to maintain stable PMF has been observed in other bacterial species as well.[30,40] The increase in internal pH as the environmental alkalinity increases above pH 7.0 (Figure 3.5), while newly observed in mycobacteria, has previously been described in other bacterial species.[41–45]

The current models for TB pathogenesis suggest that *M. tuberculosis* bacilli encounter a variety of pH environments, ranging from 5.0 to 7.6,[22–27] a range over which *M. tuberculosis* is

able to maintain a stable cytoplasmic pH. Thus, the ability of *M. tuberculosis* to survive the immunological responses of the host may be linked to the bacillus's ability to withstand acidic environments, as previously suggested by Vandal and colleagues,[39] and mycobacterial pH homeostasis may offer a potential effective drug target as proposed elsewhere.[46–48] Furthermore, if stress was related to PZA's activity, as previously suggested,[19] an increase of antibiotic efficacy might be expected in the higher pH environments tested, which does not occur. Hence, acidification of the cytosol of *M. tuberculosis* in the presence of POA_T is, likely, attributable to drug activity alone.

Pyrazinoic acid effect on proton motive force of *Mycobacterium tuberculosis* H37Ra.

While it was previously suggested POA_T causes acidification of the bacillary cytoplasm,[16] attempts to observe the phenomenon in live cells showed no change in the mycobacterial internal pH.[14,18] Still, POA_T was shown to cause a change in $\Delta\Psi$ in a concentration-dependent manner[49] and to dissipate PMF in mycobacterial membrane vesicles, through the acidification of the vesicular core.[20] The compensation mechanism between $\Delta\Psi$ and the internal pH to maintain PMF across the membrane has been widely observed in bacteria, including in *M. bovis* BCG and *M. smegmatis*.[29,30,40]

Here, the effect of POA_T on the internal pH of live mycobacterial bacilli was investigated using a constant ionic strength buffer, a common practice in classic bioenergetics studies, whereas previous attempts used traditional supplemented culture media.[14,18,49] The use of supplemented media may lead to interference caused by the components of the medium or the supplements, such as albumin. Previous reports indicated albumin adsorbs POA_T (up to 75% with 10% albumin in the medium), as well as, fluorescent dyes similar to the ones used in the present work.[36,50]

Albumin, however, does not adsorb PZA.[36] Thus, a constant ionic strength buffer (supplemented by glucose and KCl) was used as the assay medium to estimate the impact of POA_T in the pH environment of the cytoplasm, following previously published recommendations.[38] The use of MMA buffer overcame two potential sources of interference: the buffer was designed to contain exclusively Good's buffers, avoiding the use of buffers (such as phosphate or citrate) that could penetrate the cytoplasmic membrane and buffer cytoplasmic pH changes caused by POA_T. Additionally, the MMA buffer maintains constant ionic strength (100 mM) within the range of pH values used throughout the work presented here (5.5-8.5), preventing variations in ionic strength that could obfuscate the effect of POA_T on the mycobacterial PMF homeostasis. Therefore, the use of MMA buffer was instrumental to observe the disruption of PMF in *M. tuberculosis*.

The percentage of ΔpH remaining after dosage with POA_T in different pH environments was determined and the results plotted in Figure 3.6. The decrease in internal pH shown is dependent on the concentration of POA_T and on the environmental pH, with the highest drug efficacy observed at the lowest pH tested (pH 5.5). The dissipation of ΔpH by POA_T is supported by previous reports on mycobacterial membrane vesicles[20] and the pH-dependent effect is consistent with the observations of the growth inhibition assays (Figure 3.3 and Figure 3.4), suggesting that both phenomena stem from a similar mechanism. The cytoplasmic acidification was independent of exposure to acidic environment (Figure 3.5) and, therefore, the pH-dependent effect is likely caused by POA_T exposure to the external environment. Hence, the observations suggest POA_T, after PZA's deamidation, leaves the cell via an unknown mechanism, which is supported by previous observations.[18]

The percentage of $\Delta\Psi$ remaining after treatment with POA_T in different pH environments (Figure 3.7) was determined using the fluorescence dye $DiOC_2(3)$, which exhibited a similar

behavior to the assay on ΔpH. The dissipation of both ΔpH and ΔΨ results in the collapse of PMF upon administration of POA_T. The ΔΨ dissipation is supported by observations reported elsewhere.[49] Previous work showed that, in low pH environments (pH 5.0-5.5), the activity of POA_T is comparable to the effect of dinitrophenol and benzoic acid, two compounds known to dissipate PMF.[49] The pH-dependence on the dissipation of both ΔpH (seen in Figure 3.6) and ΔΨ (shown in Figure 3.7) suggests that POA_N may be the active form of PZA and that the phenomena is determined by pK_a and the acidity of the medium. The results indicate that POA_T seems to cause a maximum of 75% ΔΨ dissipation, implied by the apparent plateau at 25% of remaining ΔΨ (Figure 3.7). The observation suggests the cytoplasmic membrane maintains structural integrity in the presence of POA_T, resulting in the containment of charged molecules other than protons, which also contribute to ΔΨ within the cytoplasm. Loss of membrane integrity would cause the complete dissipation of ΔΨ.

At the concentrations that result in 50% growth inhibition (Figure 3.4) less than 50% disruption of PMF was observed (Figure 3.6 and Figure 3.7). However, POA_T growth inhibition assays were conducted over 5 days, whereas the incubations to estimate PMF disruption were only 30 minutes long. Hence, the different incubation times are believed to reconcile the difference in growth inhibition and PMF disruption. Similarly, Lu and colleagues observed that the presence of POA_T in their mycobacterial membrane vesicle model caused PMF disruption within 20 minutes of incubation; the same report shows that POA_T treatment induces a time-dependent decrease of ATP level in *M. bovis* BCG with 83% reduction in ATP levels after incubation with POA_T for 6 days. Lu concluded that the two effects were connected and that POA_T led to the depletion of ATP through disruption of PMF.[20] The observations in the present work suggest a similar cascade effect and the growth inhibition would, therefore, be an expression of the secondary effects of POA_T.

The hypothesis that PZA targets PMF through the acidification of the cytoplasm provides an elegant explanation for previous observations, such as the slow decrease in ATP levels upon dosage with POA_T or the increased effect of PZA in non-replicating bacilli.[20,36] However, the results shown above cannot rule out a contribution by pH-induced stress in growth inhibition or POA_N acting as an inhibitor of an enzyme inside mycobacterial bacilli.

The interplay between the two components of PMF, $\Delta\Psi$ and ΔpH, was reported before in mycobacteria and other genera.[29,30,40] Bacteria use PMF to power a variety of processes, including proton-dependent efflux and oxidative phosphorylation; disruption of PMF has been associated with loss of function in these processes, as expected.[51–53] Classical PMF inhibitors like nigericin and CCCP (carbonyl cyanide-*m*-chlorophenylhydrazone), act as chemical uncouplers, so called for their ability to uncouple oxidative processes from phosphorylation in ATP synthesis. The activity of uncouplers relies on the compound's ability to transport ions, usually protons, across the cytosolic membrane and, as such, through equilibration between the cytoplasmic environment and the environment the cells are exposed to. The models for the mode of action of these compounds assume passive diffusion across the membrane or an active mechanism to facilitate the transport;[54] the uncertainty surrounding the exact mechanism is in line with recent controversy regarding drug uptake.[55–58]

In the case of uncouplers that only shuttle protons, both ΔpH and $\Delta\Psi$ are disrupted and the cytoplasmic pH equilibrates with the pH of the external medium. The activity of these proton shuttles, or protonophores, relies on the distinct acid-base equilibria within and outside the cell; the protonated (neutral) species of the protonophore serves as the proton carrier and releases the proton inside the cell, with the charged form (deprotonated) of the protonophore free to cross the membrane once more and be protonated again. Thus, protonophores show pH-dependent activity,

with their cell toxicity increasing as the external pH decreases, in a manner that correlates with the concentration of the neutral species of the compounds.[54]

Conclusions

Succinctly, the acid-base equilibrium of pyrazinoic acid drives the pH dependence of pyrazinamide-induced *M. tuberculosis* growth inhibition, which is dependent on the concentration of POA_N. Upon intracellular conversion from PZA, the POA_C in the cytoplasm rapidly undergoes acid-base equilibration with POA_N. POA_T then moves to the extracellular medium via an unknown mechanism. Once outside of the mycobacterial cell, POA_T is exposed to the lower pH of the medium, shifting the equilibrium between POA_C and POA_N towards POA_N as predicted by the HHE. As the pH of the medium is decreased, and the ΔpH across the membrane increases, the equilibrium shift is amplified. This implies that the POA_N in the medium may act as a protonophore, carrying protons through the semi-permeable cytoplasmic membrane and, on exposure to the higher pH of the cytosol, releasing protons within the cell. The resulting cytoplasmic acidification causes disruption of both ΔpH and $\Delta\Psi$, collapsing PMF, which, in turn, leads to inhibition of PMF-dependent processes and, ultimately, growth inhibition.

Materials and Methods

All reagents were purchased from Sigma-Aldrich except when noted. Middlebrook 7H9 broth was purchased from Becton Dickinson and albumin from GoldBio. The fluorescent dyes used were purchased from Invitrogen. All reagents were of, at least, reagent grade and used without further purification.

***Mycobacterium tuberculosis* H37Ra culture methods**.

M. tuberculosis H37Ra cultures were grown under standard conditions. Frozen glycerol stocks of *M. tuberculosis* H37Ra were thawed and used to inoculate Middlebrook 7H9 medium, supplemented with oleic acid-albumin-dextrose (OAD, 10% v/v), 0.1% v/v tyloxapol and 0.2% w/v casamino acids (supplemented 7H9 broth). If necessary, the pH of the medium was adjusted with sodium hydroxide or hydrogen chloride. Culture flasks were incubated at 37°C with constant agitation. Cells were harvested at an optical density at 600 nm (OD_{600}) between 0.6-0.8 and further processed according to the requirements of each experiment.

***Mycobacterium tuberculosis* H37Ra grown in acidic and alkaline environments.**

To determine the ability of *M. tuberculosis* H37Ra cells to replicate under acidic or alkaline environments, cells were grown in supplemented 7H9 broth without adjustment of pH. The culture was allowed to reach an OD_{600} within the range 0.6-0.8, upon which cells were harvested, centrifuged for 15 minutes using a Beckman CS-6R centrifuge at 1500 x g. The cells were washed with fresh medium at the desired pH (5.5, 7.0 or 8.5) and resuspended to a final OD_{600} of 0.05 in clear glass tubes (culture volume was 2 mL, with a head space of 8 mL of air). Cultures were incubated at 37°C with constant rocking. The OD_{600} was recorded every 24 hours for 5 days using a Beckman DU 640 spectrophotometer; cultures were aerated every day after OD_{600} measurements.

pH-dependent growth inhibition of *Mycobacterium tuberculosis* H37Ra by pyrazinoic acid.

The pH-dependent inhibitory effect of POA_T on the growth of *M. tuberculosis* cells was determined using the growth inhibitory assay developed by Gruppo and colleagues.[34] Cells of

M. tuberculosis H37Ra were grown, harvested, centrifuged using a Beckman CS-6R centrifuge at 1500 x g and washed with fresh culture medium (supplemented 7H9 broth). The pH of the culture media was adjusted with sodium hydroxide or hydrochloric acid to obtain pH values ranging from 6.4 to 7.3 in 0.3 pH unit intervals. The cells were then resuspended in the culture medium at the desired pH and incubated at 37°C with constant agitation until an OD_{600} between 0.6 and 0.8 was reached, to acclimatize the bacilli to the pH of the medium. The cultures were subsequently harvested, centrifuged as described above and washed with fresh medium at the desired pH value. The cells were resuspended to an OD_{600} of 0.1 and aliquots of 198 µL were transferred to 96-well microtiter plates containing one zirconia bead per well (diameter ~1 mm) to assist with agitation and aeration. Aliquots of 2 µL of a range of concentrations of POA_T dissolved in DMSO, including an aliquot containing no POA_T as a blank, were added to the plate and the OD_{600} was recorded using a BioRad Benchmark Plus plate reader. The OD_{600} was determined every 24h over 5 days, with the incubation between time points occurring at 37°C with constant rocking of the plates within a sealed plastic bag containing a damp paper towel to maintain humidity and prevent evaporation. Growth rates were calculated by determining the slope of the growth curve at each time point. The GIC_{50} values were calculated using a non-linear 4-parameter E_{max} regression model.

MMA buffer preparation.

The determination of pH homeostasis in *M. tuberculosis* and the analysis of the effect of POA_T on the internal pH of the cells required a buffer where ionic strength fluctuations across a wide pH range were minimized and the components of the buffer were unable to permeate the bacillary membrane. As such, a buffer containing 25mM of 2-(N-morpholino)ethanesulfonic acid

(MES), 25mM of 3-(N-morpholino)propanesulfonic acid (MOPS) and 50mM of 2-amino-2-methyl propanol (AMP) was prepared, following recommendations reported elsewhere, with a constant ionic strength of 50 mM.[38] pH was adjusted as required by addition of sodium hydroxide. Potassium chloride (50 mM, contributing to an overall ionic strength of the buffer of 100 mM) and glucose (90 mM) were added to each buffer solution to establish a potassium gradient and to energize the cells, respectively. The variation of ionic strength between the pH interval used throughout the work presented here (5.5-8.5) was calculated to never exceed 2%.

***Mycobacterium tuberculosis* H37Ra pH homeostasis assessment.**

The pH homeostasis of *M. tuberculosis* H37Ra cells was assessed following the protocol used by Ozkan and colleagues,[28] with minor modifications. *M. tuberculosis* H37Ra cells were grown to exponential phase as described above, harvested, and washed twice with MMA buffer at the pH of the assay (pH values tested ranged from 5.5 to 8.5, in 0.3 pH units increments). After centrifugation at 1500 x g on a Beckman CS-6R centrifuge, the cells were resuspended in MMA buffer at the required pH to an OD_{600} of 0.3 and aliquots of 198 µL were transferred to a black-walled microtiter plate with a zirconia bead in each well. Background fluorescence was recorded for 10 minutes (in 2 minute intervals) at 37°C on a Biotek Synergy HT with excitation at 440 nm and 485 nm and emission at 540 nm. After the background fluorescence was determined, 0.5 µM of BCECF-AM was added to the cells. Fluorescence was recorded until the 485/440 ratio was constant, which took between 30 to 60 minutes, depending on the pH of the MMA buffer.

Effect of pyrazinoic acid on the internal pH of *Mycobacterium tuberculosis* H37Ra cells.

M. tuberculosis H37Ra cultures were grown as described above, upon which the cells were harvested, washed twice with MMA buffer and resuspended in MMA buffer at the desired pH to an OD_{600} of 0.3, after which aliquots of 196 µL were transferred into a black-walled 96-well titer plates with one zirconia bead in each well. Fluorescence was recorded as described above, with 10 minute incubation without dye and 30 minute incubation with BCECF-AM; afterwards, aliquots of 2 µL of a range of concentrations of POA_T dissolved in DMSO (with DMSO without POA_T serving as a blank) were added to the cultures and fluorescence was recorded for another 30 minutes.

Effect of pyrazinoic acid on the transmembrane electric potential of *Mycobacterium tuberculosis* cells.

The transmembrane membrane potential was determined following a modification of the procedure originally reported by Novo and colleagues.[59] *M. tuberculosis* H37Ra cells were grown under the conditions detailed above and harvested by centrifugation. The pellet obtained was washed twice with MMA buffer and resuspended at the desired pH to a final OD_{600} of 0.3. Aliquots of the cultures were then transferred into black-walled 96-well microtiter plates with a zirconia bead in each well. Background fluorescence was obtained with a Biotek Synergy HT, using an excitation at 440 nm and emission at 540 and 590 nm, for 10 minutes (2-minute intervals) at 37°C. The membrane potential-dependent fluorescent dye $DiOC_2(3)$ was added to the wells at 2 µM and fluorescence was recorded for 30 minutes, at which point the 590/540 ratio was constant. A range of POA_T concentrations, dissolved in DMSO, was added to the wells and fluorescence measured for 30 minutes. The resulting 590/540 ratio is proportional to the transmembrane electric potential,

as described by Novo and colleagues,[59] and can be used to determine the change in membrane potential caused by POA_T.

References

(1) British Thoracic and Tuberculosis Association. Short-course chemotherapy in pulmonary tuberculosis: a controlled trial by the British Thoracic and Tuberculosis Association. *The Lancet* **1976**, *308* (7995), 1102–1104. https://doi.org/10.1016/S0140-6736(76)91085-0.

(2) British Thoracic Society. A controlled trial of six months' chemotherapy in pulmonary tuberculosis, final report: results during the 36 months after the end of chemotherapy and beyond. *Brit. J. Dis. Chest* **1984**, *78*, 330–336. https://doi.org/10.1016/0007-0971(84)90165-7.

(3) World Health Organization. *Global Tuberculosis Report 2018*; Geneva, 2018.

(4) World Health Organization. *WHO Consolidated Guidelines on Drug-Resistant Tuberculosis Treatment*; Geneva, 2019.

(5) Konno, K.; Feldmann, F. M.; McDermott, W. Pyrazinamide susceptibility and amidase activity of tubercle bacilli. *Am. Rev. Respir. Dis.* **1967**, *95* (3), 461–469. https://doi.org/10.1164/arrd.1967.95.3.461.

(6) Boshoff, H. I. M.; Mizrahi, V. Expression of *Mycobacterium smegmatis* pyrazinamidase in *Mycobacterium tuberculosis* confers hypersensitivity to pyrazinamide and related amides. *J. Bacteriol.* **2000**, *182* (19), 5479–5485. https://doi.org/10.1128/JB.182.19.5479-5485.2000.

(7) Scorpio, A.; Zhang, Y. Mutations in *pncA*, a gene encoding pyrazinamidase/nicotinamidase, cause resistance to the antituberculous drug pyrazinamide in tubercle bacillus. *Nat. Med.* **1996**, *2* (6), 662. https://doi.org/10.1038/nm0696-662.

(8) French, J. B.; Cen, Y.; Vrablik, T. L.; Xu, P.; Allen, E.; Hanna-Rose, W.; Sauve, A. A. Characterization of nicotinamidases: steady state kinetic parameters, classwide inhibition by nicotinaldehydes, and catalytic mechanism. *Biochemistry* **2010**, *49* (49), 10421–10439. https://doi.org/10.1021/bi1012518.

(9) Dillon, N. A.; Peterson, N. D.; Rosen, B. C.; Baughn, A. D. Pantothenate and pantetheine antagonize the antitubercular activity of pyrazinamide. *Antimicrob. Agents Ch.* **2014**, *58* (12), 7258–7263. https://doi.org/10.1128/AAC.04028-14.

(10) Shi, W.; Chen, J.; Feng, J.; Cui, P.; Zhang, S.; Weng, X.; Zhang, W.; Zhang, Y. Aspartate decarboxylase (PanD) as a new target of pyrazinamide in *Mycobacterium tuberculosis*. *Emerg. Microbes Infec.* **2014**, *3* (1), 1–8. https://doi.org/10.1038/emi.2014.61.

(11) Shi, W.; Zhang, X.; Jiang, X.; Yuan, H.; Lee, J. S.; Barry, C. E.; Wang, H.; Zhang, W.; Zhang, Y. Pyrazinamide inhibits *trans*-translation in *Mycobacterium tuberculosis*. *Science* **2011**, *333* (6049), 1630–1632. https://doi.org/10.1126/science.1208813.

(12) Njire, M.; Wang, N.; Wang, B.; Tan, Y.; Cai, X.; Liu, Y.; Mugweru, J.; Guo, J.; Hameed, H. M. A.; Tan, S.; et al. Pyrazinoic acid inhibits a bifunctional enzyme in *Mycobacterium tuberculosis*. *Antimicrob. Agents Ch.* **2017**, *61* (7), e00070-17. https://doi.org/10.1128/AAC.00070-17.

(13) Kim, H.; Shibayama, K.; Rimbara, E.; Mori, S. Biochemical characterization of quinolinic acid phosphoribosyltransferase from *Mycobacterium tuberculosis* H37Rv and inhibition of its activity by pyrazinamide. *PLOS ONE* **2014**, *9* (6), e100062. https://doi.org/10.1371/journal.pone.0100062.

(14) Peterson, N. D.; Rosen, B. C.; Dillon, N. A.; Baughn, A. D. Uncoupling environmental pH and intrabacterial acidification from pyrazinamide susceptibility in *Mycobacterium*

tuberculosis. *Antimicrob. Agents Ch.* **2015**, *59* (12), 7320–7326. https://doi.org/10.1128/AAC.00967-15.

(15) Salfinger, M.; Heifets, L. B. Determination of pyrazinamide MICs for *Mycobacterium tuberculosis* at different pHs by the radiometric method. *Antimicrob. Agents Ch.* **1988**, *32* (7), 1002–1004. https://doi.org/10.1128/AAC.32.7.1002.

(16) Zhang, Y.; Mitchison, D. The curious characteristics of pyrazinamide: a review. *Int. J. Tuberc. Lung Dis.* **2003**, *7* (1), 6–21.

(17) Raynaud, C.; Lanéelle, M.-A.; Senaratne, R. H.; Draper, P.; Lanéelle, G.; Daffé, M. Mechanisms of pyrazinamide resistance in mycobacteria: importance of lack of uptake in addition to lack of pyrazinamidase activity. *Microbiology* **1999**, *145* (6), 1359–1367. https://doi.org/10.1099/13500872-145-6-1359.

(18) Zhang, Y.; Scorpio, A.; Nikaido, H.; Sun, Z. Role of acid pH and deficient efflux of pyrazinoic acid in unique susceptibility of *Mycobacterium tuberculosis* to pyrazinamide. *J. Bacteriol.* **1999**, *181* (7), 2044–2049.

(19) Anthony, R. M.; den Hertog, A. L.; van Soolingen, D. 'Happy the man, who, studying nature's laws, Thro'' known effects can trace the secret cause.' Do we have enough pieces to solve the pyrazinamide puzzle?' *J Antimicrob Chemother* **2018**, *73* (7), 1750–1754. https://doi.org/10.1093/jac/dky060.

(20) Lu, P.; Haagsma, A. C.; Pham, H.; Maaskant, J. J.; Mol, S.; Lill, H.; Bald, D. Pyrazinoic acid decreases the proton motive force, respiratory ATP synthesis activity, and cellular ATP levels. *Antimicrob. Agents Ch.* **2011**, *55* (11), 5354–5357. https://doi.org/10.1128/AAC.00507-11.

(21) Hertog, A. L. den; Menting, S.; Pfeltz, R.; Warns, M.; Siddiqi, S. H.; Anthony, R. M. Pyrazinamide is active against *Mycobacterium tuberculosis* cultures at neutral pH and low temperature. *Antimicrob. Agents Ch.* **2016**, *60* (8), 4956–4960. https://doi.org/10.1128/AAC.00654-16.

(22) Nielson, D. W.; Goerke, J.; Clements, J. A. Alveolar subphase pH in the lungs of anesthetized rabbits. *PNAS* **1981**, *78* (11), 7119–7123. https://doi.org/10.1073/pnas.78.11.7119.

(23) Nyberg K; Johansson U; Johansson A; Camner P. Phagolysosomal pH in alveolar macrophages. *Environ. Health Persp.* **1992**, *97*, 149–152. https://doi.org/10.1289/ehp.9297149.

(24) Effros, R. M.; Chinard, F. P. The *in vivo* pH of the extravascular space of the lung. *J Clin Invest* **1969**, *48* (11), 1983–1996.

(25) Irwin, S. M.; Prideaux, B.; Lyon, E. R.; Zimmerman, M. D.; Brooks, E. J.; Schrupp, C. A.; Chen, C.; Reichlen, M. J.; Asay, B. C.; Voskuil, M. I.; et al. Bedaquiline and pyrazinamide treatment responses are affected by pulmonary lesion heterogeneity in *Mycobacterium tuberculosis* infected C3HeB/FeJ mice. *ACS Infect. Dis.* **2016**, *2* (4), 251–267. https://doi.org/10.1021/acsinfecdis.5b00127.

(26) Lanoix, J.-P.; Ioerger, T.; Ormond, A.; Kaya, F.; Sacchettini, J.; Dartois, V.; Nuermberger, E. Selective inactivity of pyrazinamide against tuberculosis in C3HeB/FeJ mice is best explained by neutral pH of caseum. *Antimicrob. Agents Ch.* **2016**, *60* (2), 735–743. https://doi.org/10.1128/AAC.01370-15.

(27) Masuda, M.; Sato, T.; Sakamaki, K.; Kudo, M.; Kaneko, T.; Ishigatsubo, Y. The effectiveness of sputum pH analysis in the prediction of response to therapy in patients with pulmonary tuberculosis. *PeerJ* **2015**, *3*, e1448. https://doi.org/10.7717/peerj.1448.

(28) Ozkan, P.; Mutharasan, R. A rapid method for measuring intracellular pH using BCECF-AM. *BBA-Gen. Subjects* **2002**, *1572* (1), 143–148. https://doi.org/10.1016/S0304-4165(02)00303-3.

(29) Rao, M.; Streur, T. L.; Aldwell, F. E.; Cook, G. M. Intracellular pH regulation by *Mycobacterium smegmatis* and *Mycobacterium bovis* BCG. *Microbiology* **2001**, *147* (4), 1017–1024. https://doi.org/10.1099/00221287-147-4-1017.

(30) Bakker, E. P.; Mangerich, W. E. Interconversion of components of the bacterial proton motive force by electrogenic potassium transport. *J. Bacteriol.* **1981**, *147* (3), 820–826.

(31) Vandal, O. H.; Nathan, C. F.; Ehrt, S. Acid resistance in *Mycobacterium tuberculosis*. *J. Bacteriol.* **2009**, *191* (15), 4714–4721. https://doi.org/10.1128/JB.00305-09.

(32) Fisher, M. A.; Plikaytis, B. B.; Shinnick, T. M. Microarray analysis of the *Mycobacterium tuberculosis* transcriptional response to the acidic conditions found in phagosomes. *J. Bacteriol.* **2002**, *184* (14), 4025–4032. https://doi.org/10.1128/JB.184.14.4025-4032.2002.

(33) Schnappinger, D.; Ehrt, S.; Voskuil, M. I.; Liu, Y.; Mangan, J. A.; Monahan, I. M.; Dolganov, G.; Efron, B.; Butcher, P. D.; Nathan, C.; et al. Transcriptional adaptation of *Mycobacterium tuberculosis* within macrophages: insights into the phagosomal environment. *J. Exp. Med.* **2003**, *198* (5), 693–704. https://doi.org/10.1084/jem.20030846.

(34) Gruppo, V.; Johnson, C. M.; Marietta, K. S.; Scherman, H.; Zink, E. E.; Crick, D. C.; Adams, L. B.; Orme, I. M.; Lenaerts, A. J. Rapid microbiologic and pharmacologic evaluation of experimental compounds against *Mycobacterium tuberculosis*. *Antimicrob. Agents Ch.* **2006**, *50* (4), 1245–1250. https://doi.org/10.1128/AAC.50.4.1245-1250.2006.

(35) Nurul Islam, M.; Hitchings, R.; Kumar, S.; Fontes, F. L.; Lott, J. S.; Kruh-Garcia, N. A.; Crick, D. C. Mechanism of fluorinated anthranilate-induced growth inhibition in *Mycobacterium tuberculosis*. *ACS Infect. Dis.* **2019**, *5* (1), 55–62. https://doi.org/10.1021/acsinfecdis.8b00092.

(36) Zhang, Y.; Permar, S.; Sun, Z. Conditions that may affect the results of susceptibility testing of *Mycobacterium tuberculosis* to pyrazinamide. *Journal of Medical Microbiology* **2002**, *51* (1), 42–49. https://doi.org/10.1099/0022-1317-51-1-42.

(37) Coleman, D.; Waddell, S. J.; Mitchison, D. A. Effects of low incubation temperatures on the bactericidal activity of anti-tuberculosis drugs. *J Antimicrob Chemother* **2011**, *66* (1), 146–150. https://doi.org/10.1093/jac/dkq414.

(38) Ellis, K. J.; Morrison, J. F. Buffers of constant ionic strength for studying pH-dependent processes. In *Methods in Enzymology*; Purich, D. L., Ed.; Enzyme Kinetics and Mechanism - Part C: Intermediates, Stereochemistry, and Rate Studies; Academic Press, 1982; Vol. 87, pp 405–426. https://doi.org/10.1016/S0076-6879(82)87025-0.

(39) Vandal, O. H.; Pierini, L. M.; Schnappinger, D.; Nathan, C. F.; Ehrt, S. A membrane protein preserves intrabacterial pH in intraphagosomal *Mycobacterium tuberculosis*. *Nat. Med.* **2008**, *14* (8), 849–854. https://doi.org/10.1038/nm.1795.

(40) Booth, I. R. Regulation of cytoplasmic pH in bacteria. *Microbiol. Mol. Biol. R.* **1985**, *49* (4), 359–378.

(41) Sturr, M. G.; Guffanti, A. A.; Krulwich, T. A. Growth and bioenergetics of alkaliphilic *Bacillus firmus* OF4 in continuous culture at high pH. *J. Bacteriol.* **1994**, *176* (11), 3111–3116. https://doi.org/10.1128/jb.176.11.3111-3116.1994.

(42) Hornbæk, T.; Jakobsen, M.; Dynesen, J.; Nielsen, A. K. Global transcription profiles and intracellular pH regulation measured in *Bacillus licheniformis* upon external pH upshifts. *Arch Microbiol* **2004**, *182* (6), 467–474. https://doi.org/10.1007/s00203-004-0729-6.

(43) Nannen, N. L.; Hutkins, R. W. Intracellular pH effects in lactic acid bacteria. *J. Dairy Sci.* **1991**, *74* (3), 741–746. https://doi.org/10.3168/jds.S0022-0302(91)78219-2.

(44) Kobayashi, H.; Suzuki, T.; Kinoshita, N.; Unemoto, T. Amplification of the *Streptococcus faecalis* proton-translocating ATPase by a decrease in cytoplasmic pH. *J. Bacteriol.* **1984**, *158* (3), 1157–1160.

(45) Kobayashi, H. A proton-translocating ATPase regulates pH of the bacterial cytoplasm. *J. Biol. Chem.* **1985**, *260* (1), 72–76.

(46) Darby, C. M.; Ingólfsson, H. I.; Jiang, X.; Shen, C.; Sun, M.; Zhao, N.; Burns, K.; Liu, G.; Ehrt, S.; Warren, J. D.; et al. Whole cell screen for inhibitors of pH homeostasis in *Mycobacterium tuberculosis*. *PLOS ONE* **2013**, *8* (7), e68942. https://doi.org/10.1371/journal.pone.0068942.

(47) de Carvalho, L. P. S.; Darby, C. M.; Rhee, K. Y.; Nathan, C. Nitazoxanide disrupts membrane potential and intrabacterial pH homeostasis of *Mycobacterium tuberculosis*. *ACS Med. Chem. Lett.* **2011**, *2* (11), 849–854. https://doi.org/10.1021/ml200157f.

(48) Bartek, I. L.; Reichlen, M. J.; Honaker, R. W.; Leistikow, R. L.; Clambey, E. T.; Scobey, M. S.; Hinds, A. B.; Born, S. E.; Covey, C. R.; Schurr, M. J.; et al. Antibiotic bactericidal activity is countered by maintaining pH homeostasis in *Mycobacterium smegmatis*. *mSphere* **2016**, *1* (4), e00176-16. https://doi.org/10.1128/mSphere.00176-16.

(49) Zhang, Y.; Wade, M. M.; Scorpio, A.; Zhang, H.; Sun, Z. Mode of action of pyrazinamide: disruption of *Mycobacterium tuberculosis* membrane transport and energetics by pyrazinoic acid. *J. Antimicrob. Chemother.* **2003**, *52* (5), 790–795. https://doi.org/10.1093/jac/dkg446.

(50) Laurence, D. J. R. A study of the adsorption of dyes on bovine serum albumin by the method of polarization of fluorescence. *Biochemical Journal* **1952**, *51* (2), 168–180. https://doi.org/10.1042/bj0510168.

(51) Cavari, B. Z.; Avi-Dor, Y.; Grossowicz, N. Effect of carbonyl cyanide m-chlorophenylhydrazone on respiration and respiration-dependent phosphorylation in *Escherichia coli*. *Biochem. J.* **1967**, *103* (2), 601–608. https://doi.org/10.1042/bj1030601.

(52) Anoushiravani, M.; Falsafi, T.; Niknam, V. Proton motive force-dependent efflux of tetracycline in clinical isolates of *Helicobacter pylori*. *J. Med. Microbiol.* **2009**, *58* (10), 1309–1313. https://doi.org/10.1099/jmm.0.010876-0.

(53) Rao, S. P. S.; Alonso, S.; Rand, L.; Dick, T.; Pethe, K. The protonmotive force is required for maintaining ATP homeostasis and viability of hypoxic, nonreplicating *Mycobacterium tuberculosis*. *PNAS* **2008**, *105* (33), 11945–11950. https://doi.org/10.1073/pnas.0711697105.

(54) O'Shaughnessy, K.; Hladky, S. B. Transient currents carried by the uncoupler, carbonyl cyanide *m*-chlorophenylhydrazone. *BBA-Bioenergetics* **1983**, *724* (3), 381–387. https://doi.org/10.1016/0005-2728(83)90097-X.

(55) Smith, D.; Artursson, P.; Avdeef, A.; Di, L.; Ecker, G. F.; Faller, B.; Houston, J. B.; Kansy, M.; Kerns, E. H.; Krämer, S. D.; et al. Passive lipoidal diffusion and carrier-mediated cell uptake are both important mechanisms of membrane permeation in drug disposition. *Mol. Pharmaceutics* **2014**, *11* (6), 1727–1738. https://doi.org/10.1021/mp400713v.

(56) Hannesschlaeger, C.; Horner, A.; Pohl, P. Intrinsic membrane permeability to small molecules. *Chem. Rev.* **2019**, *119* (9), 5922–5953. https://doi.org/10.1021/acs.chemrev.8b00560.

(57) Kell, D. B.; Oliver, S. G. How drugs get into cells: tested and testable predictions to help discriminate between transporter-mediated uptake and lipoidal bilayer diffusion. *Front. Pharmacol.* **2014**, *5*. https://doi.org/10.3389/fphar.2014.00231.

(58) Peters, B. J.; Groninger, A. S.; Fontes, F. L.; Crick, D. C.; Crans, D. C. Differences in interactions of benzoic acid and benzoate with interfaces. *Langmuir* **2016**, *32* (37), 9451–9459. https://doi.org/10.1021/acs.langmuir.6b02073.

(59) Novo, D.; Perlmutter, N. G.; Hunt, R. H.; Shapiro, H. M. Accurate flow cytometric membrane potential measurement in bacteria using diethyloxacarbocyanine and a ratiometric technique. *Cytometry* **1999**, *35* (1), 55–63. https://doi.org/10.1002/(SICI)1097-0320(19990101)35:1<55::AID-CYTO8>3.0.CO;2-2.

Chapter 4

Pyrazinoic acid mimics the activity of protonophores against *Mycobacterium tuberculosis*

Pyrazinamide (PZA) is an antibiotic used in combination with other anti-tubercle in standard treatment regimen for tuberculosis (TB) infections.[1] While PZA's mode of action is still unclear,[2] multiple reports show PZA requires conversion to pyrazinoate (POA_C) by a mycobacterial enzyme to exhibit antibacterial activity.[3–6] In solution, the charged, deprotonated POA_C exists in equilibrium with the neutral, protonated pyrazinoic acid (POA_N) and the total pyrazinoic acid (POA_T) in solution consists of the sum of the concentration of both forms ($POA_N + POA_C$). A recent report showed that the pH-dependent growth inhibitory effect of PZA in *Mycobacterium tuberculosis in vitro* depends on the differential concentration of POA_N between the bacillary cytoplasm and the environment.[7] The same report posits POA_N acts as an uncoupler of oxidative phosphorylation, leading to a cascade of secondary effects that leads to growth arrest and may explain the synergism PZA exhibits with other anti-tubercle drugs.

Peter Mitchell's chemiosmotic theory describes that the establishment of a proton electrochemical gradient across the membrane is generated through oxidative processes and then utilized to generate ATP.[8] Substrate oxidation during the electron transport chain (ETC) drives the generation of an electrochemical potential, designated as proton motive force (PMF), with two components associated to it: the electric potential ($\Delta\Psi$), stemming from all the charged species on both sides of the membrane, and the proton concentration gradient (ΔpH), expressed as the differential of pH environments between the cytoplasm and the extracellular medium. The dissipation of one of these components can lead to disruption of PMF, although compensatory mechanisms have been reported elsewhere.[9,10] Uncouplers of oxidative phosphorylation are a class

of compounds able to, through various mechanisms, decouple substrate oxidation from the phosphorylation of ADP into ATP.[11] Ionophores, such as valinomycin, cause PMF's disruption by dissipation of $\Delta\Psi$ alone while others, such as nigericin, act by dissipation of ΔpH alone. Valinomycin acts as a semi-permeable pore, allowing the flux of charged species (mostly K^+) through the membrane, which does not affect the proton gradient or the pH differential across the membrane. Thus, valinomycin's mechanism is electrogenic. Nigericin, however, operates as an antiporter transporter, sequestering and shuttling protons from the more acidic environment in the extracellular medium to the more neutral cytoplasm and crossing the membrane back to the extracellular space with a counterion in the form of a monovalent cation (usually K^+), making nigericin's mechanism charge neutral. These uncouplers have been used widely as controls in classical bioenergetics studies of oxidative phosphorylation. A third case of ionophoric disruption of PMF relates to chemicals that can dissipate both $\Delta\Psi$ and ΔpH; carbonyl cyanide *m*-chlorophenyl hydrazone is an example of such a compound. In solution, the neutral, protonated *N*-(3-chlorophenyl)carbonohydrazonoyl dicyanide ($CCCP_N$) exists in equilibrium with its charged, deprotonated form, 1-(3-chlorophenyl)-2-(dicyanomethylene)hydrazine-1-ide ($CCCP_C$), and the total carbonyl cyanide *m*-chlorophenyl hydrazine ($CCCP_T$) is the sum of concentrations of each species. The equilibrium between $CCCP_N$ and $CCCP_C$ drives its activity as ionophore: in an acidic environment outside the cell, a fraction of $CCCP_T$ exists as $CCCP_N$. The membrane permeability of $CCCP_N$ was shown to be higher than that of $CCCP_C$,[12] which results in $CCCP_N$ being more likely to cross the membrane than its conjugated base, $CCCP_C$. Upon exposure to the cytoplasmic environment, the higher pH leads to a different acid-base equilibrium between $CCCP_N$ and $CCCP_C$, expressed by the Henderson-Hasselbalch equation (HHE), which results in the release of protons to the cytoplasm. While the mechanism of action of $CCCP_T$ involves the efflux of $CCCP_C$ (without

a counterion), the critical event for the uncoupling activity of $CCCP_T$ is the release of protons by $CCCP_N$. Therefore, $CCCP_N$ disrupts ΔpH if its flux into the cells is greater than the flux of protons generated by the cell in the opposite direction. Furthermore, since the flux of $CCCP_C$ occurs without the use of a counterion, as in the case of nigericin, the uncoupling event caused by $CCCP_T$ is electrogenic, leading to dissipation of ΔΨ. Since the activity of $CCCP_T$ and compounds with similar mechanism relies uniquely on the transport of protons, the compounds are termed protonophores, to distinguish the activity from other ionophores. Additionally, as the mechanism described above suggests, the activity of protonophores is pH-dependent, as the flux of the protonated form of the compound is dependent on the available concentration of this form, which, in turn, depends on the pH of the solution as described by the HHE. Protonophores share structural similarities, such as the requirement of a protonatable group for activity and of a hydrophobic moiety that increases membrane solubity.[11,13]

Similarly to $CCCP_T$, small weak acids have been shown to exhibit protonophoric activity.[14] 2,4-dinitrophenol was one of the examples used by Mitchell to demonstrate protonophore-driven uncoupling in light of his chemiosmotic theory,[8] and many more weak acids exhibit analogous activity since then.[14–18] The activity of benzoic acid (BEN_N) as a food preservative was recently explained through the interaction of BEN_N and its conjugated base, benzoate (BEN_C), with membranes. The mechanism involves protonophoric activity of BEN_N.[18] Salicylic acid (SAL_N), a structural analogue of BEN_N, is an interesting example, as it exhibits activity as protonophore, as well as other, more traditional, pharmacological targets.[16,17,19] However, the chemical nature of POA_N as a weak acid is seldom considered when its mode of action is investigated, even if the structural similarity between POA_N and both BEN_N and SAL_N warrants investigation into potential similar mechanisms of action. Furthermore, evidence exists that a form of total benzoic acid

(BEN_T, equal to BEN_N + BEN_C) has a similar effect on the mycobacterial $\Delta\Psi$ as POA_T.[20] Additionally, *para*-aminosalicylic acid, a structural analogue of salicylic acid, was one of the first antibiotics discovered against *M. tuberculosis*.[21,22] The chemical structure of other anti-tubercle drugs, like isoniazid or rifampin, also shows protonatable groups that could, in theory, enable protonophoric activity to these antibiotics. Thus, the aim of the present work is to compare the activity of a number of anti-mycobacterial drugs with POA_T and structural analogues of POA_T and attempt to gain insight into the potential mechanism of action of PZA.

Results

Figure 4.1 shows the structures of the compounds used in the work presented here. The acronyms used for each compound follow the same trend throughout the text: the protonated form of the compound shows a subscript N and the deprotonated a subscript C; when referring to both

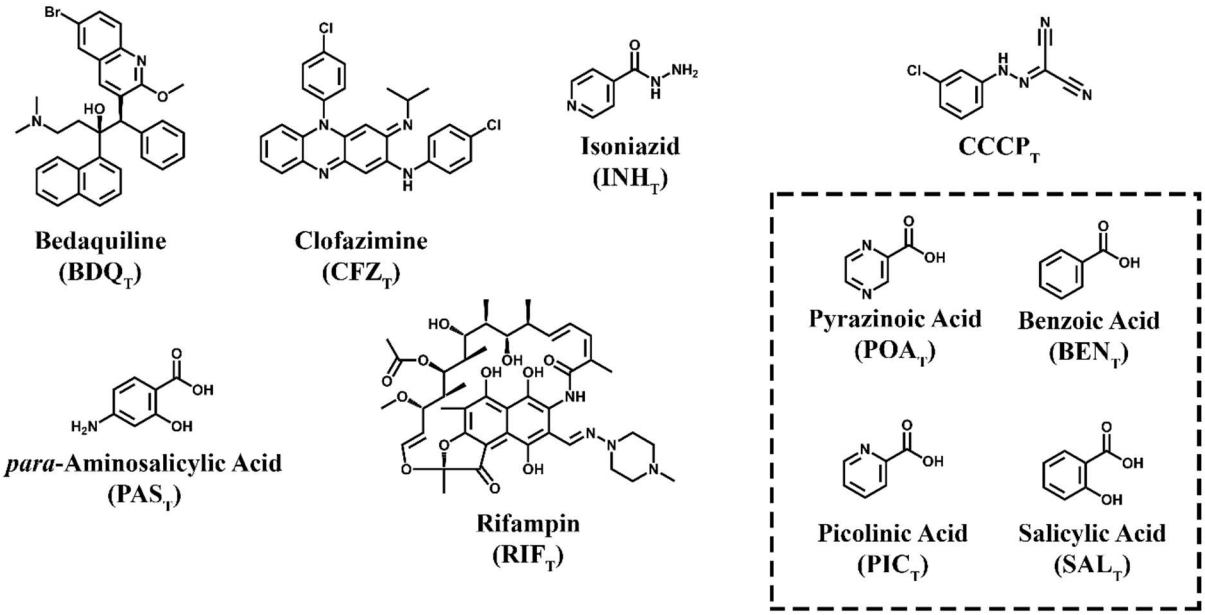

Figure 4.1 – Structures of the anti-mycobacterial drugs and POA_T structural analogues used. The dashed-line box groups POA_T with the compounds referred throughout the text as its structural analogues.

Table 4.1 – QSAR model coefficients

Compound	pK_a*	T_N (μM^{-1})	T_C (μM^{-1})	R^2
		No pH-dependent activity		
BDQ_T	8.91	24 ± 2	360 ± 160	0.30
CFZ_T	6.63	0 ± 2	6 ± 1	0.30
INH_T	3.35	0 ± 840	6.3 ± 0.4	0.01
PAS_T	3.68	100 ± 460	4.0 ± 0.5	0.01
RIF_T	6.55	50 ± 7	60 ± 4	0.00
		pH-dependent activity		
POA_T	3.62	1.10 ± 0.09	0 ± 0.0001	0.96
BEN_T	4.08	0.20 ± 0.02	0.0003 ± 0.0001	0.94
PIC_T	5.52	0.007 ± 0.001	0.0001 ± 0.0001	0.91
SAL_T	2.79	10 ± 0.5	0.0015 ± 0.0001	0.98
$CCCP_T$	5.81	0.60 ± 0.02	0.050 ± 0.003	0.98

*pK_a values obtained through Chemicalize (www.chemicalize.com).

forms or when the form present is unclear, a subscript T is used, standing for N + C, as explained above for the cases of POA_T, $CCCP_T$ and BEN_T. For compounds with multiple pK_a values, the pK_a closest to neutral pH was used (Table 4.1).

pH-dependent drug susceptibility in *Mycobacterium tuberculosis* H37Ra. The pH-dependent activity of POA_T *in vitro* has been established in multiple reports.[7,23–25] However, the effect of pH on the activity of other anti-tubercle drugs is rarely considered, despite the pathogenesis models for *M. tuberculosis* suggesting exposure to a wide range of pH environments.[26–31] Figure 4.2 shows the concentration responsible for 50% of growth inhibition

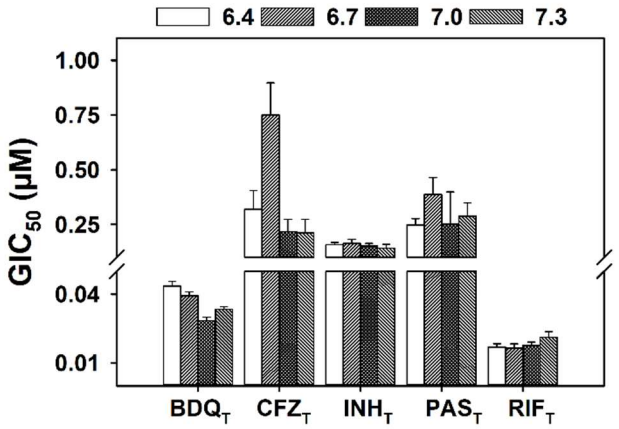

Figure 4.2 – Effect of pH on the growth inhibition of *M. tuberculosis* by known anti-tubercle drugs. *M. tuberculosis* H37Ra were incubated at 37°C in supplemented 7H9 broth with a range of concentrations of the specified antibiotic. The OD_{600} was measured every 24 hours for 5 days, with growth rates calculated by determining the slope at each time point. The GIC_{50} were calculated with the growth rates of day 5, from four independent replicates. The GIC_{50} values extracted from the E_{max} model regression are presented at each external pH tested (6.4-7.3). The error bars of each bar correspond to the standard error calculated during the regression.

(GIC_{50}) of bedaquiline (BDQ_T), clofazimine (CFZ_T), *para*-aminosalicylic acid (PAS_T), isoniazid (INH_T) and rifampin (RIF_T) over a small, physiologically relevant range of environmental pH values (6.4-7.3). All of the anti-mycobacterial drugs shown in Figure 4.2 have different molecular targets and, with the exception of BDQ_T,[32] there is no evidence reported in literature of ionophoric activity by any of the drugs. The results shown in Figure 4.2 demonstrate none of the compounds tested exhibits pH-dependent activity against *M. tuberculosis*, within the pH range tested.

The results shown in Figure 4.3 represent, graphically, the GIC_{50} values of the POA_T analogues tested, as well as the GIC_{50} values for POA_T and $CCCP_T$, over the range of environmental pH previously used (6.4-7.3). The data demonstrates POA_T, $CCCP_T$ and all of the POA_T analogues exhibit pH-dependent growth inhibitory activity against *M. tuberculosis*. Additionally, $CCCP_T$ exhibits the highest efficacy in growth inhibition of all the compounds in Figure 4.3, with SAL_T showing the lowest GIC_{50} among the POA_T analogues. All the compounds shown in Figure 4.3 also exhibited higher GIC_{50} values than the results for the compounds shown in Figure 4.2.

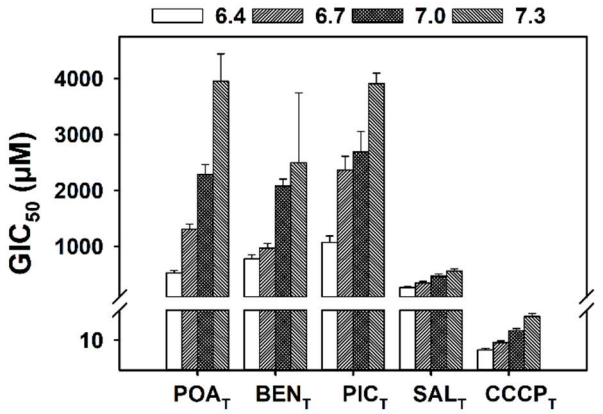

Figure 4.3 – Effect of pH on the growth inhibition of *M. tuberculosis* by POA_T, structural analogues of POA_T and $CCCP_T$. Mycobacterial cultures were grown in supplemented 7H9 broth at 37°C and incubated with a range of concentration of the specified compound for 5 days. The OD_{600} was measured every 24h and growth rates determined by calculating the slope of the growth curve at each time point. The GIC_{50} values shown were determined with the growth rates of day 5 regression of an E_{max} model for each environmental pH value (6.4-7.3), using four replicates. The error bars shown correspond to the standard error extracted during the regression.

Modeling pH-dependent activity in *Mycobacterium tuberculosis* H37Ra. Quantitative structure-activity relationship (QSAR) models have been previously used to determine the activity of drugs or poisons with pH-dependent properties. The model presented in Equation 4.1 (and Equation 4.2 in the Materials and methods section) was derived (Appendix A) from acid-base equilibrium chemistry and adapted from the work of Könemann and Musch.[33] The GIC_{50} values obtained during the drug susceptibility assays were used and the goodness of fit to the model (Equation 4.1) was determined, with the coefficients T_N and T_C extracted from the fit. T_N stands for the inverse of the concentration of the protonated form of the compound tested responsible for 50% of the growth inhibition caused by that form and T_C stands for the inverse of the concentration of the deprotonated form of the compound tested responsible for 50% of the growth inhibition enacted by the deprotonated species.

$$\frac{1}{GIC_{50}} = T_N \cdot \frac{10^{-pH}}{10^{-p} + 10^{-p}{}_a} + T_C \cdot \frac{10^{-pK_a}}{10^{-pH+1} - pK_a} \qquad \text{Equation 4.1}$$

The coefficients T_N and T_C and the coefficient of determination (R^2) for each of the compounds used in the present work are shown in Table 4.1. As expected, the compounds that showed no

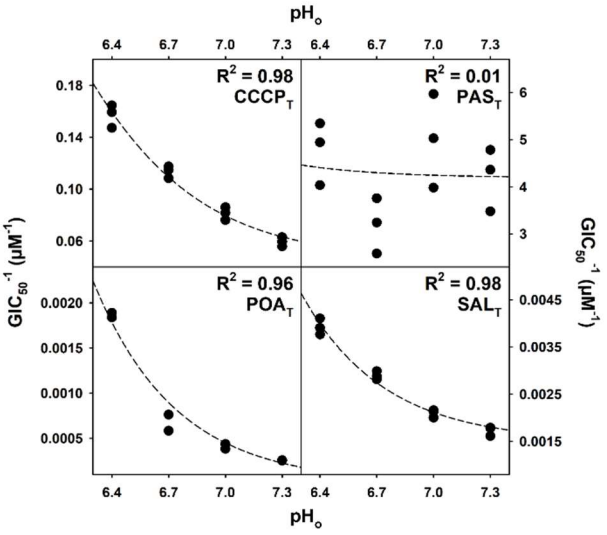

Figure 4.4 – Regression of the QSAR model for $CCCP_T$, PAS_T, POA_T and SAL_T. The GIC_{50} values (three independent replicates) obtained during the drug susceptibility assay were fitted to the model described Equation 4.1 and plotted as a function of external pH (pH_o). The R^2 values were calculated based on the residuals of the regression, and the curves (full line) generated with the coefficients determined during the regression.

pH-dependent activity exhibit poor goodness of fit, while the compounds with clear pH-dependent activities fit the model. Figure 4.4 shows the graphically representation of the fit, including the experimental GIC_{50} points, for $CCCP_T$, PAS_T, POA_T and SAL_T, as a function of the environmental pH used for each GIC_{50} determination. As Figure 4.4 shows, the model behavior for $CCCP_T$, POA_T and SAL_T is similar, suggesting a similar pH-dependent response. Moreover, as the coefficient values show in Table 4.1, for all the compounds with high R^2 values, the value of T_N is much greater than T_C, indicating a higher efficacy of the protonated form of the compounds and/or a mechanistic requirement for the formation of the protonated form (the latter being reported to be true in both $CCCP_T$ and SAL_T, given their protonophoric activity).[16,34]

Cytoplasmic acidification by structural analogues of pyrazinoic acid in *Mycobacterium tuberculosis* H37Ra. Previous work described how POA_T causes the acidification of the cytosol of *M. tuberculosis* H37Ra and suggested the uncoupling of proton

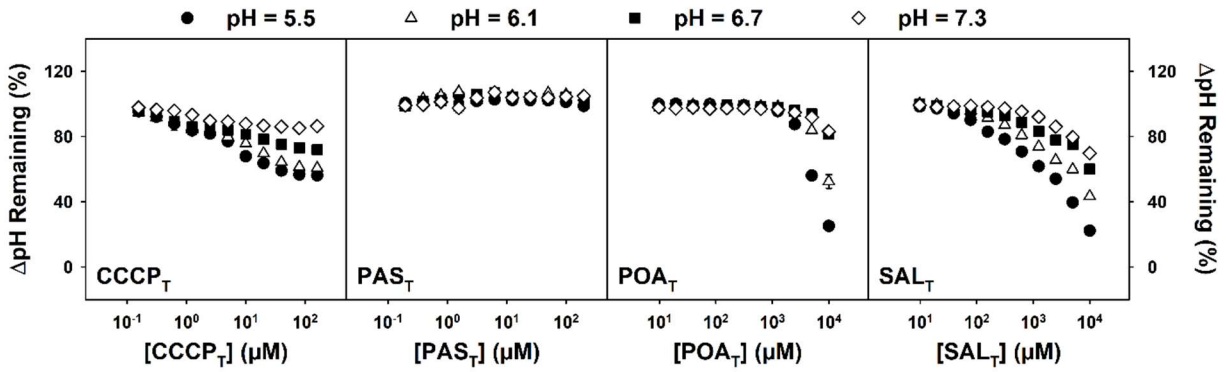

Figure 4.5 – Effect of $CCCP_T$, PAS_T, POA_T and SAL_T on ΔpH over a range of external pH values. M. tuberculosis H37Ra cells were incubated in MMA buffer containing 0.5 μM BCECF-AM at the indicated pH and concentration of the desired analogue for 30 minutes. Fluorescence was measured at 37 °C with excitation at 440 and 485 nm and emission recorded at 540 nm with four replicates for each concentration of compound. The percentage of ΔpH remaining was estimated with the BCECF's 485/440 ratio after 30 minutes of incubation with analogue divided by the estimated ΔpH (using pH 7.4 as the cytoplasmic pH); the untreated (DMSO control) was considered 100%.

motive force by POA_N.[7] However, it is unclear if the cytoplasmic acidification is a specific effect of POA_T or most drugs induce cytosolic pH decrease. Additionally, given the similar behavior in inhibition of growth, the effect on the cytosolic pH environment by $CCCP_T$ and SAL_T, both known protonophores, should determine if, as previously suggested, POA_T acts as a protonophore. Figure 4.5 shows the change in the pH gradient between the cytoplasm and the exterior environment (ΔpH) across a range of environmental pH values when the mycobacterial suspensions were exposed to concentrations of $CCCP_T$, PAS_T, POA_T or SAL_T. The drug concentrations were selected to be within the range of effective growth inhibition. As seen in Figure 4.5, $CCCP_T$, POA_T and SAL_T cause cytoplasmic acidification in a concentration dependent manner, with higher efficiency in acidification observed at the lowest environmental pH tested for all three compounds. Conversely, PAS_T does not show disruption of ΔpH within the range of growth inhibitory concentrations, suggesting the growth inhibitory mechanism is unrelated to ΔpH dissipation and, therefore, disconnected from disruption of PMF. However, the similarity shown

in Figure 4.5 (and throughout the data shown in the present work) between POA_T and two known protonophores, $CCCP_T$ and SAL_T, indicate that PZA, through the conversion to POA_N, behaves like a protonophore as its primary mechanism of action *in vitro*.

Discussion

pH-dependent drug susceptibility in *Mycobacterium tuberculosis* H37Ra. The results shown in Figure 4.2 and Figure 4.3 demonstrate that the pH-dependent effect of PZA is not observed in other anti-tubercle drugs. However, $CCCP_T$ and the structural analogues of POA_T all exhibited pH-dependent activity, similar to the growth inhibitory effect shown for POA_T here and supported by previous observations.[7] The results imply POA_T acts mechanistically like $CCCP_T$ and the POA_T analogues and the pH-dependent activity of these compounds is a consequence of their primary mode of action. The literature on the pH-dependence of PZA *in vitro* is extensive,[7,23–25] with a recent report providing the first comprehensive explanation for the phenomenon.[7] The pH-dependent activity of PZA is explained by the protonophoric activity of POA_N, first through POA_C converted from PZA within the cytoplasm and then by an acid-base equilibrium outside the cell. The mechanism relies on POA_N transporting protons from the acidic environment to the neutral cytoplasm and, consequently, disrupting the PMF in *M. tuberculosis*. This mode of action has the advantage of providing a cohesive explanation for previous observations during treatment with PZA or POA_T, such as the decrease in ATP levels upon treatment with POA_T in *Mycobacterium bovis* BCG.[35] The protonophoric activity of POA_N may also elucidate the observation that PZA's efficacy increases at lower temperatures, as the pK_a increase as the temperature decreases may be accompanied by an increase in the concentration of POA_N. Additionally, the protonophoric mechanism hypothesis provides an explanation for the synergism

of PZA with other anti-mycobacterial drugs[36,37] since, by disrupting PMF, POA_N may be indirectly inhibiting PMF-dependent efflux pumps involved in the resistance mechanism of most antibiotics; therefore, the cytosolic concentrations of anti-tubercle drugs would be theoretically higher when the efflux pumps activity is inhibited and the activity of these drugs would appear to increase.[38,39]

The effect of environmental pH on the activity of non-PZA anti-mycobacterial drugs is seldom studied, in contrast with the well-established pH-dependence of PZA *in vitro*. The drugs used in the present work were chosen to provide a range of molecular targets of *M. tuberculosis*. Thus, both BDQ_T and CFZ_T target energy production, albeit with different modes of action,[40,41] while INH_T has been linked to multiple targets, including cell wall biosynthesis inhibition, nucleic acid synthesis inhibition and reactive oxygen and nitrogen species generation.[42–48] After endogenous conversion into its active form, PAS_T is reported to inhibit the folate pathway[49,50] and RIF_T is a well-described, wide-spectrum, inhibitor of DNA-dependent RNA polymerase.[51] As Figure 4.2 demonstrates, none of the anti-mycobacterial drugs mentioned above exhibit pH-dependent activity within the range of environmental pH values tested. The observations of Bartek and colleagues support the results shown here for RIF_T,[52] but for the other antibiotics mentioned above, no previous reports on their activity at different environmental pH were found.

In *M. tuberculosis*, BDQ_T inhibits the F_1F_0-ATP synthase, binding to the a-c subunit of the F_0 complex of the ATP synthase and leading to depletion of ATP.[40] However, BDQ_T was reported to act as a H^+/K^+ ionophore in *Escherichia coli* membrane vesicles,[32] but *E. coli* lacks the BDQ_T binding site.[53] Additionally, the results in Figure 4.2 show BDQ_T exhibits no pH-dependent activity, which are supported by observations described elsewhere.[54] Thus, the data implies the ionophoric activity of BDQ_T in mycobacteria is potentially a secondary effect or only possible in cases where the BDQ_T-binding site in the ATP synthase is not present.

Figure 4.3 shows that the pH-dependent growth inhibition of POA_T is mimicked by the structural analogues used in the present work: BEN_T, PIC_T and SAL_T. Additionally, given the previous report suggesting POA_N acts as a protonophore,[7] the effect of $CCCP_T$ (a well-known protonophore) on the growth of *M. tuberculosis* was determined and the pH-dependence inhibition observed is similar to the dependence seen with POA_T and the its structural analogues. The results presented in Figure 4.3 suggest the mechanism connected to POA_T's pH-dependent activity is similar to the underlying mechanism that produces the pH-dependent activity of all the other compounds tested, which further implies that POA_N acts as a protonophore.

Modeling pH-dependent activity in *Mycobacterium tuberculosis* H37Ra. The QSAR model represented by Equation 4.1 (adapted from Könemann and Musch;[33] see Appendix A for derivation) was first utilized as a model for the pH-dependent toxicity of phenols in fish.[33,55] The theoretical framework of the model accounts for independent toxicity of the protonated and deprotonated forms of phenols, expressed by the coefficients T_N and T_C, respectively. The model was adapted to antibiotics targeting bacteria, as seen in Appendix A. The coefficients extracted when the GIC_{50} values obtained at different environmental pH values for each of the compounds used were fit to the model are shown in Table 4.1. The model fits well for the compounds exhibiting pH-dependent activity (Figure 4.3) and is a poor model for the activity of the compounds shown in Figure 4.2, as those compounds showed no dependence on the pH of the culture medium. The results, with the model regression line shown, are represented graphically in Figure 4.4 for $CCCP_T$, PAS_T, POA_T and SAL_T.

The coefficients presented in Table 4.1 indicate the previous observation that POA_N is the active form of PZA[7] is correct, as the coefficient T_C is orders of magnitude lower than T_N. The

negligible value of T_C (when compared with T_N) indicates the contribution of the deprotonated form of POA_T to the effect is also negligible and the observable effect relies solely on the protonated form. Similarly, the structure analogues of POA_T all follow the same pattern, further supporting the hypothesis of a common mechanism of action. Additionally, the concentration of POA_N responsible for 50% of the growth inhibition (inverse of T_N) corresponds to ~910 nM. A similar concentration of POA_N responsible for 50% of growth inhibition was previously reported elsewhere.[7] The equivalent concentration of $CCCP_N$ is ~1700 nM. Thus, theoretically, POA_N is twice as effective at inhibiting *M. tuberculosis* growth as $CCCP_N$. Moreover, the inverse T_N concentration for SAL_N is ~100 nM, which would make SAL_N the best compound at inhibiting mycobacterial growth from the ones shown in Figure 4.3. However, the low pK_a of POA_N and SAL_N determines that, to achieve the concentrations required to inhibit 50% of growth in neutral environments, the concentrations of POA_T and SAL_T are orders of magnitude higher than the theoretical concentrations of POA_N and SAL_N needed to induce the inhibitory effect. Conversely, given the higher pK_a, $CCCP_T$ concentrations are closer to the theoretical $CCCP_N$ concentrations to achieve a similar effect. Nonetheless, the results strongly suggest POA_N acts as a protonophore, given all the similarities described with the known protonophores $CCCP_N$ and SAL_N.

Figure 4.4 also shows the experimental results and the poor fit obtained for PAS_T, which reflect the lack of pH-dependence presented in Figure 4.2. However, PAS_T is a structural analogue of both POA_T and SAL_T, which could imply a similar behavior and mechanism. Nevertheless, the drug susceptibility assays and the QSAR model used here indicate otherwise. Previous reports showed PAS_T inhibits the folate pathway in *M. tuberculosis*.[49,56] Thus, the existence of an endogenous target of PAS_T, like suggested previously for the case of the ionophoric activity of BDQ_T,[32] seems to prevent the protonophoric activity that PAS_T's structure suggested. Besides, as

PAS_T is incorporated into the mycobacterial folate pathway as hydroxyl-dihydropteroate,[49] free cytosolic PAS_T is unlikely to exist in the concentrations required for the protonophoric activity.

Cytoplasmic acidification by structural analogues of pyrazinoic acid in *Mycobacterium tuberculosis* H37Ra. The drug susceptibility assays at a range of environmental pH values and the QSAR model used subsequently provide evidence that the pH-dependent activity of POA_T is not a universal mechanism in anti-tubercle drugs (Figure 4.2, Figure 4.3 and Figure 4.4). The QSAR model used here also implies POA_T's activity depends on the concentration of POA_N, a hallmark of protonophoric activity. Additionally, the results also support a shared mechanism of action between POA_T and $CCCP_T$, SAL_T and the other structural analogues, although not with PAS_T, as explained above. POA_T was recently shown to cause rapid cytosolic acidification in *M. tuberculosis* and to dissipate $\Delta\Psi$. These observations were interpreted as an indication of a potential protonophoric mode of action.[7] Figure 4.5 shows how the cytosolic acidification by POA_T is also observed when *M. tuberculosis* H37Ra suspensions are treated with $CCCP_T$ or SAL_T, but PAS_T causes no change in the mycobacterial transmembrane ΔpH at the range of concentration that generates PAS_T-induced growth inhibition. The cytosolic acidification caused by $CCCP_T$ is supported by observations described elsewhere.[25] A previous report by Zhang and colleagues showed similar GIC_{50} values for BEN_T and SAL_T to the ones presented here, but they failed to observe any change in the internal pH caused by the two compounds. Still, they showed BEN_T and SAL_T-induced $\Delta\Psi$ disruption in *M. tuberculosis* H37Ra (but not in *M. smegmatis*).[57]

The mechanism of acidification of the cytoplasm by $CCCP_T$ is, however, apparently distinct from that of POA_T and SAL_T. As shown in Figure 4.5, the dissipation of ΔpH by $CCCP_T$

seems to vary linearly with the concentration of the compounds while the protonophoric effect of POA_T and SAL_T correlate differently with the concentration of the drugs. These results may be interpreted as a reflection of the different protonophoric mechanisms of $CCCP_T$ and SAL_T.[14,16,17,34,58] The mechanism of $CCCP_T$ (termed A^-) involves the permeation of the protonated $CCCP_N$ through the membrane, the release of the proton upon arrival to the cytoplasm and subsequent permeation of the deprotonated $CCCP_C$ through the membrane to the extracellular medium, where $CCCP_C$ is protonated into $CCCP_N$ and the cycle may begin again.[14,34,58] The mechanism exhibits the acidification of the cytoplasm commonly associated with uncouplers. Moreover, the A^- mechanism also expresses the ability of $CCCP_T$ (and other uncouplers working through the same molecular cycle) to disrupt PMF, since the mechanism is not electron neutral, changing $\Delta\Psi$ as it does ΔpH and, therefore, causing the disruption of PMF.[34] However, the uncoupling mechanism of SAL_T has been shown to be distinct from the A^- mechanism.[14,16,17] Termed AHA^-, the mechanism involves the protonated form of the uncoupler permeating the membrane and releasing a proton upon arrival to the cytoplasmic side of the membrane, just as described with the A^- mechanism. However, while in the A^- mechanism, the uncoupler was able to permeate the membrane in its deprotonated form and reach the extracellular environment, the AHA^- mechanism requires the deprotonated form to establish a complex with a protonated form of itself, forming the AHA^- complex (in the case of SAL_T, it requires the SAL_C to form a complex with a molecule of SAL_N).[14,58] The complex is then able to permeate the membrane and the deprotonated form of the uncoupler can reach the extracellular medium, available to be protonated again and to initiate a new cycle. As with the A^- mechanism, the AHA^- mechanism can theoretically explain both the acidification of the cytoplasm and the dissipation of the transmembrane electric potential, resulting in the disruption of PMF.[16,56] While the evidence for

chemical uncoupler membrane permeation is vast,[9,10,12,16,17,34] recent controversy regarding the possibility of passive diffusion of drug-like molecules may lead to different mechanisms being postulated in the future.[59] Furthermore, the difference in ability to dissipate ΔpH by $CCCP_T$ versus POA_T or SAL_T might have a different source than the one suggested above, such as different cell envelope solubility or other physical chemical or biochemical reason.

Still, all the data presented here indicates that POA_T acts with a similar mechanism to the mode of action of SAL_T.[16,17] While SAL_T has many other reported mechanisms of action,[19] the evidence presented here indicates SAL_T behaves like a protonophore in *M. tuberculosis*. Additionally, Peters and colleagues recently suggested the anti-bacterial activity of BEN_T in acidic environments is caused by the acidification of the bacterial cytosol, in a mechanism similar to a protonophore,[18] supporting the idea that the structural analogues of POA_T share a common mechanism of action. Furthermore, previous reports showed the susceptibility of *M. tuberculosis* H37Ra and *M. smegmatis* for SAL_T and BEN_T, among other weak acids.[57] The activity of SAL_T and BEN_T was also shown to exhibit sterilizing activity against *M. tuberculosis* H37Ra.[60] However, literature on the impact of SAL_T or aspirin, the pro-drug form of SAL_T used therapeutically, in TB infections is surprisingly scarce and somewhat controversial.[61–64] While PZA exhibits activity *in vivo*, the integration of the antibiotic in the standard regimen for TB infections only occurred after the discovery of the synergism between PZA and RIF_T.[36,37] Aspirin and SAL_T, however, were shown to antagonize the activity of multiple anti-tubercle drugs.[65] Still, these studies were conducted in neutral pH environments, where SAL_T is less effective, and, therefore, the real nature of the drug-drug interactions between SAL_T and other antibiotics is still unclear. Studies conducted in mice seem to agree on mild antagonism between SAL_T and INH_T, although an increase in bacterial load clearance with a combination of aspirin and INH_T was also

observed.[61] Moreover, SAL_T was shown to synergize with PZA in a murine model,[62] and evidence of improved outcome in patients undergoing treatment with PZA (plus INH_T and ethambutol) when aspirin was added to the regimen exists.[66,67]

Conclusions

The primary mechanism of action of pyrazinamide involves the disruption of proton motive force by the active form, pyrazinoic acid. The mode of action is similar to that of carbonyl cyanide *m*-chlorophenyl hydrazone or salicylic acid, behaving as a protonophore and leading to the acidification of the mycobacterial cytoplasm. Succinctly, the work presented here demonstrated that POA_T's pH-dependent activity is mimicked by its structural analogues, such as SAL_T or BEN_T, but not by other anti-tubercle drugs or by analogues with reported endogenous molecular targets, like PAS_T. The QSAR model used here supports the requirement for the formation of POA_N in the mechanistic cycle of PZA, which is equally mimicked by the analogues tested. Conversely, the other anti-tubercle drugs tested do not exhibit such requirement. Finally, the data shows how the acidification of the cytosol of *M. tuberculosis* by POA_N is replicated with $CCCP_T$ and SAL_T, but not by PAS_T, a structural analogue of POA_T with an endogenous target. The results summarized above indicate the protonophoric activity of POA_N is the mechanism responsible for the anti-tubercle activity of PZA. Moreover, the observations with the structural analogues of POA_N suggest alternatives to PZA may exist already in old pharmaceuticals, like aspirin, or in commonly used preservatives, such as benzoic acid.

Materials and Methods

The reagents used in this work were purchased from Sigma-Aldrich, except when noted. Middlebrook 7H9 broth was purchased from Becton Dickinson and albumin from GoldBio. The fluorescent dye used in the cytosolic acidification assay was obtained from Invitrogen. All reagents were used without further purification and were, at least, of reagent grade.

***Mycobacterium tuberculosis* H37Ra culture methods.** *M. tuberculosis* H37Ra cultures were grown as reported elsewhere.[7] Briefly, frozen glycerol stocks of *M. tuberculosis* H37Ra were thawed and utilized to inoculate Middlebrook 7H9 medium, which was supplemented with oleic acid-albumin-dextrose (OAD, 10% v/v), 0.1% v/v tyloxapol and 0.2% w/v casamino acids (supplemented 7H9 broth). The pH of the medium was adjusted with hydrogen chloride or sodium hydroxide, when needed. The culture flasks were incubated at 37°C, under constant agitation. Cells were harvested when an optical density of 600 nm (OD_{600}) between 0.6-0.8 was observed. Further processing of the cultures was done according to the requirements of individual assays.

pH-dependent growth inhibition of *Mycobacterium tuberculosis* H37Ra. The growth inhibition activity of anti-tubercle drugs and POA_T analogues was determined as described previously.[68] Cells of *M. tuberculosis* H37Ra were grown and harvested, with subsequent centrifugation using a Beckman CS-6R centrifuge at 1500x g and then washed with fresh culture medium (supplemented 7H9 broth). The pH of the culture medium was adjusted as described above to obtain pH values ranging from 6.4 to 7.3 in 0.3 units intervals. Cells were resuspended in culture medium at the desired pH and incubated until an OD_{600} between 0.6-0.8 was reached, as a way to acclimatize the bacilli to the pH of the medium, as described elsewhere.[7] The cells were

then harvested, centrifuged as above and washed with fresh medium at the desired pH value. Aliquots of 198 µL of resuspended cells at an OD_{600} of 0.1 were transferred to 96-well microtiter plates containing one zirconia bead per well (diameter around 1 mm) to assist with agitation and aeration. Aliquots of 2 µL of a range of concentrations of drug dissolved in dimethyl sulfoxide (DMSO) or water (for BEN_T), including an aliquot containing no drug as a blank, were added to the plate and the OD_{600} was recorded using a BioRad Benchmark Plus plate reader. The OD_{600} was determined over 5 days, with readings every 24h. Incubation between time points occurred at 37°C with constant rocking of the plates within a sealed plastic bag containing a damp paper towel to maintain humidity and prevent evaporation. Growth rates were determined by calculation of the slope of the growth curve at each time point. The calculation of the concentration required to inhibit 50% of growth was done using a non-linear 4-parameter E_{max} regression model.

Modeling uncoupling activity in *Mycobacterium tuberculosis*. Multiple QSAR models have been proposed to determine the activity of analogues of poisons or drugs. However, the impact of pH in the activity of these compounds seldom taken into consideration. Könemann and Musch derived,[33] based on the work of Tabata,[55] a model that accounts for the specific activity of each form of an ionizable compound, which is shown in Equation 4. 1. The derivation of the model is provided in the Appendix A.

$$\frac{1}{GIC_{50}} = T_N \cdot \frac{10^{-pH}}{10^{-pH}+10^{-pK_a}} + T_C \cdot \frac{10^{-pK_a}}{10^{-pH}+10^{-pK_a}} \qquad \text{Equation 4.2}$$

with GIC_{50} corresponding to the concentration to unspecified form of a compound required to inhibit 50% of growth and T_N corresponding to the inverse of the concentration of the protonated form of the compound required to cause 50% inhibition of the effect caused by the protonated form of the compound, while T_C is the inverse of the concentration of the deprotonated form of

the compound required to cause 50% inhibition of the effect caused by the deprotonated form of the compound. pH corresponds to the environmental pH at which the GIC_{50} value was obtained and pK_a corresponds to the pK_a of the protonated form of the compound.

The GIC_{50} values obtained in the drug susceptibility assay described above were fitted to the model described by Equation 4.1 with an algorithm created in R. As T_N and T_C correspond to concentrations and, therefore, have biochemical meaning, the algorithm was designed to restrain the values of the coefficients to only values equal or above zero. The coefficients obtained from the fit are reported in Table 4.1 with standard errors obtained from the fit. The coefficient of determination was calculated with the residuals of the fit and.

Effect of pyrazinoic acid on the internal pH of *Mycobacterium tuberculosis* H37Ra cells. The assessment of the internal pH of mycobacterial cells by analogues of POA_T was performed as reported previously.[7] *M. tuberculosis* H37Ra cultures were grown as described above, upon which the cells were harvested by and washed twice with MMA buffer (a mixed buffer consisting of 25mM of MES, 25mM of MOPS and 50mM of AMP, prepared as previously communicated).[7] Cells were resuspended in MMA buffer at the desired pH to an OD_{600} of 0.3 and aliquots of 196 µL were transferred into a black-walled 96-well titer plates with one zirconia bead in each well. Background fluorescence was recorded at 37°C for 10 minutes (in 2 minute intervals) on a Biotek Synergy HT (excitation at 440 nm and 485 nm and emission at 540 nm), followed by addition of 0.5 µM of 2',7'-bis-(2-carboxyethyl)-5-(and-6)-carboxyfluorescein acetoxymethyl ester (BCECF-AM) to the cells. Fluorescence was recorded for 30 minutes. Aliquots of 2 µL of

a range of concentrations of the desired analogue of POA_T dissolved in DMSO (with DMSO without drug serving as a blank) were then added to the cultures and fluorescence was recorded for another 30 minutes.

References

(1) World Health Organization. *Global Tuberculosis Report 2018*; Geneva, 2018.

(2) Zhang, Y.; Mitchison, D. The curious characteristics of pyrazinamide: a review. *Int. J. Tuberc. Lung Dis. Off. J. Int. Union Tuberc. Lung Dis.* **2003**, *7* (1), 6–21.

(3) Konno, K.; Feldmann, F. M.; McDermott, W. Pyrazinamide susceptibility and amidase activity of tubercle bacilli. *Am. Rev. Respir. Dis.* **1967**, *95* (3), 461–469. https://doi.org/10.1164/arrd.1967.95.3.461.

(4) Boshoff, H. I. M.; Mizrahi, V. Expression of *Mycobacterium smegmatis* pyrazinamidase in *Mycobacterium tuberculosis* confers hypersensitivity to pyrazinamide and related amides. *J. Bacteriol.* **2000**, *182* (19), 5479–5485. https://doi.org/10.1128/JB.182.19.5479-5485.2000.

(5) Scorpio, A.; Zhang, Y. Mutations in *pncA*, a gene encoding pyrazinamidase/nicotinamidase, cause resistance to the antituberculous drug pyrazinamide in tubercle bacillus. *Nat. Med.* **1996**, *2* (6), 662. https://doi.org/10.1038/nm0696-662.

(6) French, J. B.; Cen, Y.; Vrablik, T. L.; Xu, P.; Allen, E.; Hanna-Rose, W.; Sauve, A. A. Characterization of nicotinamidases: steady state kinetic parameters, classwide inhibition by nicotinaldehydes, and catalytic mechanism. *Biochemistry* **2010**, *49* (49), 10421–10439. https://doi.org/10.1021/bi1012518.

(7) Fontes, F. L.; Peters, B. J.; Crans, D. C.; Crick, D. C. The acid-base equilibrium of pyrazinoic acid drives the pH dependence of pyrazinamide induced *Mycobacterium tuberculosis* growth inhibition. **2019**, (submitted).

(8) Mitchell, P. Chemiosmotic coupling in oxidative and photosynthetic phosphorylation. *Biol. Rev.* **1966**, *41* (3), 445–501. https://doi.org/10.1111/j.1469-185X.1966.tb01501.x.

(9) Bakker, E. P.; Mangerich, W. E. Interconversion of components of the bacterial proton motive force by electrogenic potassium transport. *J. Bacteriol.* **1981**, *147* (3), 820–826.

(10) Booth, I. R. Regulation of cytoplasmic pH in bacteria. *Microbiol. Mol. Biol. Rev.* **1985**, *49* (4), 359–378.

(11) Hanstein, W. G. Uncoupling of oxidative phosphorylation. *Biochim. Biophys. Acta BBA - Rev. Bioenerg.* **1976**, *456* (2), 129–148. https://doi.org/10.1016/0304-4173(76)90010-0.

(12) LeBlanc, O. H. The effect of uncouplers of oxidative phosphorylation on lipid bilayer membranes: Carbonylcyanidem-chlorophenylhydrazone. *J. Membr. Biol.* **1971**, *4* (1), 227–251. https://doi.org/10.1007/BF02431973.

(13) Heytler, P. G. [58] Uncouplers of oxidative phosphorylation. In *Methods in Enzymology*; Biomembranes Part F: Bioenergetics: Oxidative Phosphorylation; Academic Press, 1979; Vol. 55, pp 462–472. https://doi.org/10.1016/0076-6879(79)55060-5.

(14) McLaughlin, S. G.; Dilger, J. P. Transport of protons across membranes by weak acids. *Physiol. Rev.* **1980**, *60* (3), 825–863. https://doi.org/10.1152/physrev.1980.60.3.825.

(15) Dilger, J.; McLaughlin, S. Proton transport through membranes induced by weak acids: A study of two substituted benzimidazoles. *J. Membr. Biol.* **1979**, *46* (4), 359–384. https://doi.org/10.1007/BF01868755.

(16) Norman, C.; Howell, K. A.; Millar, A. H.; Whelan, J. M.; Day, D. A. Salicylic Acid Is an Uncoupler and Inhibitor of Mitochondrial Electron Transport. *Plant Physiol.* **2004**, *134* (1), 492–501. https://doi.org/10.1104/pp.103.031039.

(17) Gutknecht, J. Salicylates and proton transport through lipid bilayer membranes: A model for salicylate-induced uncoupling and swelling in mitochondria. *J. Membr. Biol.* **1990**, *115* (3), 253–260. https://doi.org/10.1007/BF01868640.

(18) Peters, B. J.; Groninger, A. S.; Fontes, F. L.; Crick, D. C.; Crans, D. C. Differences in interactions of benzoic acid and benzoate with interfaces. *Langmuir* **2016**, *32* (37), 9451–9459. https://doi.org/10.1021/acs.langmuir.6b02073.

(19) Klessig, D. F.; Tian, M.; Choi, H. W. Multiple targets of salicylic acid and its derivatives in plants and animals. *Front. Immunol.* **2016**, *7*. https://doi.org/10.3389/fimmu.2016.00206.

(20) Zhang, Y.; Wade, M. M.; Scorpio, A.; Zhang, H.; Sun, Z. Mode of action of pyrazinamide: disruption of *Mycobacterium tuberculosis* membrane transport and energetics by pyrazinoic acid. *J. Antimicrob. Chemother.* **2003**, *52* (5), 790–795. https://doi.org/10.1093/jac/dkg446.

(21) Lehmann, J. Determination of pathogenicity of tubercle bacilli by their intermediate metabolism. *The Lancet* **1946**, *247* (6384), 14–15. https://doi.org/10.1016/S0140-6736(46)91184-1.

(22) Lehmann, J. *Para*-aminosalicylic acid in the treatment of tuberculosis. *The Lancet* **1946**, *247* (6384), 15–16. https://doi.org/10.1016/S0140-6736(46)91185-3.

(23) Salfinger, M.; Heifets, L. B. Determination of pyrazinamide MICs for *Mycobacterium tuberculosis* at different pHs by the radiometric method. *Antimicrob. Agents Chemother.* **1988**, *32* (7), 1002–1004. https://doi.org/10.1128/AAC.32.7.1002.

(24) Zhang, Y.; Permar, S.; Sun, Z. Conditions that may affect the results of susceptibility testing of *Mycobacterium tuberculosis* to pyrazinamide. *J. Med. Microbiol.* **2002**, *51* (1), 42–49. https://doi.org/10.1099/0022-1317-51-1-42.

(25) Peterson, N. D.; Rosen, B. C.; Dillon, N. A.; Baughn, A. D. Uncoupling environmental pH and intrabacterial acidification from pyrazinamide susceptibility in *Mycobacterium tuberculosis*. *Antimicrob. Agents Chemother.* **2015**, *59* (12), 7320–7326. https://doi.org/10.1128/AAC.00967-15.

(26) Nielson, D. W.; Goerke, J.; Clements, J. A. Alveolar subphase pH in the lungs of anesthetized rabbits. *Proc. Natl. Acad. Sci.* **1981**, *78* (11), 7119–7123. https://doi.org/10.1073/pnas.78.11.7119.

(27) Nyberg K; Johansson U; Johansson A; Camner P. Phagolysosomal pH in alveolar macrophages. *Environ. Health Perspect.* **1992**, *97*, 149–152. https://doi.org/10.1289/ehp.9297149.

(28) Effros, R. M.; Chinard, F. P. The *in vivo* pH of the extravascular space of the lung. *J. Clin. Invest.* **1969**, *48* (11), 1983–1996.

(29) Irwin, S. M.; Prideaux, B.; Lyon, E. R.; Zimmerman, M. D.; Brooks, E. J.; Schrupp, C. A.; Chen, C.; Reichlen, M. J.; Asay, B. C.; Voskuil, M. I.; et al. Bedaquiline and pyrazinamide treatment responses are affected by pulmonary lesion heterogeneity in *Mycobacterium tuberculosis* infected C3HeB/FeJ mice. *ACS Infect. Dis.* **2016**, *2* (4), 251–267. https://doi.org/10.1021/acsinfecdis.5b00127.

(30) Lanoix, J.-P.; Ioerger, T.; Ormond, A.; Kaya, F.; Sacchettini, J.; Dartois, V.; Nuermberger, E. Selective inactivity of pyrazinamide against tuberculosis in C3HeB/FeJ mice is best explained by neutral pH of caseum. *Antimicrob. Agents Chemother.* **2016**, *60* (2), 735–743. https://doi.org/10.1128/AAC.01370-15.

(31) Masuda, M.; Sato, T.; Sakamaki, K.; Kudo, M.; Kaneko, T.; Ishigatsubo, Y. The effectiveness of sputum pH analysis in the prediction of response to therapy in patients with pulmonary tuberculosis. *PeerJ* **2015**, *3*, e1448. https://doi.org/10.7717/peerj.1448.

(32) Hards, K.; McMillan, D. G. G.; Schurig-Briccio, L. A.; Gennis, R. B.; Lill, H.; Bald, D.; Cook, G. M. Ionophoric effects of the antitubercular drug bedaquiline. *Proc. Natl. Acad. Sci.* **2018**, *115* (28), 7326–7331. https://doi.org/10.1073/pnas.1803723115.

(33) Könemann, H.; Musch, A. Quantitative structure-activity relationships in fish toxicity studies (Part 2): The influence of pH on the QSAR of chlorophenols. *Toxicology* **1981**, *19* (3), 223–228. https://doi.org/10.1016/0300-483X(81)90131-1.

(34) Kasianowicz, J.; Benz, R.; McLaughlin, S. The kinetic mechanism by which CCCP (carbonyl cyanide m-chlorophenylhydrazone) transports protons across membranes. *J. Membr. Biol.* **1984**, *82* (2), 179–190. https://doi.org/10.1007/BF01868942.

(35) Lu, P.; Haagsma, A. C.; Pham, H.; Maaskant, J. J.; Mol, S.; Lill, H.; Bald, D. Pyrazinoic acid decreases the proton motive force, respiratory ATP synthesis activity, and cellular ATP levels. *Antimicrob. Agents Chemother.* **2011**, *55* (11), 5354–5357. https://doi.org/10.1128/AAC.00507-11.

(36) British Thoracic and Tuberculosis Association. Short-course chemotherapy in pulmonary tuberculosis: a controlled trial by the British Thoracic and Tuberculosis Association. *The Lancet* **1976**, *308* (7995), 1102–1104. https://doi.org/10.1016/S0140-6736(76)91085-0.

(37) British Thoracic Society. A controlled trial of six months' chemotherapy in pulmonary tuberculosis, final report: results during the 36 months after the end of chemotherapy and beyond. *Br. J. Dis. Chest* **1984**, *78*, 330–336. https://doi.org/10.1016/0007-0971(84)90165-7.

(38) Anoushiravani, M.; Falsafi, T.; Niknam, V. Proton motive force-dependent efflux of tetracycline in clinical isolates of *Helicobacter pylori*. *J. Med. Microbiol.* **2009**, *58* (10), 1309–1313. https://doi.org/10.1099/jmm.0.010876-0.

(39) Askoura, M.; Mattawa, W.; Abujamel, T.; Taher, I. Efflux pump inhibitors (EPIs) as new antimicrobial agents against Pseudomonas aeruginosa. *Libyan J. Med.* **2011**, *6* (1), 5870. https://doi.org/10.3402/ljm.v6i0.5870.

(40) Hards, K.; Robson, J. R.; Berney, M.; Shaw, L.; Bald, D.; Koul, A.; Andries, K.; Cook, G. M. Bactericidal mode of action of bedaquiline. *J. Antimicrob. Chemother.* **2015**, *70* (7), 2028–2037. https://doi.org/10.1093/jac/dkv054.

(41) Yano, T.; Kassovska-Bratinova, S.; Teh, J.-S.; Winkler, J.; Sullivan, K.; Isaacs, A.; Schechter, N. M.; Rubin, H. Reduction of clofazimine by mycobacterial type 2 NADH:Quinone oxidoreductase: A pathway for the generation of bactericidal levels of reactive oxygen species. *J. Biol. Chem.* **2010**, jbc.M110.200501. https://doi.org/10.1074/jbc.M110.200501.

(42) Winder, F. G. A.; Collins, P.; Rooney, S. A. Effects of isoniazid on mycolic acid synthesis in *Mycobacterium tuberculosis* and on its cell envelope. *Biochem. J.* **1970**, *117* (2), 27P-27P. https://doi.org/10.1042/bj1170027Pa.

(43) Takayama, K.; Wang, L.; David, H. L. Effect of isoniazid on the in vivo mycolic acid synthesis, cell growth, and viability of *Mycobacterium tuberculosis*. *Antimicrob. Agents Chemother.* **1972**, *2* (1), 29–35. https://doi.org/10.1128/AAC.2.1.29.

(44) Gangadharam, P. R. J.; Harold, F. M.; Schaefer, W. B. Selective inhibition of nucleic acid synthesis in *Mycobacterium tuberculosis* by isoniazid. *Nature* **1963**, *198* (4881), 712–714. https://doi.org/10.1038/198712b0.

(45) Wengenack, N. L.; Rusnak, F. Evidence for isoniazid-dependent free radical generation catalyzed by *Mycobacterium tuberculosis* KatG and the isoniazid-resistant mutant KatG(S315T). *Biochemistry* **2001**, *40* (30), 8990–8996. https://doi.org/10.1021/bi002614m.

(46) Timmins, G. S.; Master, S.; Rusnak, F.; Deretic, V. Requirements for nitric oxide generation from isoniazid activation in vitro and inhibition of mycobacterial respiration *in vivo*. *J. Bacteriol.* **2004**, *186* (16), 5427–5431. https://doi.org/10.1128/JB.186.16.5427-5431.2004.

(47) Shoeb, H. A.; Bowman, B. U.; Ottolenghi, A. C.; Merola, A. J. Enzymatic and nonenzymatic superoxide-generating reactions of isoniazid. *Antimicrob. Agents Chemother.* **1985**, *27* (3), 408–412. https://doi.org/10.1128/AAC.27.3.408.

(48) Sipe, H. J.; Jaszewski, A. R.; Mason, R. P. Fast-flow EPR spectroscopic observation of the isoniazid, iproniazid, and phenylhydrazine hydrazyl radicals. *Chem. Res. Toxicol.* **2004**, *17* (2), 226–233. https://doi.org/10.1021/tx0341759.

(49) Zheng, J.; Rubin, E. J.; Bifani, P.; Mathys, V.; Lim, V.; Au, M.; Jang, J.; Nam, J.; Dick, T.; Walker, J. R.; et al. *Para*-aminosalicylic acid is a prodrug targeting dihydrofolate reductase in *Mycobacterium tuberculosis*. *J. Biol. Chem.* **2013**, *288* (32), 23447–23456. https://doi.org/10.1074/jbc.M113.475798.

(50) Chakraborty, S.; Gruber, T.; Barry, C. E.; Boshoff, H. I.; Rhee, K. Y. Para-Aminosalicylic Acid Acts as an Alternative Substrate of Folate Metabolism in Mycobacterium tuberculosis. *Science* **2013**, *339* (6115), 88–91. https://doi.org/10.1126/science.1228980.

(51) Lancini, G.; Pallanza, R.; Silvestri, L. G. Relationships between bactericidal effect and inhibition of ribonucleic acid nucleotidyl-transferase by rifampicin in *Escherichia coli* K-12. *J. Bacteriol.* **1969**, *97* (2), 761–768.

(52) Bartek, I. L.; Reichlen, M. J.; Honaker, R. W.; Leistikow, R. L.; Clambey, E. T.; Scobey, M. S.; Hinds, A. B.; Born, S. E.; Covey, C. R.; Schurr, M. J.; et al. Antibiotic bactericidal activity is countered by maintaining pH homeostasis in *Mycobacterium smegmatis*. *mSphere* **2016**, *1* (4), e00176-16. https://doi.org/10.1128/mSphere.00176-16.

(53) Preiss, L.; Langer, J. D.; Yildiz, Ö.; Eckhardt-Strelau, L.; Guillemont, J. E. G.; Koul, A.; Meier, T. Structure of the mycobacterial ATP synthase Fo rotor ring in complex with the

anti-TB drug bedaquiline. *Sci. Adv.* **2015**, *1* (4), e1500106. https://doi.org/10.1126/sciadv.1500106.

(54) Haagsma, A. C.; Podasca, I.; Koul, A.; Andries, K.; Guillemont, J.; Lill, H.; Bald, D. Probing the interaction of the diarylquinoline TMC207 with its target mycobacterial ATP synthase. *PLOS ONE* **2011**, *6* (8), e23575. https://doi.org/10.1371/journal.pone.0023575.

(55) Tabata, K. Toxicity of ammonia to aquatic animals with reference to the effect of pH and carbonic acid. *Bull Tokai Reg Fish Res Lab* **1962**, *34*, 67–74.

(56) Gutknecht, J. Aspirin, acetaminophen and proton transport through phospholipid bilayers and mitochondrial membranes. *Mol. Cell. Biochem.* **1992**, *114* (1), 3–8. https://doi.org/10.1007/BF00240290.

(57) Zhang, Y.; Zhang, H.; Sun, Z. Susceptibility of *Mycobacterium tuberculosis* to weak acids. *J. Antimicrob. Chemother.* **2003**, *52* (1), 56–60. https://doi.org/10.1093/jac/dkg287.

(58) Neumcke, B.; Bamberg, E. The action of uncouplers on lipid bilayer membranes. In *Lipid bilayers and biological membranes: dynamic properties*; Dekker: New York, 1975; Vol. 3, pp 215–253.

(59) Kell, D. B.; Oliver, S. G. How drugs get into cells: tested and testable predictions to help discriminate between transporter-mediated uptake and lipoidal bilayer diffusion. *Front. Pharmacol.* **2014**, *5*. https://doi.org/10.3389/fphar.2014.00231.

(60) Wade, M. M.; Zhang, Y. Effects of weak acids, UV and proton motive force inhibitors on pyrazinamide activity against *Mycobacterium tuberculosis in vitro*. *J. Antimicrob. Chemother.* **2006**, *58* (5), 936–941. https://doi.org/10.1093/jac/dkl358.

(61) Byrne, S. T.; Denkin, S. M.; Zhang, Y. Aspirin antagonism in isoniazid treatment of tuberculosis in mice. *Antimicrob. Agents Chemother.* **2007**, *51* (2), 794–795. https://doi.org/10.1128/AAC.01145-06.

(62) Byrne, S. T.; Denkin, S. M.; Zhang, Y. Aspirin and ibuprofen enhance pyrazinamide treatment of murine tuberculosis. *J. Antimicrob. Chemother.* **2007**, *59* (2), 313–316. https://doi.org/10.1093/jac/dkl486.

(63) Eisen, D. P.; McBryde, E. S.; Walduck, A. Low-Dose Aspirin and Ibuprofen's Sterilizing Effects on Mycobacterium tuberculosis Suggest Safe New Adjuvant Therapies for Tuberculosis. *J. Infect. Dis.* **2013**, *208* (11), 1925–1927. https://doi.org/10.1093/infdis/jit476.

(64) Vilaplana, C.; Marzo, E.; Tapia, G.; Diaz, J.; Garcia, V.; Cardona, P.-J. Ibuprofen therapy resulted in significantly decreased tissue bacillary loads and increased survival in a new murine experimental model of active tuberculosis. *J. Infect. Dis.* **2013**, *208* (2), 199–202. https://doi.org/10.1093/infdis/jit152.

(65) Schaller, A.; Sun, Z.; Yang, Y.; Somoskovi, A.; Zhang, Y. Salicylate reduces susceptibility of *Mycobacterium tuberculosis* to multiple antituberculosis drugs. *Antimicrob. Agents Chemother.* **2002**, *46* (8), 2636–2639. https://doi.org/10.1128/AAC.46.8.2636-2639.2002.

(66) Horsfall, P. A. L.; Plummer, J.; Allan, W. G. L.; Girling, D. J.; Nunn, A. J.; Fox, W. Double blind controlled comparison of aspirin, allopurinol and placebo in the management of arthralgia during pyrazinamide administration. *Tubercle* **1979**, *60* (1), 13–24. https://doi.org/10.1016/0041-3879(79)90051-5.

(67) Schoeman, J. F.; Janse van Rensburg, A.; Laubscher, J. A.; Springer, P. The role of aspirin in childhood tuberculous meningitis. *J. Child Neurol.* **2011**, *26* (8), 956–962. https://doi.org/10.1177/0883073811398132.

(68) Gruppo, V.; Johnson, C. M.; Marietta, K. S.; Scherman, H.; Zink, E. E.; Crick, D. C.; Adams, L. B.; Orme, I. M.; Lenaerts, A. J. Rapid microbiologic and pharmacologic evaluation of experimental compounds against *Mycobacterium tuberculosis*. *Antimicrob. Agents Chemother.* **2006**, *50* (4), 1245–1250. https://doi.org/10.1128/AAC.50.4.1245-1250.2006.

Chapter 5

Salicylic acid replicates the drug-drug interactions of pyrazinoic acid with other anti-tubercle drugs

Pyrazinamide (PZA) is a first-line anti-tubercle drug, despite its addition to the standard regiment in the treatment of tuberculosis (TB) infections happening decades after its discovery as an anti-mycobacterial agent.[1] Against *Mycobacterium tuberculosis*, the etiological cause of TB infections, the *in vitro* activity of PZA was shown to be pH-dependent, the mechanism of which was recently reported as depending on the protonophoric activity of pyrazinoic acid (POA), PZA's active form.[2] Additionally, PZA is known to synergize with rifampin (RIF),[3] another first-line antibiotic, reducing the standard time of treatment in half.[4,5] PZA was also shown to synergize with second-line antibiotic and it is currently part of most regimens for multi- and extensive-drug resistant TB infections.[6,7] However, despite the recent elucidation on the mechanism of action of PZA,[2] the mechanism behind the synergism with RIF is still unknown. Moreover, the behavior of PZA (or its active form, POA) in combination has seldom been described *in vitro*, in particular when its pH-dependence is taken into consideration.[8]

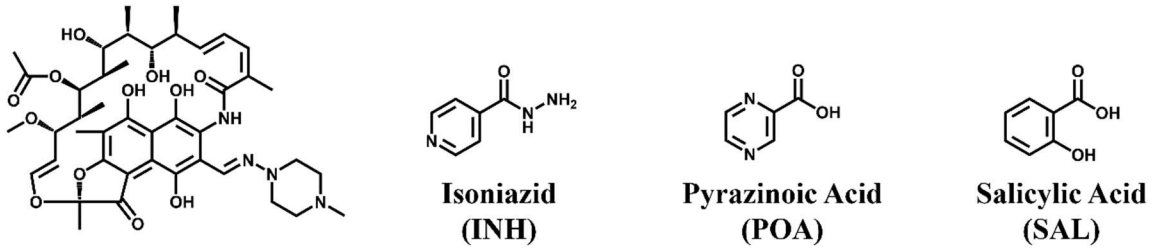

Figure 5.1 – Structures of anti-mycobacterial drugs used.

Salicylic acid (SAL), the active form of aspirin, is a structural analogue of POA (Figure 5.1) and acts in a similar manner to POA against *M. tuberculosis in vitro*.[2] Additionally, SAL enhances the recovery of patients with TB infections.[9] The activity of SAL against *M. tuberculosis* was also reported in a mouse model.[10] However, the study of SAL's interactions with other anti-tubercle drugs is scarce. In a murine model, SAL was shown to be antagonistic with isoniazid (INH), another first-line antibiotic used in TB infections.[11] Given the recent evidence that SAL is more potent than POA *in vitro* and the widespread use and availability of multiple approved formulations of it, SAL is a potential new agent against *M. tuberculosis* infections.

The synergism shown by PZA with other drugs is a type of drug-drug interaction, which also includes concepts of additivism and antagonism. Strict definitions of these terms are still subject to much debate,[12] but it is generally accepted that synergy expresses an increased effect of a combination of treatments that is not simply explained by the addition of the effects of the treatments alone. Similarly, antagonism is defined in opposition to synergy, as the overall effect of the treatments in combination decreases compared to the expected addition of effects of these treatments alone. Additivism is, therefore, when the effects of the drugs do not overlap, as the effect of the combination is what is expected of the addition of the effects of the single treatments.[12] However, multiple methods of determining what typo of drug-drug interaction occurs in a given combination have been proposed.[12–15] Of these, the median effect principle (MEP) method has seen wide use in the biomedical field, in particular in cancer research.[16] The MEP method was derived through biochemical principles, stemming from the mass-action law.[17] It was also shown to contain the four major equations in the biomedical field (the Michaelis-Menten equation, the Henderson-Hasselbalch equation, the Hill equation and the Scatchard equation) and claims have been put forward that the MEP equation provides an unified theory for dose-effect phenomena.[13]

However, the expansion of the MEP equation to allow drug combinations is still its most widely used application.[16] The MEP method also allows for determination of the type of interaction in a combination for the duration of the effect (expressed as a factor f_a, standing for fraction affected). For long duration regimens, such as the standard combination therapy used in TB infections, the interactions in a combination can vary over time and understanding how the combination interactions evolve throughout the treatment provides an advantage other methods of determining drug-drug interactions lack.[13] Thus, the present work aims to understand the interaction between POA or SAL, both reported to act through the same mechanism against *M. tuberculosis*, and RIF or INH, standard drugs in the treatment of TB, using the MEP method.

Results

Median effect principle of anti-tubercle drugs combination. Pairwise combinations between POA or SAL and RIF or INH were studied using checkerboard assays. The use of the checkerboard design allows for the generation of growth rates when the culture is exposed to different molar ratios of the combination of drugs.[18] For the extent of the work presented here, the results shown reflect the analysis of the ratio of POA or SAL to INH of 300:1 and the ratio of POA or SAL to RIF of 5200:1, which were chosen because these ratios provide the highest number of points in the checkerboard setup used. Other ratios were also analyzed with similar observations to the ones reported for the ratios indicated above (data not shown).

Figure 5.2 shows the MEP plot, first described by Chou and Talalay,[17] for the drug combinations used in the present work at pH 6.4. The results for the other pH environments tested

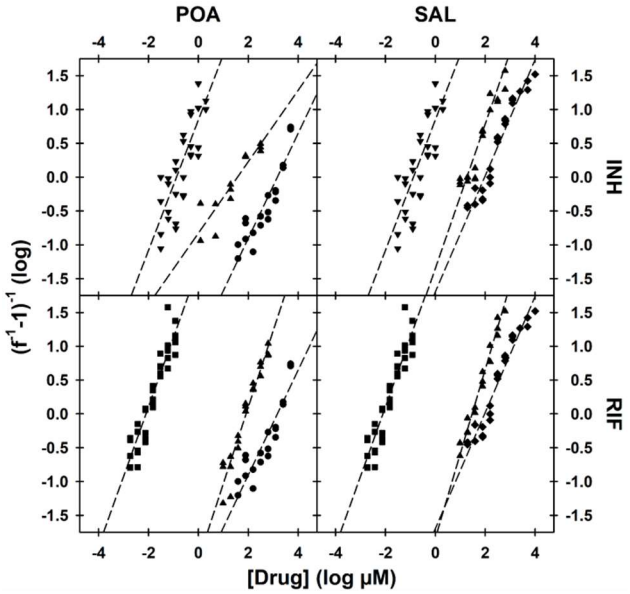

Figure 5.2 – Median effect principle plot of the drug combinations (pH 6.4). The growth rates obtained from the checkerboard assays were converted to fraction of the system affected (f_a) by dividing the growth rate of the specific concentration by the growth rate of the untreated control (DMSO blank) and subtracting this value from 1. The linearization of the data points followed Equation 5.3 (see Materials and Methods). The results shown are similar to the ones obtained when the pH of the medium was 6.7 or 7.0 and the results shown are the collection of three independent replicates. Downward triangles represent the treatment of INH alone, circles correspond to POA alone, diamonds refer to SAL alone and squares signify RIF alone. Upward triangles represent the combination treatment of the pair of compounds tested in each quadrant at specific molar ratios.

(6.7 and 7.0) is similar (data not shown), with the main difference corresponding with a translation of the POA or SAL curve to reflect the decrease in efficacy. The MEP plot enables the calculation of the median effect coefficients that determine dose-effect curves: the median effect (akin to an IC_{50} or an MIC_{50}) and the shape of the curve, which is given by the slope of the curve (see the derivation of Equation 5.3 in the Materials and Methods section). The data points represented with triangles in each quadrant represent the combination of the two drugs, while the other two curves correspond to treatment with each drug in the combination used alone. Mechanistic inference is possible with the MEP plot: as the curve of the combination of all pairs shown in Figure 5.2 is not parallel to the curves of the drugs of the combination alone, Chou and Talalay report the drugs in the combination have mutually non-exclusive mechanisms, which implies different targets. The

observations is supported by the reported mechanism of action of RIF, INH, POA and SAL in *M. tuberculosis*.[2,19–22]

Synergy index of drug combinations. The coefficients obtained from the MEP are used to simulate the behavior of the molar ratios of the combinations tested as a function of f_a, as previously described.[13,17] The simulation, obtained from Equation 5.6 (derived in the Materials and Methods section), allows to determine the combination at different stages of the growth inhibition. As f_a represents the fraction of growth inhibition obtained by the drug combination used, with 1 being complete inhibition, the results shown in Figure 5.3 demonstrate how the different pairwise combination tested in the present work act from no inhibition to complete growth inhibition. The grey areas represented in Figure 3 arise from a conservative estimation of the additivity region and were adapted from the semi-quantitative numbers suggested by Chou elsewhere.[13]

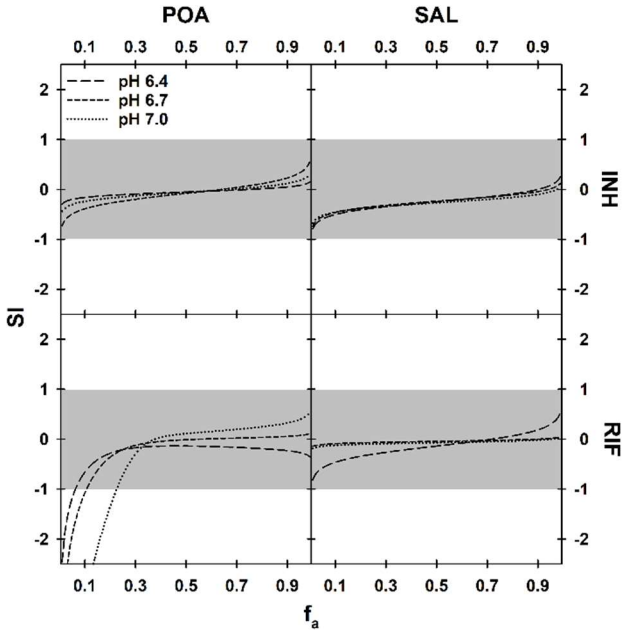

Figure 5.3 – Synergy index plot of the combinations at different pH environments. The synergy index values were obtained through Equation 5.5 and Equation 5.6 (Materials and Methods), from the coefficients obtained with the median effect principle equation (Equation 5.3). The area shaded in grey corresponds to the conservative region of additive effect.

The combinations shown in Figure 5.3 are consistently additive in their effect in growth inhibition. The combination of POA with RIF shows some antagonism at lower stages of the growth inhibition (low f_a) but becomes additive after about 10-20% of the effect occurs. The rest of the combinations (POA/INH, SAL/INH and SAL/RIF) are additive across all values of f_a. The combinations using SAL are similar to the combinations using POA. Additionally, despite the pH-dependent activity of both POA and SAL,[2,23] no pH-dependent drug-drug effect is observed.

Discussion

Median effect principle of anti-tubercle drugs combination. Multiple methodologies to determine, quantitatively or qualitatively, drug-drug interactions have been proposed over the years.[12] Traditionally, the fractional inhibitory concentration (FIC) method has been used to study the interactions of anti-tubercle drugs. The FIC method provides an easy, quick and conservative way to estimate synergism *in vitro*,[18,24] despite arguments that the FIC method conservative ranges of additivity are too conservative and lead to cases of synergism being qualified as additive.[25]

However, the correlation between *in vitro* drug-drug interactions and the effect of combinations *in vivo* was previously shown to be more accurate when more conservative estimations were used.[26] While the FIC method is widely used in microbiology, other methods have found success and extensive use in medicine, in particular the MEP method. Proposed by Chou and Talalay,[17] the MEP method stems from the biochemical mass-action law, while most other methods used to estimate drug-drug interactions have an empirical or merely statistical root.[12] The biochemical origin of the MEP method allows for some inferences on the mechanistic natures of the drugs in the combination,[16] which may help in cases where the targets of the drugs studied are not properly characterized.[17] Furthermore, the MEP method allows the analysis of the

combination across all stages of the effect (expressed by f_a), which, while possible with the FIC method, can be technically difficult.[17] Additionally, while it was not the approach used in the present work, the MEP method can theoretically be used with a low number of data points, with Chou arguing it can be used by determining the effect of two unique concentrations of the combination (if the effect of the individual drugs is known).[13] The advantages provided by the MEP method in the determination of drug-drug interactions were the reason for its use in the present work instead of the more traditional FIC method.

Figure 5.2 shows the MEP plot of the combinations tested in the present work. The linear regressions of the data points permit the determination of the MEP coefficients, in particular the median effect concentration of each drug when administered alone and of the combination. The results shown in Figure 5.2 correspond to the study of the combinations when the medium of the culture was at pH 6.4, but other pH environments where tested to obtain the MEP coefficients (pH 6.7 and pH 7.0). Different pH environments were employed given the pH-dependent activity of POA and SAL (while RIF and INH were shown to exhibit no such dependence, which supported the observations of the present work).[2] The median effect concentrations of the drugs tested, when used alone, were similar to the values reported elsewhere.[2]

Chou and Talalay derived the MEP and postulated the MEP plot also indicates the type of interaction between the drugs in the combination: either mutually exclusive (as expected in Loewe additivity) or mutually non-exclusive (which, they argue, produces an interaction in line with Bliss independence).[17] A mutually exclusive combination indicates that the drugs in the combination affect the same target and the MEP plot reflects this type of combination when the linear regression of all treatments shown (all drugs alone and the combination) are parallel. In cases where the curves of the drugs when administered alone are parallel, but the curve of the combination is not

parallel to the others, Chou and Talalay conclude the combination is mutually non-exclusive. As the results shown in Figure 5.2 indicate, the POA or SAL combined with INH or RIF behave as a mutually non-exclusive combination at pH 6.4 (the same was observed for pH 6.7 and 7.0, data not shown). Greco and colleagues presented a critique to the derivation of Chou and Talalay for mutual non-exclusive combinations, arguing that Chou's and Talalay's derivation only applies when the slope of the combination equals 1.[12] However, in the case presented here, the slopes of all combinations, regardless of the pH, is 0.95 ± 0.18, which is within the error allowed by the Chou-Talalay derivation for a strict mutually non-exclusive interaction.[17] Additionally, the different mechanisms of action of RIF, INH and POA (or SAL) imply mutually non-exclusive interactions for the combinations tested. As such, for further analysis of the drug-drug interactions of the combinations tested here, the present work assumed the combinations behaved as mutually non-exclusive combinations.

Synergy index of drug combinations. The synergy index (SI) is an extension on the concept of the previously derived combination index (CI, partially derived in the Materials and Methods section).[17] The CI is used to describe the type of interaction of a combination of drugs as synergistic, antagonistic or additive.[16] Derived from the MEP, and, therefore, conforming to the mass-action law, the CI allows the determination of the impact of different treatments in combination, including when the treatments are not chemical (such as the case of the impact of radiation treatments in anti-cancer chemotherapeutics).[13] The CI plot (versus f_a) was also shown to replicate the results of more traditional methodologies, like the construction of isobolograms, to determine synergism.[13,16] The CI plot provides a simple visual representation of the combination behavior across the range of the effect (represented by f_a), with strict ranges for each type of

interaction: CI below 1 for synergism, equal to 1 for additivism and above 1 for antagonism.[17] The asymmetrical ranges complicate the analysis of CI plots, mainly when comparisons between the amplitude of synergism and antagonism are drawn. To simplify the analysis, the present work proposes the use of the negative common logarithm of CI. If a strict interpretation of CI was taken, the factor resulting of the logarithmic transformation (seen in Equation 5.6, in the Materials and Methods section), called synergy index (SI), allows for symmetrical values of synergy and antagonism, with additivism corresponding to a SI value of 0, positive values corresponding to synergism and negative values to antagonism. However, as suggested for CI values, more conservative intervals can be applied, to account for experimental error or the complexity of the systems studied that add variability to the results.[13] The present work considered any value of SI between -1 and 1 as representing additivism, with values below -1 reflecting antagonism and values above 1 synergism.

Figure 5.3 shows the SI plot of the combinations tested in the present work, at the different pH values used. The results indicate that, using the conservative ranges defined above, POA in combination with either INH or RIF exhibits additivity for all the values of f_a (when in combination with INH) or for the majority of the effect (as seen with RIF). The different pH values had no impact on the interaction of POA with INH; when POA is in combination with RIF, the interaction exhibits some pH-dependence, but the type of interaction does not change dramatically. Additionally, the results shown in Figure 5.3 correspond to specific molar ratios (300:1 with INH and 5200:1 with RIF), but other ratios were analyzed, with comparable results (data not shown). The *in vitro* drug-drug interactions of PZA (or its active form, POA) with INH or RIF have seldom been reported in literature, but the results presented here do not reflect the interactions reported for *in vivo* synergism between RIF and PZA,[3,4] while antagonism was been reported for INH when

used in combination with PZA in the mouse model.[27] Antagonism between POA and INH were also previously reported *in vitro*, in cultures at acidic pH (5.6).[8]

Similarly, Figure 5.3 also presents the results obtained for the combinations of SAL with INH or RIF. For both combinations, the results indicate additivism across all values of f_a, with no significant pH-dependent effect observable. When compared together, the combinations with POA and with SAL are comparable, as was expected given their similar mechanism of action.[2] As with POA, while the results shown in Figure 5.3 correspond only to fixed molar rations (300:1 with INH and 5200:1 with RIF), other concentration ratios were analyzed and produced similar results (data not shown). Reports on anti-tubercle combinations including SAL are scarce, but one report suggests SAL antagonizes with INH and RIF *in vitro*.[28] Additionally, SAL and INH were shown to be mildly antagonistic in a mouse model,[11] although SAL (given as aspirin) was shown to improve the outcome of patients treated for tuberculosis with a combination of PZA, INH and ethambutol.[29,30] However, SAL remains a candidate for potential substitution of PZA, as it was recently shown to act against *M. tuberculosis* through the same mechanism as POA, the active form of PZA.[2] Moreover, SAL was shown to have anti-tubercle effects in the murine model before.[9] As described above, PZA has been shown to synergize with RIF *in vivo*, both in animal models and patients,[3,4] but POA was shown here to be mildly antagonistic or purely additive when in combination with RIF. It is possible the same happens with SAL and, either by an effect only possible in the host or some other physiological mechanism, the drug-drug interactions of SAL with RIF (or even INH) are distinct in animal models from the ones reported here for an *in vitro* model.

The work presented here determined the drug-drug interactions in the context of growth inhibition *in vitro*. The methodology used cannot distinguish between live cells and dead cells in

the culture medium, as optical density is only a measurement of light scattering and dead cells scatter light as live cells do. Moreover, synergy assays conducted *in vivo* determine bacterial clearance instead of growth inhibition.[3] Hence, the conflicting accounts of synergism between the data shown above and the reported for PZA *in vivo* may be explained by the methodologies used. The similar behavior of SAL and POA *in vitro*, however, suggests the possibility of similar behavior *in vivo* and, therefore, the use of a delivery formulation of SAL may be possible to treat tuberculosis.

Conclusions

The *in vitro* drug-drug interactions of salicylic acid with anti-tubercle compounds, rifampin and isoniazid, are similar to those seen with pyrazinoic acid, the active form of pyrazinamide. Briefly, the work presented here showed how the combinations of pyrazinoic acid or salicylic acid with rifampin or isoniazid behave in a mutually non-exclusive, confirming the combination results from the two individual drugs in the combination acting through different molecular mechanisms. Moreover, the median effect concentrations are comparable with growth inhibitory concentrations reported previously, supporting the use of the median effect principle to determine drug-drug interaction in *M. tuberculosis*. The present work also introduces the synergy index, a numerical value to evaluate drug-drug interactions. The synergy index of the combinations tested here show mostly additivism, suggesting that combinations containing pyrazinoic acid behave similarly to the combinations with salicylic acid. The conservative analysis of drug-drug interactions shown here suggests interaction seen *in vivo* with pyrazinamide (or with its active form, pyrazinoic acid) can be replicated with salicylic acid, which indicates salicylic acid is a potential alternative to pyrazinamide.

Materials and Methods

The chemicals used in the present work were purchased from Sigma Aldrich, except when specified otherwise. Albumin was obtained from GoldBio and Middlebrook 7H9 broth from Becton Dickinson. All reagents were of reagent grade or higher and were used without further purification.

***Mycobacterium tuberculosis* H37Ra culture methods.** *M. tuberculosis* H37Ra cultures were grown as previously reported.[23] Succinctly, frozen glycerol stocks of *M. tuberculosis* H37Ra were thawed and used to inoculate fresh Middlebrook 7H9 medium supplemented with oleic acid-albumin-dextrose (OAD, 10% v/v), 0.1% v/v tyloxapol and 0.2% w/v casamino acids. The pH of the supplemented 7H9 broth was adjusted with hydrogen chloride or sodium hydroxide as needed. Culture flasks were incubated with constant agitation at 37°C and cells were harvested when an optical density at 600 nm (OD_{600}) between 0.6-0.8 was observed. The cells were further processed according to the requirements of the checkerboard assays.

Checkerboard assays to determine drug-drug interactions between anti-tubercle drugs in *M. tuberculosis* H37Ra. Checkerboard assays were designed and executed as described before.[18] *M. tuberculosis* H37Ra cultures were grown as described above and cells harvested and washed twice with fresh supplemented 7H9 medium. The mycobacterial cells were then centrifuged at 1500 x g on a Beckman CS-6R centrifuge and resuspended in fresh supplemented 7H9 medium at the desired pH to achieve an OD_{600} of 0.1. Aliquots of 196 µL of cell suspension were then transferred to 96-well microtiter plate with each well containing a zirconia bead (diameter ~1 mm) to assist with agitation and aeration. Aliquots of 2 µL of a range of concentrations of the desired

drugs dissolved in dimethyl sulfoxide (DMSO) were prepared and transferred to the microtiter plate, generating a gradient where each well has a unique combination of concentrations of the two drugs. This was produced by adding the range of concentrations of one drug horizontally (right left) and the range of concentrations of the other drug vertically (up down). A blank (no drugs) well was generated by addition of aliquots of 2 µL of DMSO twice. Each pairwise combination was tested in triplicate. The OD_{600} of the plate was then recorded every 24 hours, for 5 days, using a BioRad Benchmark Plus plate reader. Between measurements, the plates were incubated at 37°C with constant rocking, within a sealed plastic bag with a damp paper towel to preserve humidity. The growth rate of each individual treatment was calculated as the slope of the growth curve over the 5 days of incubation. The growth rates were utilized to posterior analysis of the drug-drug interactions between each pair of drugs, as described below.

Median effect principle analysis. The median effect principle (MEP) was first proposed and derived by Chou and Talalay.[17] The method describes the general theory for dose and effect, based on the mass-action law principle.[13] The MEP stems from the correlation shown in Equation 5.1:

$$\frac{f_a}{f_u} = \left(\frac{D}{D_M}\right)^m \qquad \text{Equation 5.1}$$

where D represents the dose of the substance tested, f_a the fraction of the system affected by D and f_u the fraction of the system unaffected by the substance dose. The median-effect dose, D_M, stands for the dose that causes the median-effect (such as an IC_{50}, a MIC_{50} or a LD_{50}). The exponent m controls the shape of the effect curve, which can be hyperbolic (m = 1), sigmoidal (m > 1) or a flat sigmoid (m < 1).[13] As $f_a + f_u = 1$, Equation 5.1 can be expressed as:

$$\frac{f_a}{1-f_a} = \left(\frac{D}{D_M}\right)^m \qquad \text{Equation 5.2}$$

In the present work, f_a was calculated by finding the value of f_u first, which was determined by dividing the growth rate of each point by the growth rate of the untreated well (DMSO control), for each replicate and each drug combination. Then, f_a was obtained by subtracting the calculated f_u from one. To facilitate the calculation of D_M and m, Chou and Talalay suggest a linearization method,[17] as shown by Equation 5.3:

$$\log_{10}\left(\frac{f_a}{1-f_a}\right) = m \cdot \log_{10}(D) - m \cdot \log_{10}(D_M) \qquad \text{Equation 5.3}$$

Moreover, the linear plot defined by Equation 5.3 has interesting properties, when combinations of drugs are considered, as will be explored below.

The recent elucidation of the mechanism of action of POA makes clear that, when used in combination with RIF or INH, the drug-drug interaction is mutually non-exclusive, given the different mechanism of action of the drugs.[2,19–22] Similarly, SAL was shown to act as a protonophore in *M. tuberculosis* and, as such, behaves like POA when used in combination with RIF or INH.[2] Chou and Talalay describe how the different targets can be inferred from the graphical representation of Equation 3.[17] They describe how the curve of a mutually exclusive combination should be parallel to the curves of each drug in the combination when used alone. However, when the combination is mutually non-exclusive, i.e. each drug acts independently and, therefore, has a distinct target, the linear curve of the combination is not parallel to the curves of the drugs in the combination when used independently. Furthermore, the purely additive interaction between two mutually non-exclusive drugs is defined by Equation 5.4:[17]

$$\frac{D_A}{(D_M)_A} + \frac{D_B}{(D_M)_B} + \frac{D_A \cdot D_B}{(D_M)_A \cdot (D_M)_B} = 1 \qquad \text{Equation 5.4}$$

with D_A and D_B corresponding to the dose of drugs A and B, respectively, and $(D_M)_A$ and $(D_M)_B$ the median-effect dose of drugs A and B. If the resulting value of Equation 4 is below 1, then the

combination is synergistic and, conversely, if the value is above 1, the drugs are antagonistic. Hence, a combination index (CI) can be expressed as shown in Equation 5.5:

$$\mathrm{CI} = \frac{\mathrm{D_A}}{(\mathrm{D_\%})_\mathrm{A}} + \frac{\mathrm{D_B}}{(\mathrm{D_\%})_\mathrm{B}} + \frac{\mathrm{D_A \cdot D_B}}{(\mathrm{D_\%})_\mathrm{A} \cdot (\mathrm{D_\%})_\mathrm{B}} \qquad \text{Equation 5.5}$$

where $(D_\%)_A$ and $(D_\%)_B$ stand for the effect caused by drug A and B, respectively, at a given value of f_a (or a given percentage of the system affected), as derived by Chou and Talalay.[17]

Graphically, a plot of CI versus f_a shows the behavior of a given combination over the range of f_a values. However, the areas of antagonism (from >1 to infinite) and synergy (<1 to 0) are not symmetrical and having the "midpoint" between the antagonism and synergy at 1 is also not intuitive. To solve these issues, the present work proposes the use of the synergism index (SI), where the logarithmic transformation shown in Equation 5.6 is applied to CI.

$$\mathrm{SI} = -\log_{10} \mathrm{CI} \qquad \text{Equation 5.6}$$

The use of SI makes the graphical representation more intuitive and the synergy and antagonism areas are symmetrical. As such, the graph of SI versus f_a shows additivity when SI equals 0. For values of SI above 0 the interaction is synergistic while for values below 0 the interaction is antagonistic. However, the granularity of the data obtained through the checkerboard assay described above is low and, as in other method using checkerboard assays,[18] the present work opted to define the limits of additivity as more conservative, following the suggestions previously described by Chou.[13] As such, additive interactions are defined as interaction with a SI value between -1 and 1, with synergy and antagonism being defined by SI values above 1 or below -1, respectively.

References

(1) Zhang, Y.; Mitchison, D. The curious characteristics of pyrazinamide: a review. *Int. J. Tuberc. Lung Dis. Off. J. Int. Union Tuberc. Lung Dis.* **2003**, *7* (1), 6–21.

(2) Fontes, F. L.; Rooker, S. A.; Lynn-Barbe, J. K.; Crans, D. C.; Crick, D. C. Pyrazinoic acid mimics the activity of protonophores against *Mycobacterium tuberculosis*. **2019**, (in preparation).

(3) Tasneen, R.; Tyagi, S.; Williams, K.; Grosset, J.; Nuermberger, E. Enhanced bactericidal activity of rifampin and/or pyrazinamide when combined with PA-824 in a murine model of tuberculosis. *Antimicrob. Agents Chemother.* **2008**, *52* (10), 3664–3668. https://doi.org/10.1128/AAC.00686-08.

(4) British Thoracic and Tuberculosis Association. Short-course chemotherapy in pulmonary tuberculosis: a controlled trial by the British Thoracic and Tuberculosis Association. *The Lancet* **1976**, *308* (7995), 1102–1104. https://doi.org/10.1016/S0140-6736(76)91085-0.

(5) British Thoracic Society. A controlled trial of six months' chemotherapy in pulmonary tuberculosis, final report: results during the 36 months after the end of chemotherapy and beyond. *Br. J. Dis. Chest* **1984**, *78*, 330–336. https://doi.org/10.1016/0007-0971(84)90165-7.

(6) World Health Organization. *Global Tuberculosis Report 2018*; Geneva, 2018.

(7) World Health Organization. *WHO Consolidated Guidelines on Drug-Resistant Tuberculosis Treatment*; Geneva, 2019.

(8) Dickinson, J. M.; Aber, V. R.; Mitchison, D. A. Bactericidal activity of streptomycin, isoniazid, rifampin, ethambutol, and pyrazinamide alone and in combination against *Mycobacterium tuberculosis*. *Am. Rev. Respir. Dis.* **2015**. https://doi.org/10.1164/arrd.1977.116.4.627.

(9) Vilaplana, C.; Marzo, E.; Tapia, G.; Diaz, J.; Garcia, V.; Cardona, P.-J. Ibuprofen therapy resulted in significantly decreased tissue bacillary loads and increased survival in a new murine experimental model of active tuberculosis. *J. Infect. Dis.* **2013**, *208* (2), 199–202. https://doi.org/10.1093/infdis/jit152.

(10) Byrne, S. T.; Denkin, S. M.; Zhang, Y. Aspirin and ibuprofen enhance pyrazinamide treatment of murine tuberculosis. *J. Antimicrob. Chemother.* **2007**, *59* (2), 313–316. https://doi.org/10.1093/jac/dkl486.

(11) Byrne, S. T.; Denkin, S. M.; Zhang, Y. Aspirin antagonism in isoniazid treatment of tuberculosis in mice. *Antimicrob. Agents Chemother.* **2007**, *51* (2), 794–795. https://doi.org/10.1128/AAC.01145-06.

(12) Greco, W. R.; Bravo, G.; Parsons, J. C. The search for synergy: a critical review from a response surface perspective. *Pharmacol. Rev.* **1995**, *47* (2), 331–385.

(13) Chou, T.-C. Theoretical basis, experimental design, and computerized simulation of synergism and antagonism in drug combination studies. *Pharmacol. Rev.* **2006**, *58* (3), 621–681. https://doi.org/10.1124/pr.58.3.10.

(14) Breitinger, H.-G. Drug synergy: mechanisms and methods of analysis. *Toxic. Drug Test.* **2012**. https://doi.org/10.5772/30922.

(15) Tallarida, R. J. Quantitative methods for assessing drug synergism. *Genes Cancer* **2011**, *2* (11), 1003–1008. https://doi.org/10.1177/1947601912440575.

(16) Chou, T.-C. Drug combination studies and their synergy quantification using the Chou-Talalay method. *Cancer Res.* **2010**, 0008-5472.CAN-09–1947. https://doi.org/10.1158/0008-5472.CAN-09-1947.

(17) Chou, T.-C.; Talalay, P. Quantitative analysis of dose-effect relationships: the combined effects of multiple drugs or enzyme inhibitors. *Adv. Enzyme Regul.* **1984**, *22*, 27–55. https://doi.org/10.1016/0065-2571(84)90007-4.

(18) Ramón-García, S.; Ng, C.; Anderson, H.; Chao, J. D.; Zheng, X.; Pfeifer, T.; Av-Gay, Y.; Roberge, M.; Thompson, C. J. Synergistic drug combinations for tuberculosis therapy identified by a novel high throughput screen. *Antimicrob. Agents Chemother.* **2011**, AAC.00474-11. https://doi.org/10.1128/AAC.00474-11.

(19) Lancini, G.; Pallanza, R.; Silvestri, L. G. Relationships between bactericidal effect and inhibition of ribonucleic acid nucleotidyl-transferase by rifampicin in *Escherichia coli* K-12. *J. Bacteriol.* **1969**, *97* (2), 761–768.

(20) Winder, F. G. A.; Collins, P.; Rooney, S. A. Effects of isoniazid on mycolic acid synthesis in *Mycobacterium tuberculosis* and on its cell envelope. *Biochem. J.* **1970**, *117* (2), 27P-27P. https://doi.org/10.1042/bj1170027Pa.

(21) Gangadharam, P. R. J.; Harold, F. M.; Schaefer, W. B. Selective inhibition of nucleic acid synthesis in *Mycobacterium tuberculosis* by isoniazid. *Nature* **1963**, *198* (4881), 712–714. https://doi.org/10.1038/198712b0.

(22) Wengenack, N. L.; Rusnak, F. Evidence for isoniazid-dependent free radical generation catalyzed by *Mycobacterium tuberculosis* KatG and the isoniazid-resistant mutant KatG(S315T). *Biochemistry* **2001**, *40* (30), 8990–8996. https://doi.org/10.1021/bi002614m.

(23) Fontes, F. L.; Peters, B. J.; Crans, D. C.; Crick, D. C. The acid-base equilibrium of pyrazinoic acid drives the pH dependence of pyrazinamide induced *Mycobacterium tuberculosis* growth inhibition. **2019**, (submitted).

(24) Hsieh, M. H.; Yu, C. M.; Yu, V. L.; Chow, J. W. Synergy assessed by checkerboard: a critical analysis. *Diagn. Microbiol. Infect. Dis.* **1993**, *16* (4), 343–349. https://doi.org/10.1016/0732-8893(93)90087-N.

(25) Berenbaum, M. C. Correlations between methods for measurement of synergy. *J. Infect. Dis.* **1980**, *142* (3), 476–478. https://doi.org/10.1093/infdis/142.3.476.

(26) Chadwick, E. G.; Shulman, S. T.; Yogev, R. Correlation of antibiotic synergy *in vitro* and *in vivo*: use of an animal model of neutropenic gram-negative sepsis. *J. Infect. Dis.* **1986**, *154* (4), 670–675. https://doi.org/10.1093/infdis/154.4.670.

(27) Almeida, D.; Nuermberger, E.; Tasneen, R.; Rosenthal, I.; Tyagi, S.; Williams, K.; Peloquin, C.; Grosset, J. Paradoxical effect of isoniazid on the activity of rifampin-pyrazinamide combination in a mouse model of tuberculosis. *Antimicrob. Agents Chemother.* **2009**, *53* (10), 4178–4184. https://doi.org/10.1128/AAC.00830-09.

(28) Schaller, A.; Sun, Z.; Yang, Y.; Somoskovi, A.; Zhang, Y. Salicylate reduces susceptibility of *Mycobacterium tuberculosis* to multiple antituberculosis drugs. *Antimicrob. Agents Chemother.* **2002**, *46* (8), 2636–2639. https://doi.org/10.1128/AAC.46.8.2636-2639.2002.

(29) Horsfall, P. A. L.; Plummer, J.; Allan, W. G. L.; Girling, D. J.; Nunn, A. J.; Fox, W. Double blind controlled comparison of aspirin, allopurinol and placebo in the management of arthralgia during pyrazinamide administration. *Tubercle* **1979**, *60* (1), 13–24. https://doi.org/10.1016/0041-3879(79)90051-5.

(30) Schoeman, J. F.; Janse van Rensburg, A.; Laubscher, J. A.; Springer, P. The role of aspirin in childhood tuberculous meningitis. *J. Child Neurol.* **2011**, *26* (8), 956–962. https://doi.org/10.1177/0883073811398132.

Chapter 6

Concluding Remarks

Tuberculosis continues to be the cause of millions of deaths every year. With the rise in cases of multi- and extensive-drug resistant patients, the importance of understanding the infection and the anti-tubercle drugs available becomes more dramatic. Pyrazinamide, part of the standard treatment regimen and of most of the drug combination regimens available for resistant cases,[2] is an antibiotic like few. Despite the discovery of its anti-mycobacterial properties in the 1950s, its molecular target was unclear until now. The work presented here conclusively shows pyrazinamide acts as uncoupler of proton motive force. After entering the mycobacterial bacillus, pyrazinamide undergoes enzymatic conversion to pyrazinoate. Until now, the ultimate fate of pyrazinoate was unknown. The results described above demonstrate that pyrazinoate leaves the cell and, in the more acidic extracellular environment, enters in an acid-base equilibrium with pyrazinoic acid. The difference between both forms is only a single proton, but like other uncouplers, the entry of pyrazinoic acid and release of that proton is part of a cycle that leads to cytosolic acidification. The results presented here also reveal that pyrazinamide, under the form of pyrazinoic acid, exerts protonophoric activity. Pyrazinoic acid was shown in Chapter 3 to dissipate the electric potential across the mycobacterial cell, which, together with the evidence presented in the same chapter of cytoplasmic acidification, implies the mechanism is electrogenic. Additionally, the data shown in Chapter 4 supports the protonophoric mechanism of pyrazinoic acid, with a mathematical model developed to validate the hypothesis and the positive comparison with other known protonophores. Chapter 4 also shows that salicylic acid, the active form of aspirin, is active against *Mycobacterium tuberculosis in vitro*, showing higher efficacy than

pyrazinoic acid. The potential for the use of salicylic acid (or any of the pharmacologically available formulations in the market) may have a great impact in the field.

Chapter 5 provides the first step in assessing the potential of salicylic acid as an alternative to pyrazinamide. The results presented in that chapter show how the drug-drug interactions of pyrazinoic acid with either rifampin or isoniazid are mimicked by salicylic acid *in vitro*. *In vivo*, pyrazinamide is well-known to reduce the time of treatment in half when added to the standard combination therapy. It remains to be determined if salicylic acid induces the same effect when added to the regimen, but the initial observations in Chapter 5 are optimistic.

The discovery of protonophoric activity as primary mechanism of pyrazinamide activity creates a new research and development space for the discovery of new anti-tubercle drugs with the same mode of action. Preliminary studies conducted during the work presented above indicate the structural motifs of the hydrophobic moiety may play a role in the efficacy of the compounds tested; therefore, structure-activity relationship models can be developed to increase the efficacy of this class of compounds. Moreover, the studies presented here were all conducted *in vitro*, making it essential for the further development of the protonophoric anti-tubercle class of compounds to be tested *in vitro*. Finally, from the purely biochemical perspective, a better understanding of the rates at each step of the mechanism for these compounds could facilitate the design of future antibiotics; increasing the rate of membrane diffusion of both protonated and deprotonated forms or developing similar compounds with higher pK_a values that retain high efficacy may result in a reduced time of treatment similar to the one achieved when pyrazinamide was first introduced into the standard regimen against tuberculosis.

Appendix A

Derivation of the pH-dependent activity model.

Modeling the pH-dependent activity of relevant drugs or toxins has been the subject of extensive literature. The following model is adapted from Könemann and Musch,[1] with more detailed explanation and further development and interpretation.

For an ionizable molecule, such as pyrazinoic acid in protonated form (Figure A1, abbreviated as POA_N), it is theoretically possible for either or both the protonated and deprotonated forms of the compound exhibit an effect. In the example of POA_N, both POA_N and its deprotonated form, pyrazinoate (POA_C) can potentially exhibit activity. The assumption is that any observable effect results from the additivity of the effect of both forms of the molecule. Hence, the effect of an ionizable molecule can be expressed as

$$\frac{[HA]+[A^-]}{EC_{50}} = T_N \cdot [HA] + T_C \cdot [A^-] \qquad \text{Equation A1}$$

where $[HA]$ and $[A^-]$ stand for the concentrations of the protonated and deprotonated forms of the molecule, respectively. EC_{50} corresponds to the overall concentration of the molecule (or $[HA]+[A^-]$) that causes 50% of the observable effect. The specific effect of each form is expressed by T_N and T_C, as the inverse of the concentration responsible for 50% of the effect caused by $[HA]$

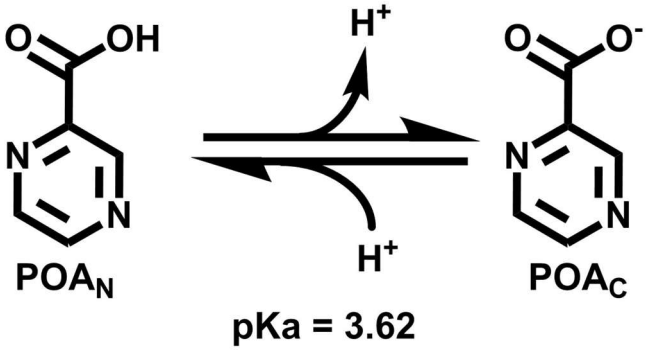

Figure A1 – Acid-base equilibrium of pyrazinoic acid (POA_N) with pyrazinoate (POA_C). The pK_a shown was obtained with theorical calculation with Chemicalize (www.chemicalize.com)

(in the case of T_N) or $[A^-]$ (in the case of T_C):

$$\frac{1}{EC_{50}^N} = T_N \quad \text{Equation A2}$$

$$\frac{1}{EC_{50}^C} = T_C \quad \text{Equation A3}$$

with EC_{50}^N representing the concentration of HA that causes 50% of the effect of HA and EC_{50}^C is the concentration of A^- responsible for 50% of the effect caused by A^-.

The ionizable molecule exists in an acid-base equilibrium in solution. The equilibrium, which, following acid-base chemistry, can be expressed as

$$\frac{[H^+]\cdot[A^-]}{[HA]} = K_a \quad \text{Equation A4}$$

with K_a corresponding to the acid equilibrium constant of the reversible reaction

$$HA \rightleftarrows H^+ + A^- \quad \text{Equation A5}$$

In which H^+ represents the proton released in the reaction. In the example of POA_N and POA_C, the equilibrium reaction takes the form of

$$POA_N \rightleftarrows H^+ + POA_C \quad \text{Equation A6}$$

When the effect is defined at the concentration EC_{50}, Equation A1 can be simplified, as follows:

$$[HA] + [A^-] = EC_{50} \quad \text{Equation A7}$$

allowing for the expression of $[HA]$ and $[A^-]$ in terms of K_a, H^+ and EC_{50}, as follows (using Equation A4 and Equation A7):

$$[HA] = \frac{[H^+]}{[H^+]+K_a} \cdot EC_{50} \quad \text{Equation A8}$$

and

$$[A^-] = \frac{K_a}{[H^+]+K_a} \cdot EC_{50} \quad \text{Equation A9}$$

Substituting Equation A7, Equation A8 and Equation A9 in Equation A1 yields

$$1 = T_N \cdot \frac{[H^+]}{[H^+]+K_a} \cdot EC_{50} + T_C \cdot \frac{K_a}{[H^+]+K_a} \cdot EC_{50} \qquad \text{Equation A10}$$

or

$$\frac{1}{EC_{50}} = T_N \cdot \frac{[H^+]}{[H^+]+K_a} + T_C \cdot \frac{K_a}{[H^+]+K_a} \qquad \text{Equation A11}$$

While $[H^+]$ and K_a can be easily calculated, it is commonly to express both in terms of pH and pK_a, respectively, for commodity of smaller numbers. The relationship between pH and $[H^+]$ follows

$$[H^+] = 10^{-pH} \qquad \text{Equation A12}$$

While the relationship between pK_a and K_a arises, in a similar manner, from

$$K_a = 10^{-pK_a} \qquad \text{Equation A13}$$

and the substitution of these equalities in Equation A11 results in

$$\frac{1}{EC_{50}} = T_N \cdot \frac{10^{-p}}{10^{-pH}+10^{-pK_a}} + T_C \cdot \frac{10^{-pK_a}}{10^{-pH}+10^{-pK_a}} \qquad \text{Equation A14}$$

Equation A14 (or Equation A11, if $[H^+]$ and K_a are used) can be analyzed further if each term of the equation is interpreted as dominant in terms of the corresponding effect of each form of the ionizable molecule. Könemann and Musch make a reference to this differential effect in terms of membrane solubility, suggesting it is common to observe a higher toxicity for the protonated form of phenols.[1] The dominance of one of the forms can also be interpreted as a specific effect requiring a specific form or an indication of a kinetic limiting step requiring the formation of a specific form of the molecule. Additionally, the dominance of a particular form in the overall effect can be a reflection of a combination of the factors described above. The dominance of a form is expressed by the value of its corresponding term, i.e., if T_N has an absolute value much higher than T_C, the protonated form has a dominant effect compared to the effect resulting from the deprotonated form.

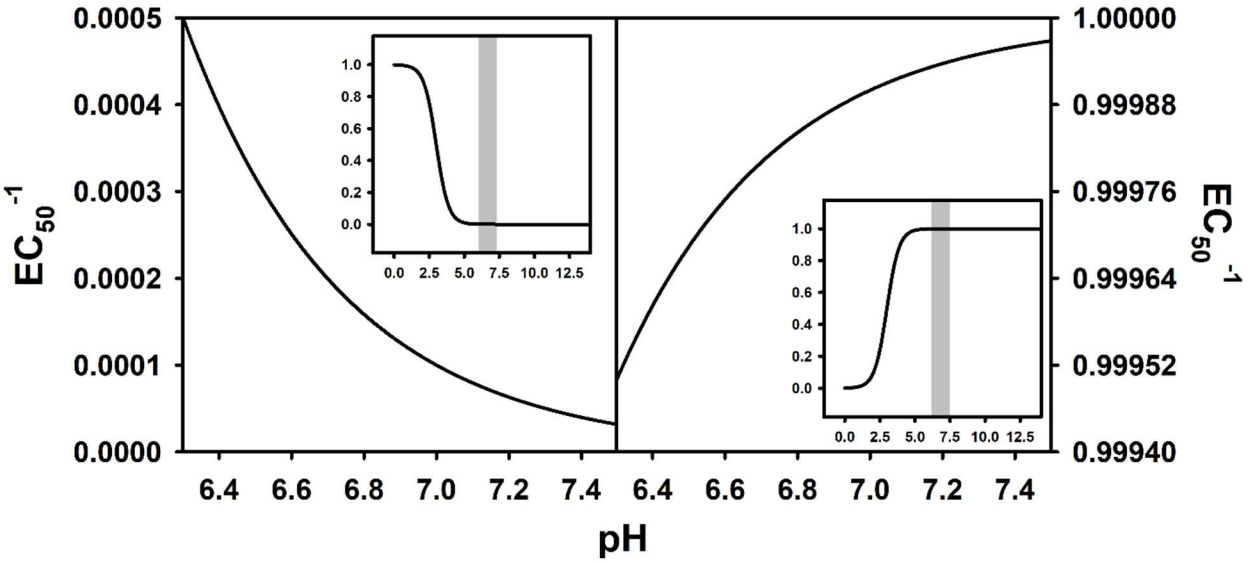

Figure A2 – Simulation of the curves described by Equation A14 in the cases of $T_N = 1$ and $T_C = 0$ (left panel) or $T_N = 0$ and $T_C = 1$ (right panel). The pK_a used for this simulation equals 3.

The dominance of a species can also be determined graphically, as seen in Figure A2. The theoretical case of an ionizable molecule with a pK_a of 3.0 is shown, with the panel on the left representing the dominance of its protonated form and the panel on the right the dominance of the deprotonated form. The panel of the left of Figure A2 shows the curve described by Equation A14 when T_N is 1 and T_C is 0, with particular focus in the range of pH values used to determine the growth inhibitory concentrations (GIC_{50}) for pyrazinoic acid and the other compounds tested in the present work. As the left panel of Figure A2 shows, when the protonated form has a dominant effect, the inverse of EC_{50} increases with the decrease of pH (which is seen in Chapter 4, Figure 4.4, for CCCP, POA_T and SAL_T). Conversely, the right panel of Figure A2 shows the curve of Equation A14 when T_N is 0 and T_C equals 1, results in the diametrically opposed trend seen in the left panel. The dominance of the deprotonated form would be expressed as an increase in the inverse of EC_{50} values when pH increases. The theoretical case of no dominance (where the numerical value of T_N is close to the value of T_C) would result in a curve with no slope or a small slope. However, these molecules are impossible to distinguish from molecules which effect is not

pH-dependent. While the numerical values of T_N and T_C presented in Table 2 were determined with non-linear curve fitting methods, Könemann and Musch provide a linearization of Equation A11 that may prove to be useful in cases where such methods are not available or difficult to use.[1] From Equation A10,

$$1 = T_N \cdot \frac{([H^+]+K_a-K_a)}{[H^+]+K_a} \cdot EC_{50} + T_C \cdot \frac{K_a}{[H^+]+K_a} \cdot EC_{50} \qquad \text{Equation A15}$$

as the consecutive addition and subtraction of K_a is neutral. Then

$$1 = T_N \cdot \frac{[H^+]+K_a}{[H^+]+K_a} \cdot EC_{50} - T_N \cdot \frac{K_a}{[H^+]+K_a} \cdot EC_{50} + T_C \cdot \frac{K_a}{[H^+]+K_a} \cdot EC_{50} \quad \text{Equation A16}$$

which can be simplified to

$$\frac{1}{EC_{50}} = T_N - (T_N - T_C) \cdot \frac{K_a}{[H^+]+K_a} \qquad \text{Equation A17}$$

The resulting Equation A17 generates a linear curve when the inverse of EC_{50} is used in the y-axis and $\frac{K_a}{[H^+]+K_a}$ is used as x-axis. The resulting curve provides an easy way to determine T_N, since it corresponds with the y-intercept and the slope can then be used to determine T_C.

The derivation presented here used the concentrations that cause 50% of the effect because of the use of GIC_{50} values in the work with pyrazinoic acid and other anti-tubercle compounds. However, it is noteworthy to point out that other percentages of effect can be used, like 90% or 99%, with the results translating to those percentages of effect across all coefficients (EC, T_N and T_C).

References.

(1) Könemann, H.; Musch, A. Quantitative structure-activity relationships in fish toxicity studies (Part 2): The influence of pH on the QSAR of chlorophenols. *Toxicology* **1981**, *19* (3), 223–228. https://doi.org/10.1016/0300-483X(81)90131-1.